

MIXTURE FORMATION AND COMBUSTION
CHARACTERISTICS OF DIESEL-HYDROGEN
DUAL FUEL ENGINE



DOCTOR OF PHILOSOPHY
UNIVERSITI MALAYSIA PAHANG

DECLARATION OF THESIS AND COPYRIGHT

Author's full name : WIDODO BUDI SANTOSO

Date of birth : 26th MAY 1969

Title : MIXTURE FORMATION AND COMBUSTION
CHARACTERISTICS OF DIESEL-HYDROGEN DUAL
FUEL ENGINE

Academic Session : SEMESTER 2 2015/2016

I declare that this thesis is classified as:

- CONFIDENTIAL** (Contains confidential information under the Official Secret Act 1972)*
- RESTRICTED** (Contains restricted information as specified by the organization where research was done)*
- OPEN ACCESS** I agree that my thesis to be published as online open access (Full text)

I acknowledge that Universiti Malaysia Pahang reserve the right as follows:

1. The Thesis is the Property of University Malaysia Pahang
2. The Library of University Malaysia Pahang has the right to make copies for the purpose of research only.
3. The Library has the right to make copies of the thesis for academic exchange.

Certified By:

A8267827

PROF. DATO' DR. ROSLI BIN ABU BAKAR

New IC/Passport Number

Name of Supervisor

Date:

Date:



**Universiti
Malaysia
PAHANG**
Engineering • Technology • Creativity

SUPERVISOR'S DECLARATION

I hereby declare that I have checked this thesis and in my opinion, this thesis is adequate in terms of scope and quality for the award of the degree of Doctor of Philosophy in Mechanical Engineering (Automotive).

(Supervisor's Signature)

Full Name : PROF. DATO' DR. ROSLI BIN ABU BAKAR

Position : PROFESSOR, FACULTY OF MECHANICAL ENGINEERING, UMP

Date :

UMP

STUDENT'S DECLARATION

I hereby declare that the work in this thesis is my own except for quotations and summaries which have been duly acknowledged. The thesis has not been accepted for any degree and is not concurrently submitted for award of other degree.

(Author's Signature)

Full Name : WIDODO BUDI SANTOSO

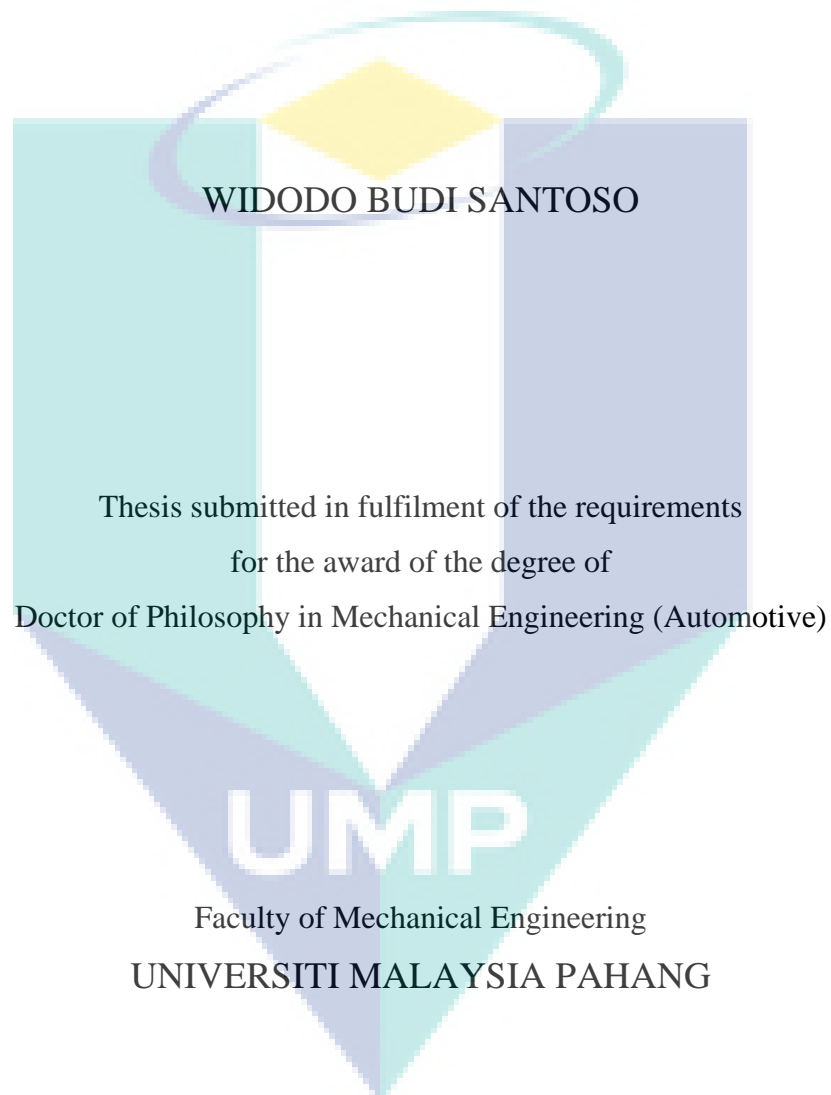
Position : PHD STUDENT

Date :

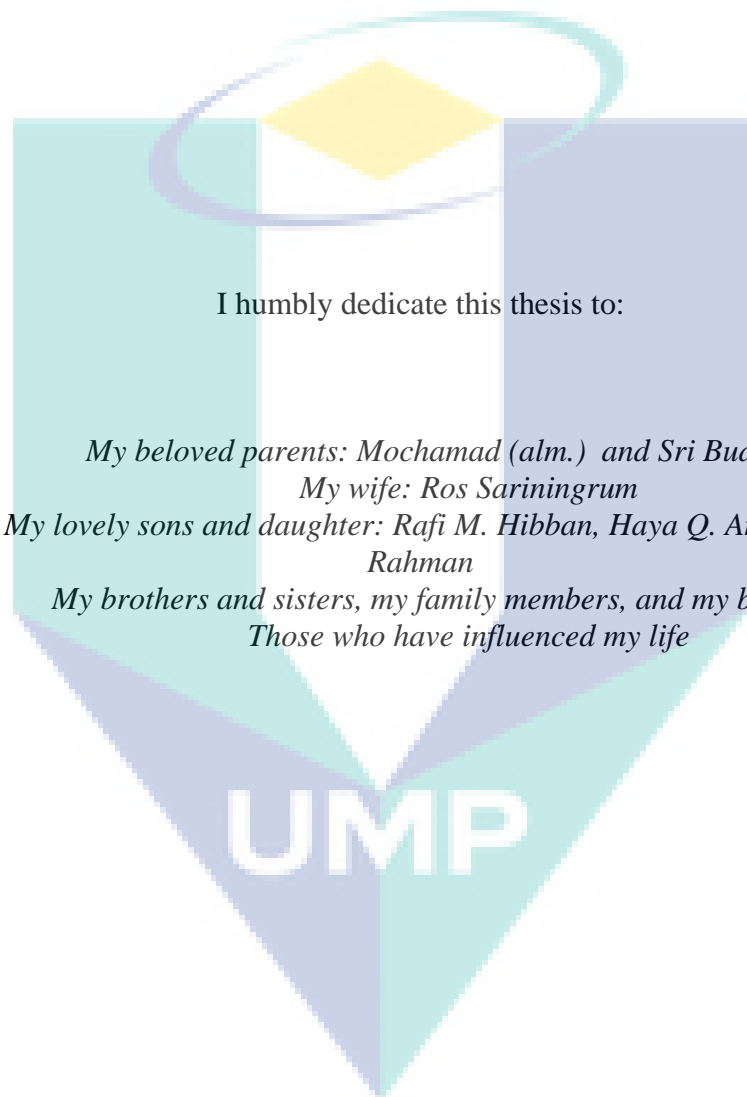


UMP

MIXTURE FORMATION AND COMBUSTION CHARACTERISTICS
OF DIESEL-HYDROGEN DUAL FUEL ENGINE



OCTOBER 2016



I humbly dedicate this thesis to:

My beloved parents: Mochamad (alm.) and Sri Budi Utami

My wife: Ros Sariningrum

My lovely sons and daughter: Rafi M. Hibban, Haya Q. Amani, Hanif A. Rahman

*My brothers and sisters, my family members, and my best friends
Those who have influenced my life*

ACKNOWLEDGEMENTS

I am grateful and would like to express my sincere gratitude to my supervisor Professor Dato' Dr. Rosli Abu Bakar for his germinal ideas, invaluable guidance, continuous encouragement and constant support in making this research possible. He has always impressed me with his outstanding professional conduct, his strong conviction for science. I also would like to express special thanks to my former co-supervisor Dr. Sugeng Ariyono for his suggestions and co-operation throughout the study. I also sincerely thanks for the time spent proofreading and correcting my many mistakes.

My sincere thanks go to all members of the staff of the Mechanical Engineering Department, UMP, who helped me in many ways and made my stay at UMP pleasant and unforgettable. Many special thanks go to members of Internal Combustion Engine Lab., LIPI Bandung for their excellent co-operation, inspirations and supports during this study. Special thanks go to Head of Research Centre for Electrical Power and Mechatronics for providing me the simulation (AVL FIRE CFD Code) and experimental facilities.

I acknowledge my sincere indebtedness and gratitude to my parents for their love, dream and sacrifice throughout my life. I acknowledge the sincerity of my parents-in-law, who consistently encouraged me to carry on my higher studies in Malaysia. I am also grateful to my wife, daughter and son for their sacrifice, patience, and understanding that were inevitable to make this work possible. I cannot find the appropriate words that could properly describe my appreciation for their devotion, support and faith in my ability to attain my goals. Special thanks should be given to my supervisory committee members. I would like to acknowledge their comments and suggestions, which was crucial for the successful completion of this study.

The logo of Universiti Malaysia Perlis (UMP) is a large, stylized letter 'V' shape. The top part of the 'V' is a light blue arc. The two sides of the 'V' are filled with a light blue color, and the bottom point is a light purple color. The letters 'UMP' are written in white, bold, sans-serif font across the center of the 'V' shape.

UMP

ABSTRACT

Among the alternative fuels, hydrogen shows great potential as fuel and energy carrier. The advantages of using hydrogen as fuel for internal combustion engine is amongst other a long-term renewable and less polluting fuel, non-toxic, odourless, and has wide range flammability. This thesis deals with the utilization of hydrogen as fuel for diesel engine under dual fuel operation. Hydrogen is mixed with air or injected in the intake manifold before entering combustion chamber. Small amount of diesel fuel is injected to promote ignition. A modified experimental setup based on a single cylinder direct injection diesel engine together with 3D computational model was employed. The model incorporates detailed chemical kinetics for the oxidation of hydrogen and diesel fuel represented by the primary reference fuel consists of n-heptane and isoctane. During the combustion processes, the turbulence-chemistry interaction was accounted for. In the experimental part of this study, the effects of introducing hydrogen in varying flow rates on engine performance, combustion, and emission in the DI diesel engine were investigated. The corresponding results were further used to validate the simulation model. The simulation provides the mean calculation results and also the spatial and temporal distributions of temperature, cylinder pressure, velocity, and species mass fractions which are key data for the interpretation of the combustion processes. Experimental results showed that hydrogen addition at certain flow rate gave a different influence on the combustion, depending on the amount of the pilot diesel fuel or the engine load. Hydrogen addition at the low load reduced the cylinder pressure. On the other hand, it increased the cylinder pressure at higher loads. Simulation revealed that for the same hydrogen flow rate, higher load resulted in a faster combustion and earlier start of ignition. Hydrogen percentage of about 70 % based on energy sharing would be the maximum amount for a good combustion efficiency and stability. In depth investigation by simulation showed that the burning of hydrogen-air mixtures essentially occurs around the regions in the vicinity of the spray with high temperature. When diesel fuel vapour reached its flammability limit at high temperature, the ignition started. Hydrogen-air mixture oxidized at some degree crank angle after the commencement of the ignition. Fast combustion was observed during the diesel oxidation. When most of pilot diesel fuel has been oxidized, the combustion became slower. Hydrogen-air mixture oxidation was mainly due to flame propagation until the end of expansion stroke. The amount of the hydrogen that can be converted into the combustion products seems to be defined by the amount of the diesel pilot fuel. Some valuable insight and new ideas were identified through the extensive experimental and numerical investigation into the diesel-hydrogen dual fuel engine. Incorporating a detailed pilot fuel injection model which can provide more accurate results for pilot injection, developing an improved kinetic model for dual fuel combustion processes with gaseous fuel as the main fuel, and developing an improved heat transfer model which suit for dual fuel combustion are amongst area of future research.

ABSTRAK

Antara bahan api alternatif, hidrogen merupakan potensi besar sebagai bahan api dan pengangkut tenaga. Kelebihan menggunakan hidrogen sebagai bahan api bagi enjin pembakaran dalam adalah antara lain dalam jangka panjang boleh diperbaharui dan ianya kurang pencemaran, tidak toksik, tidak berbau, dan mempunyai pelbagai kemudahbakaan. Tesis ini berkaitan dengan penggunaan hidrogen sebagai bahan api untuk enjin diesel di bawah penggunaan dua bahan api. Hidrogen bercampur dengan udara atau disuntik dalam pancarongga pengambilan sebelum memasuki kebuk pembakaran. Jumlah kecil bahan api diesel disuntik untuk memulakan pencucuhan. Persediaan pembakaran diubahsuai berdasarkan enjin diesel silinder tunggal dengan menggunakan model pengiraan 3D. Model ini menggabungkan kinetik kimia yang terperinci bagi pengoksidaan hidrogen dan bahan api diesel yang mewakili bahan api rujukan utama yang terdiri daripada n-heptane dan isooctane. Semasa proses pembakaran, interaksi pergolakan-kimia telah diambilkira. Dalam kajian ujikaji, kesan-kesan dari pengenalan hidrogen dalam berbeza kadar aliran terhadap prestasi enjin, pembakaran, dan pencemaran dalam enjin diesel DI telah diuji. Keputusan yang sama terus digunakan untuk mengesahkan model simulasi. Simulasi yang menyediakan keputusan pengiraan purata serta pengagihan ruang dan masa daripada suhu, tekanan silinder, halaju dan pecahan besar-besaran spesies yang merupakan data penting bagi kajian proses pembakaran. Keputusan menunjukkan bahawa penambahan hidrogen pada kadar aliran tertentu memberi pengaruh yang berbeza ke atas pembakaran, bergantung kepada jumlah bahan api atau beban enjin. Penambahan hidrogen pada beban rendah mengurangkan tekanan silinder. Di samping itu, ia meningkatkan tekanan silinder pada beban yang lebih tinggi. Simulasi menunjukkan bahawa bagi hidrogen dengan kadar aliran yang sama, beban yang lebih tinggi menyebabkan pembakaran lebih cepat dan pencucuhan lebih awal. Hidrogen dalam 70 % berdasarkan perkongsian tenaga merupakan jumlah maksimum untuk kecekapan pembakaran yang baik dan kestabilan. Analisis mendalam menggunakan simulasi menunjukkan bahawa pembakaran campuran udara hidrogen pada dasarnya berlaku sekitar kawasan sekitar sembur dengan suhu yang tinggi. Apabila wap bahan api diesel sampai takat kemudahbakaan pada suhu yang tinggi, pencucuhan bermula. Campuran hidrogen-udara teroksida beberapa sudut engkol selepas bermulanya pencucuhan dengan memberi kesan kepada pembakaran cepat semasa pengoksidaan diesel. Apabila kebanyakan bahan api diesel telah teroksida, pembakaran menjadi lebih perlahan. Pengoksidaan campuran hidrogen-udara ini adalah disebabkan oleh penyebaran api sehingga ke penghujung lejang pengembangan. Jumlah hidrogen yang boleh ditukar menjadi hasil-hasil pembakaran seolah-olah ditakrifkan oleh jumlah bahan api diesel. Beberapa pendapat yang bernilai serta idea-idea baru telah dikenal pasti melalui siasatan ujikaji dan simulasi yang banyak ke dalam enjin dua bahan api diesel-hidrogen. Antara kajian penyelidikan akan datang iaitu: memasukkan model suntikan bahan api perintis yang terperinci guna memberikan hasil yang lebih tepat untuk suntikan perintis, membangunkan model kinetik yang lebih baik untuk proses pembakaran dua bahan api dengan bahan api gas sebagai bahan api utama, dan membangunkan model pemindahan haba yang lebih baik yang sesuai untuk pembakaran dua bahan api.

TABLE OF CONTENTS

	Page
DECLARATION	
TITLE PAGE	i
DEDICATION	ii
ACKNOWLEDGEMENTS	iii
ABSTRACT	iv
ABSTRAK	v
TABLE OF CONTENTS	vi
LIST OF TABLES	x
LIST OF FIGURES	xi
LIST OF SYMBOLS	xv
LIST OF ABBREVIATION	xvii
CHAPTER 1 INTRODUCTION	
1.1 Background	1
1.2 Hydrogen as a Fuel	2
1.2.1 Hydrogen Production	2
1.2.2 Hydrogen Storage	3
1.3 Hydrogen Economy	4
1.4 Problem Statement	4
1.5 Objectives of the Study	5
1.6 Scope of the Study	6
1.7 Organization of the Thesis	7
CHAPTER 2 LITERATURE REVIEW	
2.1 Introduction	8
2.2 Dual Fuel Engine	8
2.3 Hydrogen Combustion Properties	9

2.3.1	Wide Flammability Range	10
2.3.2	High Auto-Ignition Temperature	12
2.3.3	Low Ignition Energy	12
2.3.4	Small Quenching Distance	13
2.3.5	Low Density	14
2.4	Experiments on Dual Fuel Engine with Diesel-Hydrogen	14
2.4.1	Gaseous Fumigation	14
2.4.2	Gaseous Fuel Injection	19
2.4.3	Cyclic Variation	21
2.5	Dual Fuel Modelling	22
2.5.1	Thermodynamics Modelling	22
2.5.2	Phenomenological Modelling	23
2.5.3	Multi-Dimensional Modelling	25
2.6	Summary	28
CHAPTER 3 EXPERIMENTAL DETAIL AND COMPUTATIONAL MODELLING		
3.1	Introduction	30
3.2	Experimental Details	30
3.2.1	Experimental Setup	30
3.2.2	Dynamometer	32
3.2.3	Pressure Transducer	33
3.2.4	Crank Angle Encoder	34
3.2.5	Dynamometer Control and Engine Indicating System	35
3.2.6	Air Intake and Fuel Supply System	35
3.2.7	Exhaust Emission Analysis System	36
3.2.8	Experimental Uncertainty	37
3.2.9	Experimental Procedure	41
3.2.10	Parameters of Engine Performance	41
3.3	Model Development	43
3.3.1	Generation of Computational Mesh	43
3.3.2	Setting the Boundary and Initial Conditions	45
3.3.3	Governing Equations	47

3.3.4	Turbulence Model	48
3.3.5	Spray and Atomization Model	50
3.3.6	Integration of Chemical Kinetics	51
3.3.7	Numerical Solution	54
3.4	Summary	54

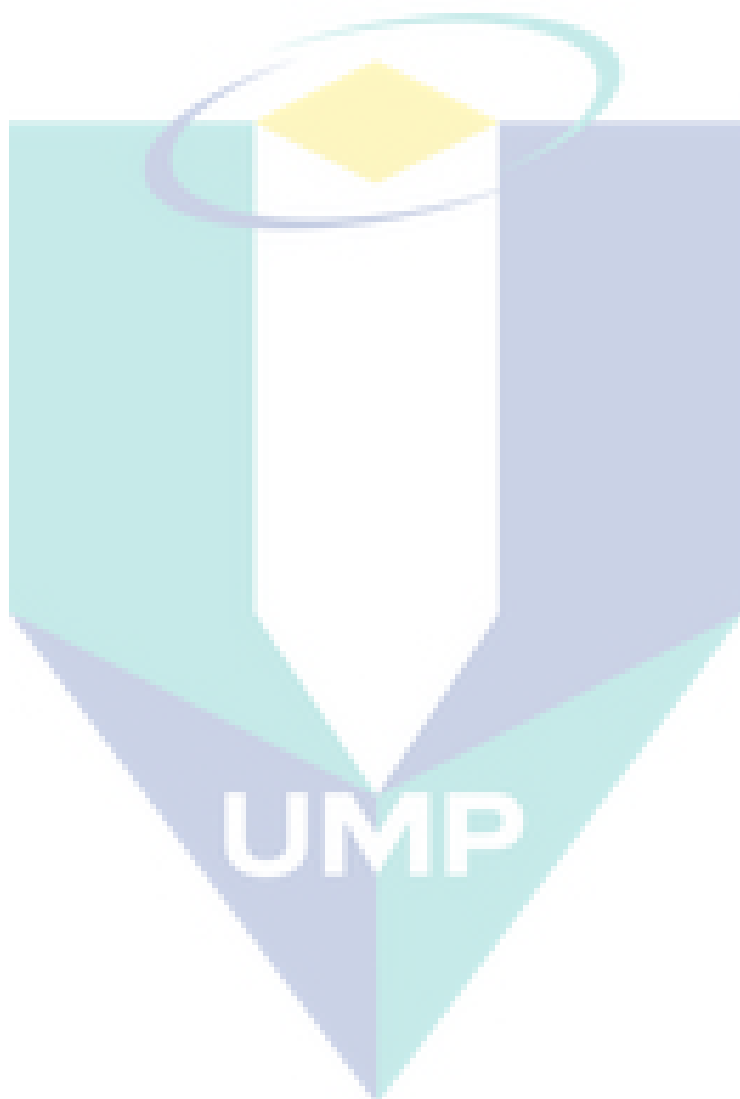
CHAPTER 4 RESULTS AND DISCUSSION

4.1	Introduction	56
4.2	Engine Performance	56
4.2.1	Diesel-Hydrogen Energy Sharing	56
4.2.2	Brake Specific Energy Consumption	59
4.2.3	Brake Thermal Efficiency	61
4.2.4	Emissions Analysis	63
4.3	Cyclic Variability of Dual Fuel Combustion	66
4.4	Combustion Characteristics	72
4.5	Numerical Investigation of Dual Fuel Combustion	77
4.5.1	Mesh Independence Test	77
4.5.2	Validation of Diesel Simulation	78
4.5.3	Validation of Dual Fuel Simulation	81
4.5.4	Characteristics of Mixture Formation	83
4.5.5	Effects of Hydrogen Addition on Engine Combustion	86
4.5.6	Characteristics of Diesel Dual Fuel During Compression and Combustion	92
4.6	Summary	113

CHAPTER 5 CONCLUSIONS AND RECOMMENDATION FOR FUTURE WORK

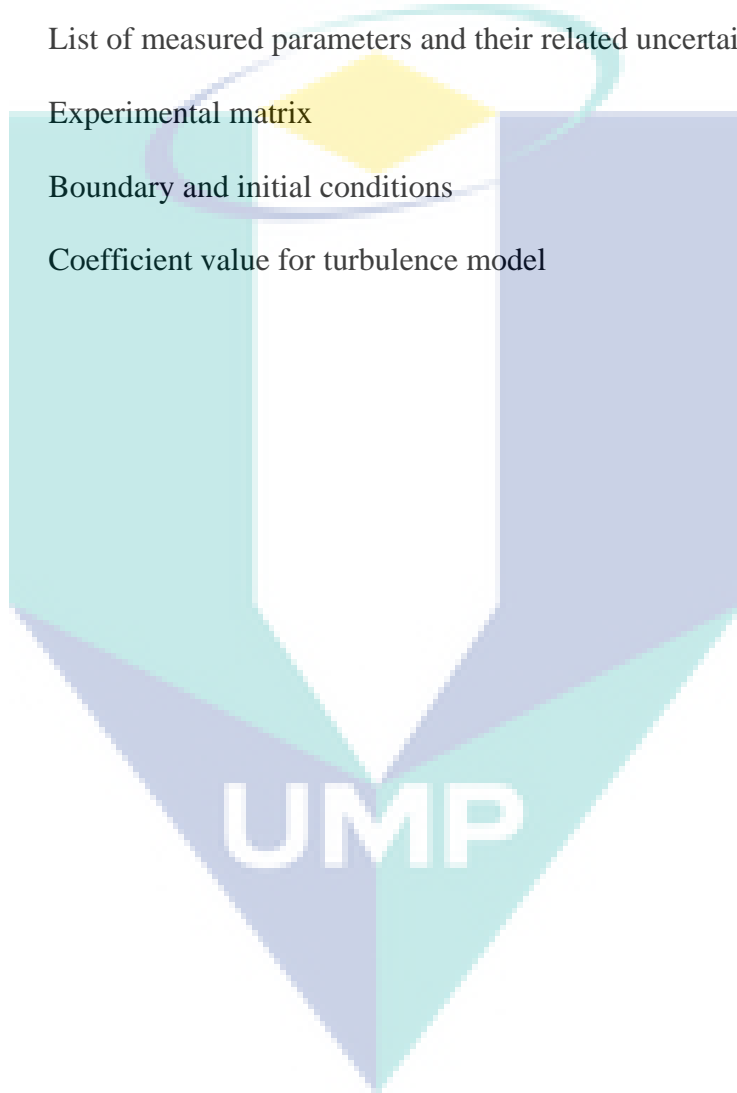
5.1	Summary of Findings	114
5.1.1	Dual Fuel Experiment	114
5.1.2	Cyclic Variability	115
5.1.3	CFD Simulation	115
5.2	Contributions of the Present Work	116
5.3	Recommendation for Future Work	116

REFERENCES	118
APPENDICES	
A LIST OF PUBLICATION	126
B PRF CHEMICAL KINETICS	127



LIST OF TABLES

Table	Title	Page
2.1	Fuel properties at 25 °C and 1 atm	10
3.1	Engine Specification	31
3.2	List of measured parameters and their related uncertainties	40
3.3	Experimental matrix	41
3.4	Boundary and initial conditions	46
3.5	Coefficient value for turbulence model	50



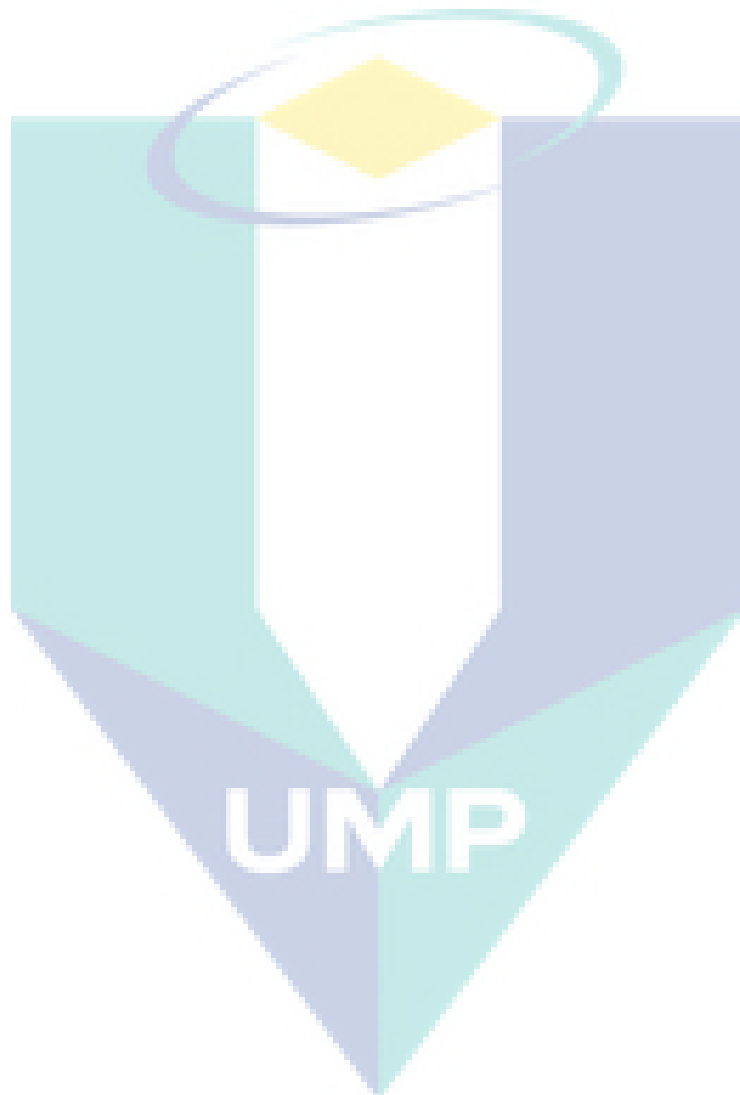
LIST OF FIGURES

Figure	Title	Page
1.1	Pathways of hydrogen production from non-renewable, sustainable, and renewable primary energy source.	3
2.1	Flammability ranges of comparative fuels at atmospheric temperature	11
2.2	Variation of hydrogen flammability limit with temperature	11
2.3	Minimum ignition energy in relation to equivalence rate at atmospheric pressure	13
2.4	A schematic zone division during combustion process	24
2.5	Definition of the burning zone before (a) and after (b) the initiation of combustion	25
3.1	Schematic of experimental setup	31
3.2	Arrangement of engine and dynamometer	32
3.3	Kistler 6061B water cooled pressure transducer	33
3.4	Arrangement of crank angle encoder	34
3.5	Instruments in the control room	35
3.6	Schematic of the exhaust system	37
3.7	Generation of computational model: (a) 2D piston bowl and spray target, (b) definition of block structure, (c) 2D mesh, (d) final 3D mesh	45
3.8	Boundary conditions	46
4.1	Diesel energy sharing at various speeds	58
4.2	Effect of hydrogen addition on needle lift, engine operation at 2000 rpm, 5 Nm	59
4.3	Variation of BSEC with hydrogen enrichment	60
4.4	Variation of brake thermal efficiency	62
4.5	Variation of NO _x with load and hydrogen flow rate	64

4.6	Variation of smoke number with load and hydrogen flow rate	65
4.7	Variation of CO ₂ emission with load and hydrogen flow rate	66
4.8	Cylinder pressure variation in diesel dual fuel engine operation	68
4.9	IMEP variation due to hydrogen addition at 5 and 20 Nm load	70
4.10	Accumulative heat release at 20 Nm load engine operation	71
4.11	Coefficient of variation of IMEP at variable load and hydrogen flow rate	71
4.12	Cylinder pressure at various load and hydrogen flow rate at 2000 rpm	73
4.13	Rate of heat release at 2000 rpm, 5 Nm	74
4.14	Rate of pressure rise under hydrogen enrichment	75
4.15	Rate of heat release at 2000 rpm, 10 Nm	75
4.16	Rate of heat release at 2000 rpm, 15 Nm	76
4.17	Rate of heat release of engine operation at high load	77
4.18	CFD meshes for study of mesh sensitivity	78
4.19	Mesh independent test; engine operating at 2000 rpm, 10 Nm	78
4.20	Validation of simulation result of diesel combustion at 2000 rpm	79
4.21	Rate of pressure rise for diesel combustion at 2000 rpm	80
4.22	Comparison of cylinder pressure for dual fuel operation	82
4.23	The injection rate and the evaporated fuel mass: case 2000 rpm, 20 Nm, H ₂ flow = 42.8 l/min	83
4.24	Spray evolution and the mass fraction distribution of diesel fuel: 2000 rpm, 20 Nm, H ₂ flow = 42.8 l/min	84
4.25	Simulation result of the effect of H ₂ addition on cylinder pressures	86
4.26	Simulation result of the effect of H ₂ addition on rate of heat release	87
4.27	Radicals (H ₂ O ₂ and OH) mass fraction decomposition and formation	88
4.28	Time-histories of average OH mass fraction	89
4.29	Effect of hydrogen addition on temperature	90

4.30	Time-histories of average hydrogen mass fraction	91
4.31	Effect of hydrogen addition on hydrogen conversion rate	92
4.32	Velocity diesel (nC7H16) mass fraction distribution at 12 °CA before TDC	93
4.33	Temperature and species mass fraction distribution at 12 °CA before TDC	94
4.34	Temperature distribution at 4 °CA before TDC	96
4.35	Carbon monoxide mass fraction distribution at 4 °CA before TDC	96
4.36	OH mass fraction distribution at 4 °CA before TDC	97
4.37	Carbon dioxide mass fraction distribution at 4 °CA before TDC	97
4.38	Time-histories of average carbon monoxide and carbon dioxide concentration.	98
4.39	Hydrogen mass fraction distribution from 5 °CA BTDC until TDC, cut plane along the spray axis	99
4.40	Hydrogen mass fraction distribution from 5 °CA BTDC until TDC, cut plane at Z =-5 mm	100
4.41	Temperature distribution across the spray axis from 5 °CA BTDC until TDC	101
4.42	Temperature distribution from 5 °CA BTDC until TDC, cut plane Z=-5 mm	102
4.43	Oxygen mass fraction distribution across the spray axis from 5 °CA BTDC until TDC	103
4.44	Oxygen mass fraction distribution from 5 °CA BTDC until TDC, cut plane Z =-5 mm.	104
4.45	Time-histories of mean n-heptane and hydrogen concentration	105
4.46	Progress of temperature distribution from 4 °CA-20 °CA ATDC	106
4.47	Progress of hydrogen mass fraction distribution from 4 °CA-20 °CA ATDC	107
4.48	Oxygen mass fraction distribution from 5 °CA-20 °CA ATDC	108
4.49	Hydrogen mass fraction distribution during the end of combustion	110

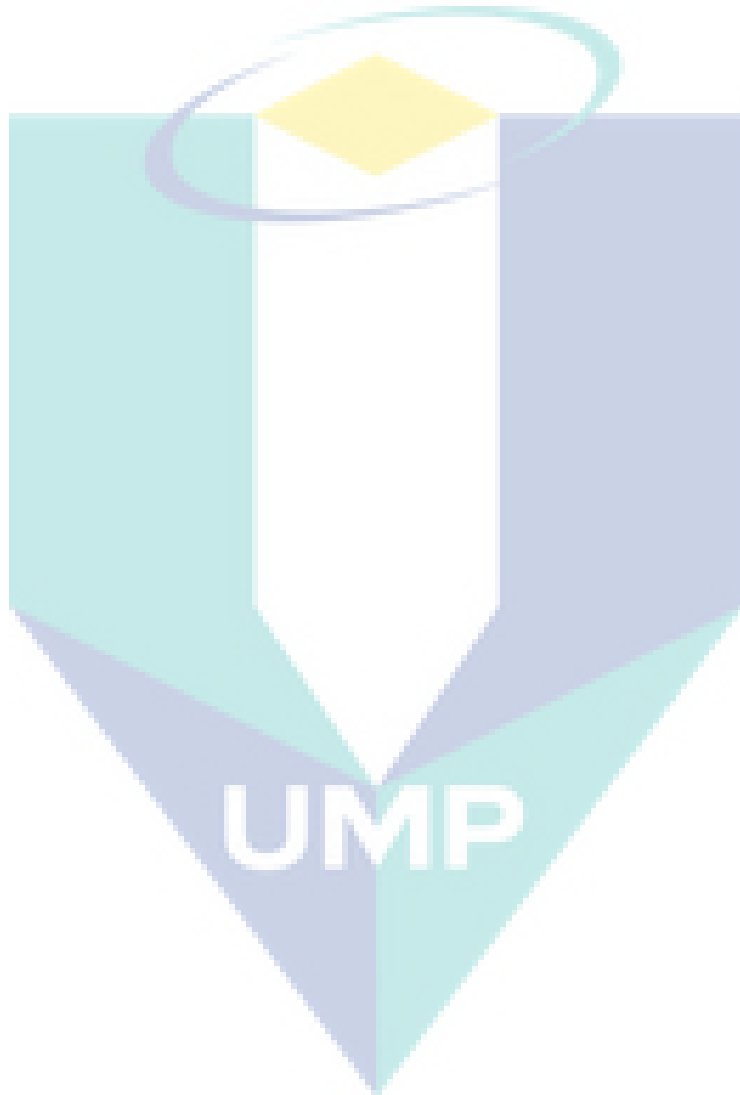
	phase (50-65 °CA after TDC)	
4.50	Velocity distribution during the end of combustion phase (50-65 °CA after TDC)	111
4.51	Temperature distribution during the end of combustion phase (50-65 °CA after TDC)	112



LIST OF SYMBOLS

A	Exponential factor
B	Temperatur dependence factor
E	Activation energy
C_1	Spray constant
LHV_{H_2}	Hydrogen low heating value
LHV_{diesel}	Diesel low heating value
k	Turbulent kinetic energy
\dot{m}_{air}	Air mass flow rate
\dot{m}_{diesel}	Diesel mass flow rate
Me	Effective torque
\dot{m}_{H_2}	Hydrogen mass flow rate
n	Engine speed
Pe	Effective power
Q_w	Wall heat flux
r_0	Initial droplet diameter
r_{new}	Droplet diameter
T	Temperature
T	Taylor number
u_{rel}	Relative velocity
We	Webber number
Z	Ohnesorge number
α	Crank angle
ε	Dissipation rate

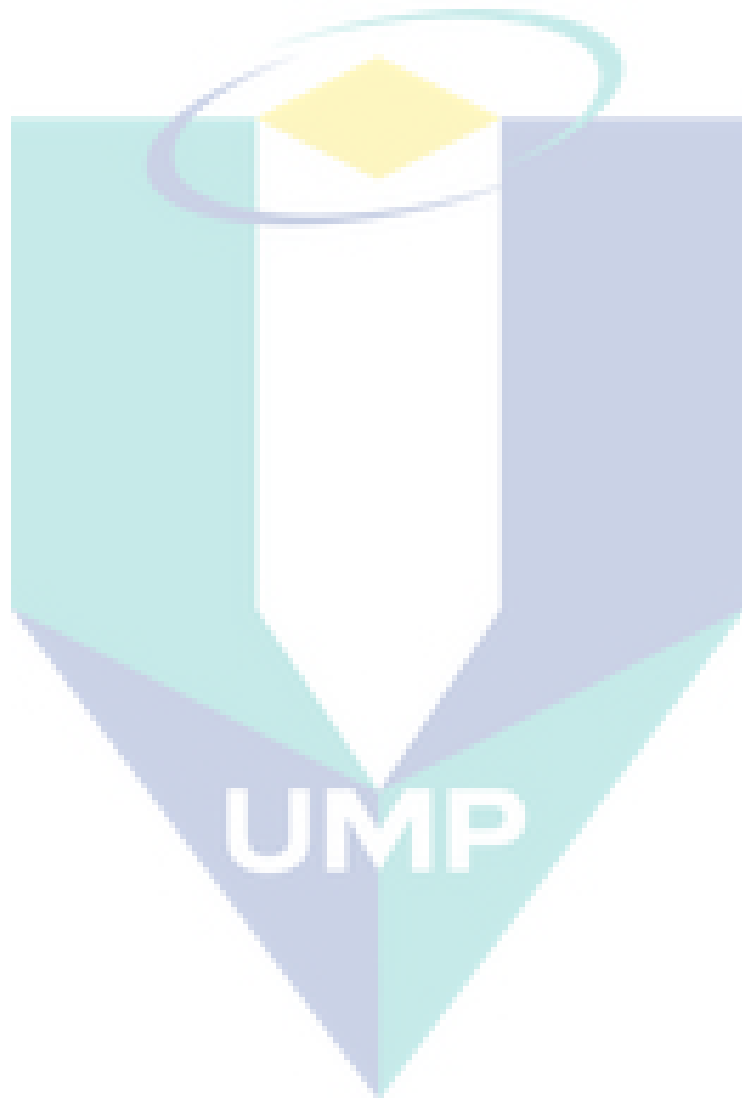
μ	Viscosity
λ	Wave length
Ω	Drop surface growth rate



LIST OF ABBREVIATIONS

1D	One dimensional
3D	Three dimensional
ATDC	After top dead centre
BSEC	Brake specific energy consumption
BSFC	Brake specific fuel consumption
BTDC	Before top dead centre
CA	Crank angle
CFD	Computational fluid dynamics
CI	Compression ignition
CNG	Compressed natural gas
CO	Carbon oxide
CO ₂	Carbon dioxide
DF	Dual fuel
DI	Direct injection
EGR	Exhaust gas recirculation
EOI	End of injection
FSN	Filter smoke number
IMEP	Indicated mean effective pressure
ISFC	Indicated specific fuel consumption
NO _x	Nitrogen oxides
PaSR	Partially Stirred Reactor
REGR	Reformed exhaust gas recirculation
SOI	Start of ignition

TDC	Top dead centre
THC	Total hydro carbon
TPI	Timed port injection
WSR	Well Stirred Reactor



CHAPTER 1

INTRODUCTION

1.1 BACKGROUND

The concept of saving energy, reducing pollution, protecting the environment, and developing long-term energy supply has been increasingly become people attention. Research funding relating to alternative fuel and energy carrier is increasing on both national and international level. Such a big concern on future energy supply is triggered by the alarming rate of fossil fuels. The energy stored in hydrocarbon fuels (solid, liquid, gas) was, is, and will be widely consumed by internal combustion engine as it is abundant, cheap, and convenient. However, such a widespread use of fossil fuels results in two problems of oil supply and environment degradation (Leon, 2008).

Efforts have been made to utilize alternative energy resources strategically, including intensification, diversification, and conservation. Alternative fuels such as alcohol, gas (CNG, LPG, biogas, producer gas, and hydrogen) have been studied intensively (Abdelaal & Hegab, 2012; Dhole, Yarasu, Lata, & Priyam, 2014; Lata, Misra, & Medhekar, 2012; Mohamed Ibrahim, Varuna Narasimhan, & Ramesh, 2015). Among those alternative fuels, hydrogen shows great potential (Sharma & Ghoshal, 2015). The advantages of using hydrogen as a fuel for internal combustion engine is amongst other a long-term renewable and less polluting fuel, non-toxic, odourless, and has wide range flammability (Fulton, Lynch, & Marmora, 1993). This research project deals with the utilization of hydrogen as fuel for diesel engine under dual fuel operation. Hydrogen cannot be used directly in a diesel engine because its auto-ignition

temperature is higher than that of diesel fuel. One alternative method is to use hydrogen in enrichment or induction. Hydrogen is mixed with air or injected in the intake manifold before entering combustion chamber. Small amount of diesel fuel, called pilot fuel, is injected to promote ignition. This “dual fuel” engine has the advantage to switch back to conventional diesel operation in case of shortfall in gas supply. There is no major modification needed for this kind of combustion mode (Karim, 2015). These benefits lead researchers worldwide to investigate the utilization of gas including hydrogen as fuel for diesel engine.

1.2 HYDROGEN AS A FUEL

Hydrogen can be regarded as a perfect fuel because it probably satisfied most of the desirable characteristics of such a fuel. Abundantly available and clean-burning, hydrogen has very high energy content and offers little or no harmful emissions. Hydrogen can be used as fuel for a wide range of applications, including power generation, industrial, residential, and transportation (Das, 1996; Hollinger & Bose, 2008)

1.2.1 Hydrogen Production

Hydrogen is supposed to be the most potent fuel among the chemical fuels, and it is natural that mankind moves towards using it soon. Fortunately, it is the most abundant element on earth and in the universe, and it is also the cleanest. Pure hydrogen as the strongest chemical fuel allows to suppress CO₂ and particulate emissions almost completely (depending upon the process of hydrogen production) and to lower the NO_x emissions (depending upon the energy conversion system used) (Leon, 2008). However, hydrogen is not only the strongest chemical fuel; it also serves as an “energy carrier”. At present, the only energy carrier that can be synthesized efficiently without materials limitations and in real-time is hydrogen. Furthermore, the combustion of hydrogen leads to the release of water to the atmosphere and the cycle is closed naturally (Hočevár & Summers, 2008; Zuetel, Borgschulte, & Schlapbach, 2008)

Hydrogen in liquid and gas form can be produced in several different ways, as can be seen in Figure 1.1. Obviously, interest focuses on those ways of hydrogen

production that are *sustainable* (like biomass) or, even better, *renewable* (like solar, wind, geothermal, hydro, etc.). Two basic options exist for producing hydrogen. One way is to separate the hydrogen from hydrocarbons through processes referred to as reforming or fuel processing. The second way to produce hydrogen is from water using the process of electrolysis to dissociate water into its separate hydrogen and oxygen constituents. Based on energy input, the production processes can be grouped into electrochemical, thermochemical, photochemical, and their combinations (Steinfeld, 2014).

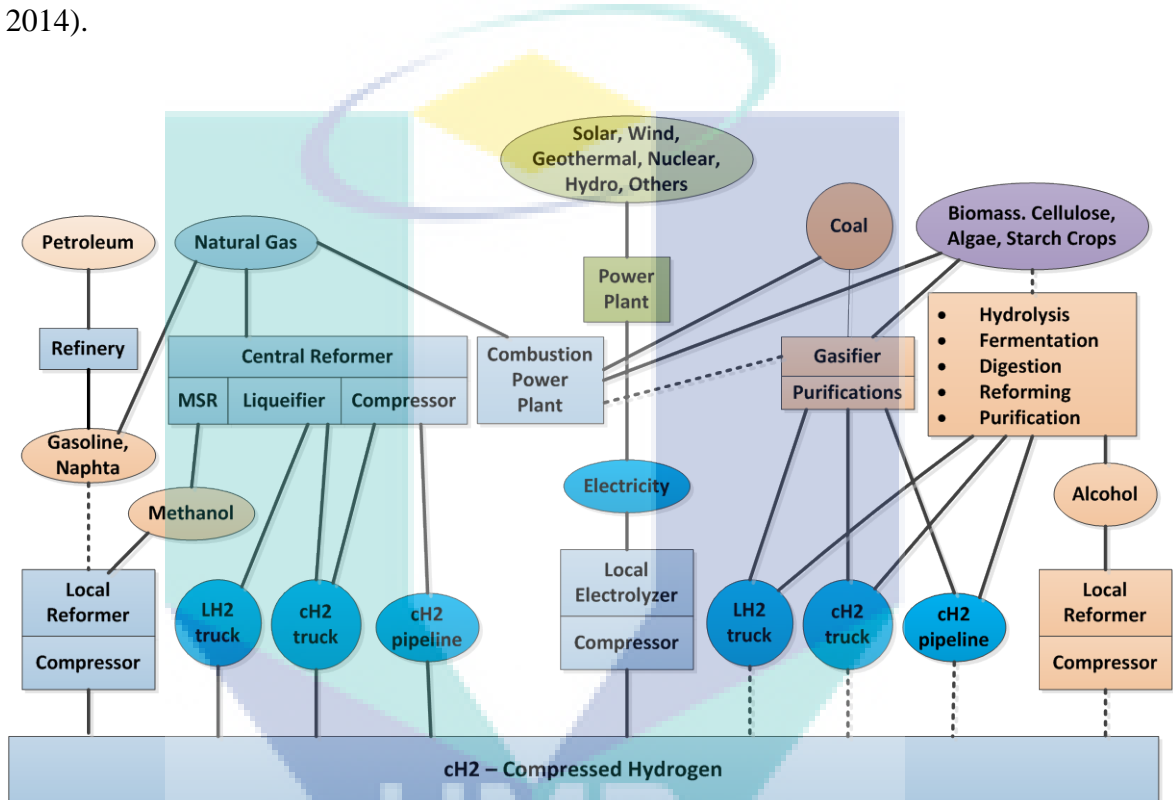


Figure 1.1. Pathways of hydrogen production from non-renewable, sustainable, and renewable primary energy source.

Source: Hočevár and Summers (2008)

1.2.2 Hydrogen Storage

For a successful application of hydrogen as an energy carrier, hydrogen should be stored safely and efficiently for variable periods of time. For that purpose, a safe and efficient means of storing hydrogen is required in mobile, portable, and stationary applications. At the same time, simple handling and low costs should be taken into consideration. It is clear that for efficient storage, hydrogen density was increased by

reducing the volume taken by the gas under normal temperature and pressure conditions (Stetson, Bowman, & Olson, 2014). As a consequence, the “usual state” of hydrogen has to be changed in order to store it efficiently. This can be accomplished by increasing the pressure, decreasing the temperature below the critical temperature or by reducing the repulsion interaction between hydrogen molecules by binding them with another material. A number of hydrogen storage options have been proposed, along with some of their identified strengths and weaknesses. The following three main options emerged: compressed hydrogen storage (CGH₂), cryogenic hydrogen storage (LH₂), and solid storage of hydrogen (SSH₂) (Leon, 2008; Stetson et al., 2014).

1.3 HYDROGEN ECONOMY

The so-called hydrogen economy is a long-term project that can be defined as an effort to change the current energy system to one which attempts to combine the cleanliness of hydrogen as an energy carrier with the efficiency of fuel cells (FCs) as devices to transform energy into electricity and heat (Marbán & Valdés-Solís, 2007). In other words, a hydrogen economy is when both hydrogen and electricity become the main energy carrier (Sherif, Barbir, & Veziroglu, 2014). For the future of the worldwide energy supply three goals must be fulfilled: security in the energy supply, environmental protection and the utilization of energy sources that promote the economic growth of societies. For a transition to a hydrogen economy through the operation of market forces, hydrogen technologies must compete effectively with fossil fuels and other alternatives to them. In particular, devices that use hydrogen e.g. fuel cell or H₂ICE must compete successfully with devices that use competing fuels (e.g. hybrid propulsion systems)(Ekins, 2010).

1.4 PROBLEM STATEMENT

Environmental concern and depletion of fossil fuel has become issues in the last decade. Efforts have been made to find renewable and environmentally friendly fuels. Hydrogen fuel was considered as a renewable and sustainable solution for both issues (Midilli & Dincer, 2008). It is often stated that fuel cells are a key technology of the twenty first century (de Palacio & Busquin, 2003). Although this statement is debatable, it is certain that fuel cells are an enabling technology for a future hydrogen economy.

Using pure hydrogen and air, fuel cells convert the chemical energy of the fuel directly into electricity with high efficiency, and they produce only water, thus eliminating all local emissions (Friedrich et al., 2008). However, the availability of economical and efficient fuel cell will not be realized with the coming years. The conventional diesel and gasoline engines remain the prime movers in the transportation, commerce, and power generation sectors (Reitz, 2013). Among them, the diesel engine is the most efficient compared with that gasoline engine. However, effort is still needed to deal with diesel emission of nitrogen oxide and particulates (Lloyd & Cackette, 2001), while at the same time improving the fuel economy. Various approaches are considered including exhaust gas after-treatment such as SCR and engine combustion process improvement (Brookshear, Nam, Nguyen, Toops, & Binder, 2015; Gu, Chun, & Song, 2015; Kang & Choi, 2016; Saravanan & Nagarajan, 2009; Valencia et al., 2014). Dual fuel engine is a typical effort to improve the combustion process.

Engine experiments, which are usually costly, are commonly used to analyse the dual fuel engine combustion process. Compared with the extensive research on the modelling of diesel engines, they are only a few references on the cycle simulation and CFD simulation of dual fuel (diesel-hydrogen) engines. This is mainly due to the complexity of the combustion process (Masood, Ishrat, & Reddy, 2007). Most of simulation studies of dual fuel combustion were focused on the small amount of hydrogen energy sharing (An et al., 2013; An et al., 2014; Deb, Sastry, Bose, & Banerjee, 2015). Thus, to fill these gaps, a complementary experimental and simulation works are conducted to achieve a better understanding on the mixture formation and combustion process in the diesel-hydrogen dual fuel engines operating at wide range energy sharing. Main parameters influencing the combustion process are also investigated.

1.5 OBJECTIVES OF THE STUDY

The objectives of this study are as follows:

- (i) To investigate experimentally the performance, combustion, and emission of diesel-hydrogen dual fuel engine
- (ii) To analyse the cyclic variability of diesel-hydrogen dual fuel engine

- (iii) To study mixture formation of dual fuel engine by multidimensional simulation
- (iv) To validate the chemical kinetics incorporated in the CFD code and to investigate numerically the combustion process of dual fuel engine

1.6 SCOPE OF THE STUDY

This thesis attempts to investigate the mixture formation and combustion processes in the dual fuel engine. The scopes of the study include:

- (i) Modify a stationary, single cylinder diesel engine to run under dual fuel mode. Hydrogen admission is realized by installing the mixer in the intake manifold.
- (ii) Hydrogen flow rate was 21.4 - 49.6 litre/min, equivalent to 22 – 99 % energy sharing, depending on engine speed and load.
- (iii) Combustion analysis for experimental works is based on cylinder pressure trace and its derivative parameters.
- (iv) Engine modelling is conducted in the compression and expansion stroke where both valves are closed. Computational grid dependency test is conducted to achieve reasonable results with a relatively short computing time.
- (v) The detailed chemical kinetic is constructed from previous studies. It combines the diesel surrogate (n-heptane and iso-octane) and hydrogen mechanism. Tuning on some parameter constants are made to meet the experimental results.
- (vi) The developed engine simulation model is only suited for normal engine operation; no abnormal combustion phenomena are considered such as knock and backfire.
- (vii) The validation of the dual fuel simulation is accomplished with certain cases in experimental observations completed within this work.
- (viii) The obtained results may only valid for the engine used in this study

1.7 ORGANIZATION OF THE THESIS

In Chapter 2, a review of the most important findings of the work related to the objectives of the present study is given. This review summarized the property of hydrogen compared with other gaseous fuel, the experimental works and simulation studies. Based on this review, some issues can be drawn as a stepping-stone for the present study. Chapter 3 describes the experimental setup and computational modelling. Engine modification, coupling the engine to the dynamometer, instrumentation, and experimental procedure are discussed briefly. Development of engine model, the governing equation, setup the calculation, spray model, combustion model, and implementation of detailed kinetics mechanism into CFD code is described. Chapter 4 discusses and analyses the experimental and simulation results. Effects of hydrogen addition on the engine performance, combustion, and emissions are discussed. Cyclic variability due to hydrogen addition at different load is analysed accordingly. Simulation of the combustion processes of diesel spray in the homogeneously premixed hydrogen-air mixture is presented. The effect of different parameters on the mixture formation and combustion processes are investigated. Chapter 5 concludes with a brief summary, discussion, and suggestion for further research.

The logo of UMP (Universitas Muhammadiyah Purwokerto) is a large, stylized shield shape. It is composed of several overlapping triangles in shades of teal, light blue, and yellow. The letters 'UMP' are written in a bold, white, sans-serif font across the center of the shield.

UMP

CHAPTER 2

LITERATURE REVIEW

2.1 INTRODUCTION

The purpose of this chapter is to provide a review of past research efforts related to diesel dual fuel engine, utilization of hydrogen for internal combustion engine fuel, and modelling of dual fuel combustion. A review of other relevant research studies is also provided. The review is organized chronologically to offer insight to how past research efforts have laid the groundwork for subsequent studies, including the present research effort. The review is detailed so that the present research effort can be properly tailored to add to the present body of literature as well as to justify the scope and direction of the present research effort.

2.2 DUAL FUEL ENGINE

A dual fuel engine is a converted diesel engine in which the gaseous fuel is mixed with the air, and ignited by injected a small amount of liquid fuel (pilot fuel). Dual fuel engines which have common features with both spark-ignition engines and diesel engines provide an opportunity for liquid petroleum fuel by gaseous fuels (natural gas, syngas, hydrogen, and other gaseous fuels). Gaseous fuel was introduced into the intake manifolds by mixers or gas injectors while maintaining the original diesel injection system.

The most common type of dual fuel engines is the one with diesel pilot fuel injected into the mixture of gaseous fuel and the inducted air. Such engines have a relative simple control system, less cyclic variation under normal operational conditions, higher thermal efficiency than spark ignited gaseous fuel engines, and with the capacity to revert to normal diesel operation at the driver's demand (Shioji, Ishiyama, & Ikegami, 2000). Diesel engines with high compression ratio are generally suitable when high thermal efficiency is desired. Gaseous fuels have high octane numbers, and therefore, suitable for engines with relatively high compression ratio due to its knock resistance. Furthermore, gaseous fuels also promise to produce less polluting exhaust (Sahoo, Sahoo, & Saha, 2009)

There are many advantages of diesel dual fuel over their dedicated diesel and spark ignition gaseous engines. Dual fuel engines can operate on a gaseous fuel with diesel pilot or on diesel alone in case of shortfall in gas supply. The ability to switch back to diesel alone operation make dual fuel engine attractive both in vehicular and stationary application. Another advantage is that an existing diesel engine can be converted to dual fuel engine with relative ease. No major modification is needed (Karim, 2015). The original cylinder can be used without modification and the compression ratio can be retained because of CNG's or hydrogen's good antiknock characteristics.

2.3 HYDROGEN COMBUSTION PROPERTIES

Hydrogen is the simplest and most abundant element in the universe. However, hydrogen is not available in pure form as primary energy source, but always chemically bound, e.g. in water, hydrocarbons (oil, natural gas, coal, biomass) (Leon, 2008). As a fuel hydrogen is no more dangerous than methane of gasoline, but it need a different treatment to handle it due to its different properties (Das, 1996). The property of hydrogen compared with methane is given in Table 2.1.

A number of researches have been focused on dual fuel engine operation with gaseous fuel including hydrogen, both as supplement or primary fuel (de Moraes, Mendes Justino, Valente, Hanriot, & Sodré, 2013; Deb et al., 2015; Köse & Ciniviz, 2013). According to Lanz (2001), the advantages of using hydrogen as fuel for internal

combustion engine are: a long-term renewable and less polluting fuel, non-toxic, odourless and results in complete combustion, wide range flammability, and high auto-ignition temperature. Other hydrogen properties that would be a challenge to solve when using it for internal combustion engine fuel: low ignition energy, small quenching distance, and low density.

Table 2.1
Fuel Properties at 25°C and 1 atm

Property	Hydrogen	CNG
Density (kg/m ³)	0.0824	0.72
Flammability limit (% vol in air)	4-75	4.3-15
Flammability limit (ϕ)	0.1-7.1	0.4-1.6
Autoignition temperature in air (K)	858	723
Minimum ignition energy (mJ)	0.02	0.28
Flame velocity(m/s)	1.85	0.38
Adiabatic flame temperature (K)	2480	2214
Quenching distance (mm)	0.64	2.1
Stoichiometric fuel/air mass ratio	0.029	0.069
Stoichiometric volume fraction (%)	29.53	9.48
Lower heating value (MJ/kg)	119.7	45.8
Heat of combustion (MJ/kg _{air})	3.37	2.9

Source: (White, Steeper, & Lutz, 2006)

2.3.1 Wide Flammability Range

Flammability ranges refer to the range of compositions, for fixed temperature and pressure, within which an explosive reaction is possible when an external ignition source is introduced. The information on flammability limits is quite useful in fire safety. For instance, flammability limits help in determining if storing a fuel in a tank is safe or not (McAllister, Chen, & Fernandez-Pello, 2011). Hydrogen has a wide flammability range in comparison with all other fuels as shown in Figure 2.1. As a result, hydrogen can be combusted in an internal combustion engine over a wide range of fuel-air mixtures. These flammability limits widen with increasing temperature as illustrated in Figure 2.2. A significant advantage of this is that hydrogen can run on a lean mixture (Verhelst & Wallner, 2009). A lean mixture is one in which the amount of fuel is less than the theoretical, stoichiometric or chemically ideal amount needed for combustion with a given amount of air. Combustion temperature is lower that produce

lower NO_x emission. However, this result in significant reduction of power and may necessitate the use of a turbo charger to increase the power (Hollinger & Bose, 2008).

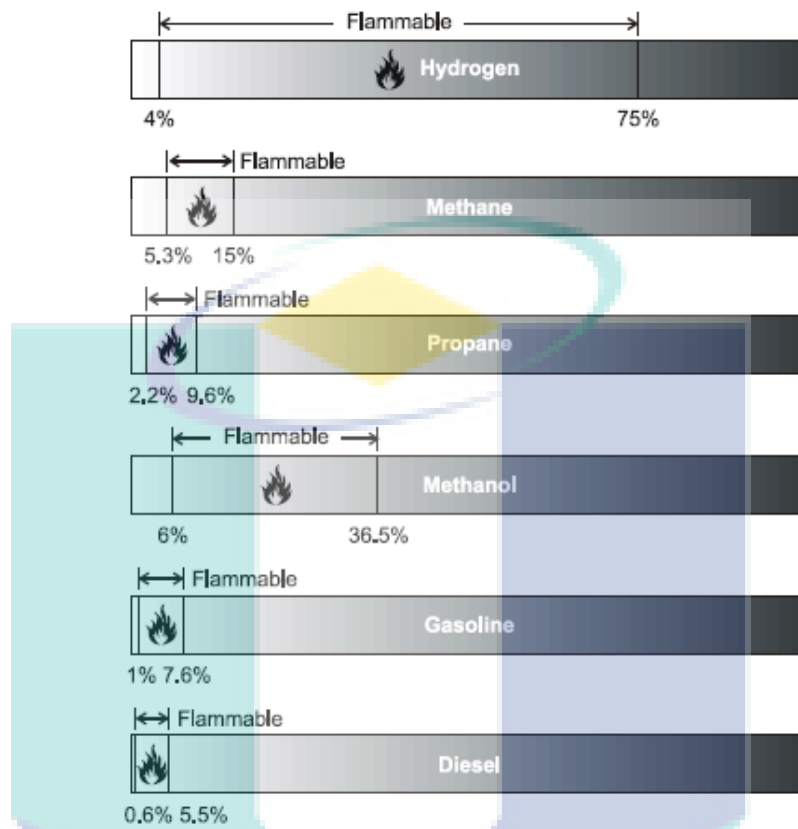


Figure 2.1. Flammability ranges of comparative fuels at atmospheric temperature.

Source: (Lanz, 2001)

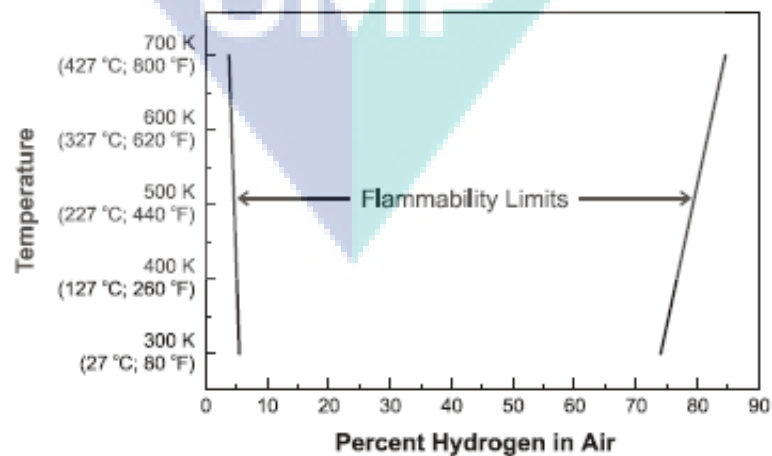


Figure 2.2. Variation of hydrogen flammability limit with temperature.

Source: (Lanz, 2001)

2.3.2 High Auto-ignition Temperature

Ignition is the mechanism leading to the onset of an aggressive combustion reaction and characterized by a rapid increase of the species temperature. It is often classified in two ways: spontaneous ignition, also known as auto-ignition, and piloted ignition which occurs with the assistance of external source (McAllister et al., 2011). The auto-ignition temperature is the minimum temperature required to initiate self-sustained combustion in a combustible fuel mixture in the absence of a source of ignition (Lanz, 2001). Hydrogen has a relatively high auto-ignition temperature of 858 K (Perry & Green, 1984; Saravanan, Nagarajan, Dhanasekaran, & Kalaiselvan, 2007b). This temperature has important implications when a hydrogen–air mixture is compressed. This property of hydrogen allows higher compression ratios to be used in a hydrogen engine than in a hydrocarbon engine. This higher compression ratio is important because it is related to the thermal efficiency of the system. On the other hand, hydrogen is difficult to ignite in a compression ignition (CI) or diesel configuration, because the temperatures needed for those types of ignition are relatively high (Gupta, 2009). Hence, it requires the use of external ignition source such as a pilot diesel fuel in dual fuel engines.

2.3.3 Low Ignition Energy

Hydrogen has a very low ignition energy requirement. This low ignition energy makes a hydrogen-fueled engine susceptible to pre-ignition (Hollinger & Bose, 2008). Hydrogen ignition energy compared to other gaseous fuels as shown in Figure 2.3 (White et al., 2006). The amount of energy needed to ignite hydrogen is about one order of magnitude less than that required for gasoline. This enables hydrogen engines to ignite lean mixtures and ensures prompt ignition. The minimum ignition energy of hydrogen stoichiometric mixture at atmospheric condition is about 0.02 mJ, which is about 10-fold less than that required for gasoline (0.24 mJ) (Gupta, 2009; McAllister et al., 2011; White et al., 2006). Unfortunately, the low ignition energy means that hot gases and hot spots on the cylinder can serve as sources of ignition, creating problems of premature ignition and flashback. In piloted ignition with spark plug, there is an optimal spacing of electrodes that results in a minimum energy required for ignition. The minimum ignition energy addresses the ignition of the combustible mixture only,

but does not guarantee that the combustion reaction will continue to propagate through the mixture (McAllister et al., 2011).

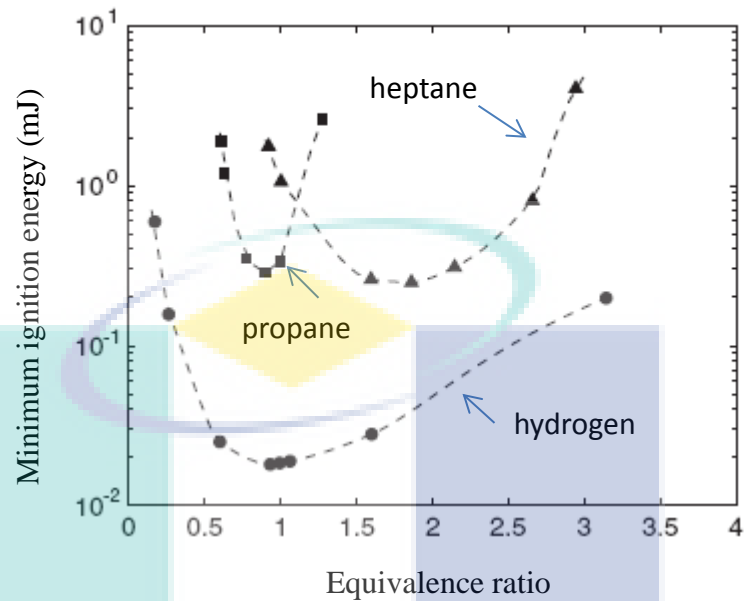


Figure 2.3. Minimum ignition energy in relation to equivalence rate at atmospheric pressure.

Source: (White et al., 2006)

2.3.4 Small Quenching Distance

The quenching gap (or quenching distance) describes the flame extinguishing properties of a fuel when used in an internal combustion engine. Specifically, the quenching gap relates to the distance from the cylinder wall that the flame extinguishes due to heat lost (Shudo, Nabetani, & Nakajima, 2001). The main physical effect lies in the balance between the heat generated by the combustion reaction and the heat lost to the adjacent material (McAllister et al., 2011). The quenching gap of hydrogen is approximately 3 times less than that of other gaseous fuels, such as natural gas as seen in Table 2.1. Consequently, hydrogen flames travel closer to the cylinder wall than other fuels before they extinguish. Thus, it is more difficult to quench a hydrogen flame than a gasoline flame. The smaller quenching distance can also increase the tendency for backfire since the flame from a hydrogen-air mixture more readily passes a nearly closed intake valve, than a hydrocarbon-air flame (Gupta, 2009).

2.3.5 Low Density

Hydrogen has very low density. This results in two problems when used in an internal combustion engine. Firstly, a very large volume is necessary to store enough hydrogen to give a vehicle an adequate driving range. Its storage is associated with either high pressures (thus requiring heavy vessels) or extremely low temperatures, and/or combination with other materials (Sebastian, Thomas, & Roger, 2014). Secondly, the energy density of a hydrogen-air mixture, and hence the power output, is reduced.

2.4 EXPERIMENTS ON DUAL FUEL ENGINE WITH DIESEL-HYDROGEN

2.4.1 Gaseous Fumigation

Hydrogen cannot be used directly in a diesel engine because its auto-ignition temperature is higher than that of diesel fuel. One alternative method is to use hydrogen in enrichment or induction. Hydrogen is mixed with air or injected in the intake manifold before entering combustion chamber. Small amount of diesel fuel, called pilot fuel, is injected to promote ignition. This dual fuel engine has the advantage to switch back to conventional diesel operation in case of shortfall in gas supply. These benefits lead researchers worldwide to investigate the utilization of gas including hydrogen as fuel for diesel engine.

Rao, Shrivastava, and Bhakta (1983) made an attempt to burn hydrogen in compression ignition engines that were operated on a dual fuel mode. Small proportions of hydrogen were introduced into the intake manifold, and ignition was initiated by injecting diesel fuel in the conventional manner. Such an operation resulted in an increase of thermal efficiency at full load, a reduction in exhaust temperature and an increase in maximum pressure. Nitrogen oxides in the exhaust were observed to increase, and the hydrocarbon emissions reduced as expected. Closed vessel explosions were conducted to study the effect of adding a hydrocarbon to a hydrogen-air mixture on the flame propagation velocities.

An experimental study was undertaken to investigate the combustion and emission of dual fuel engine by varying the injection timing over extremely wide range (Tomita, Kawahara, Piao, & Fujita, 2001). The injection timing can be changed over a wide range from 62.7 °CA BTDC to 3.2 °CA ATDC. It was shown that both smoke and NO_x are almost zero when the injection timing is extremely advanced about 40-50 °CA BTDC. In this situation, the diesel fuel is well mixed with air or hydrogen-air mixture and the initial combustion becomes mild. The reduction of NO_x emission was due to lean premixed combustion with the absence of the region of high temperature of burned gas. It was found that the ignition delay increased when hydrogen is inducted. The fumigation of a large amount of hydrogen reduced the intake air.

Kumar, Ramesh, and Nagalingam (2003) used a small quantities of hydrogen on unmodified diesel engine to improve the performance and emissions level. Results indicated an increase in the brake thermal efficiency at a certain percentage of hydrogen mass shared at maximum power output. Smoke, HC, and CO emissions were all reduced. However, NO level was increased due to high combustion rate at full load operation. Ignition delay, peak pressure and maximum rate of pressure rise were also increased in the dual fuel mode of operation. Combustion duration was reduced due to higher flame speed of hydrogen. Higher premixed combustion rate was observed with hydrogen induction. On the whole, it is concluded that induction of small quantities of hydrogen can significantly enhance the performance of a vegetable oil/diesel fuelled diesel engine.

The application of exhaust gas-assisted fuel reforming in CI engines has been studied by Tsolakis, Megaritis, and Wyszynski (2003). Experiments were conducted in a single-cylinder DI diesel engine fuelled by conventional diesel and also by a biodiesel mixture. The study consisted two parts. First, the effects of exhaust gas recirculation (EGR) and addition of small amounts of hydrogen on the combustion and exhaust emissions were investigated. The engine was run at constant load by reducing the amount of diesel fuel when hydrogen was introduced to maintain constant indicated mean effective pressure (IMEP). Thus, it involved fuel replacement by hydrogen rather than hydrogen addition. Second, the feasibility of producing hydrogen “on-board” by incorporating a laboratory reforming mini reactor in the engine exhaust system. Prototype catalysts and different reaction conditions were examined. The results from

the first part of the study showed that partial replacement of diesel fuel by hydrogen combined with EGR resulted in simultaneous reductions of smoke and nitrogen oxides emissions (NO_x) without significant changes to engine efficiency. In the second part of the study, it was shown that the amount of hydrogen required to achieve these beneficial effects potentially can be produced by exhaust gas-assisted reforming of the hydrocarbon fuel.

In the other study, it has been shown that the exhaust gas fuel reforming technique has the potential to provide a way of controlling diesel engine exhaust emissions (Tsolakis, Hernandez, Megaritis, & Crampton, 2005). The technology involves the incorporation of a reformer in the engine EGR loop. Fresh fuel was injected in the reactor, where it was reformed by catalytic reaction with exhaust gas. The produced hydrogen-rich gas was then fed back into the engine as reformed EGR (REGR). Thus, in this way, the engine in effect operates in dual fuel operation mode. In this study, the particulate emissions of the diesel-hydrogen fuelled engine were studied using an electrical low pressure impactor (ELPI). The work was performed by simulating the operation of an optimized engine-reformer system by feeding the engine with simulated reformat containing 24 % hydrogen. The particle size and mass distribution were not affected significantly, but the particle total number and mass were reduced considerably, compared to the standard diesel fuelling.

In another contribution of Tsolakis and Megaritis (2005), the exhaust gas fuel reformer was applied to assist the premixed charge compression ignition operation by substituting part of the main fuel with hydrogen-rich gas. The technique involves the injection of hydrocarbon fuel into a catalytic reformer fitted into the EGR system, so that the produced gas mixture is fed back to the engine as REGR. The application of REGR resulted in a higher premixed combustion rate and reduction of the diffusion combustion phase. It could be a potential technique in terms of achieving reduction of smoke and NO_x emissions.

Study on carburetted hydrogen in a single cylinder, naturally aspirated DI diesel engine was carried out by Pundir and Kumar (2007). Combustion events and smoke emissions were investigated. Inducting hydrogen with its energy share above 15 % resulted in a sharp decrease in ignition delay (ID), very high peak pressure rates,

increases in smoke and loss in fuel efficiency were observed. Hydrogen addition with energy share of about 30 % reduced the ignition delay and increased the peak rates of pressure rise. Smoke emissions at low hydrogen induction rates reduced slightly but increased sharply above 15 to 20 % hydrogen energy share. Hydrogen mixed with air appears to actively participate in pre-combustion reactions leading to decrease in ignition delay and its consequent effects on combustion pressure–time history, smoke emissions and efficiency.

Saravanan and Nagarajan (2008a) investigated the hydrogen as an air-enrichment medium with diesel as an ignition source in a stationary diesel engine system to improve engine performance and reduce emissions. The stationary diesel-hydrogen dual fuel engine can be operated with less fuel than neat diesel operations, resulting in lower smoke level and particulate emission. This H₂-enriched system enables the realization of higher brake thermal efficiency hence specific energy consumption (SEC). NO_x emissions were also reduced except at full load operation.

In their investigation, Saravanan, Nagarajan, Kalaiselvan, and Dhanasekaran (2008) adopted exhaust gas recirculation (EGR) technique in a hydrogen-enriched diesel engine. It was found that the brake thermal efficiency of dual fuel without EGR is higher than that of neat diesel operation. Using EGR slightly decreased the efficiency, but it was still better than that of the single diesel operation. Usage of hydrogen in dual fuel mode with EGR technique results in lowered smoke level, particulate and NO_x emissions. Dual fuel operation without EGR resulted in the lowest smoke and unburned HC. EGR reduced NO_x emission effectively due to lower combustion temperature.

The effects of load, speed, EGR level and hydrogen addition level on the emissions from a modern diesel engine equipped with common rail injection has been investigated by McWilliam, Megaritis, and Zhao (2008) . It was found that CO, FSN, and THC increase with EGR but NO_x emission decrease drastically. Inversely, CO, FSN, and THC emission decrease with hydrogen, but NO_x increases. This inverse relationship will allow the combination of EGR and hydrogen induction to be optimized to minimize both FSN and NO_x. When hydrogen was introduced the peak cylinder pressure was increased, as was the rate of cylinder pressure rise. The position of the peak cylinder pressure was delayed as hydrogen addition increased. This together with

the obtained heat release patterns shows an increase in ignition delay, and a higher proportion of premixed combustion.

The role and benefit of hydrogen in a modern common rail turbocharged automotive diesel engine has been reported by Lilik, Zhang, Herreros, Haworth, and Boehman (2010). Hydrogen substitution yields modest emission reductions with limited penalty on engine performance. Hydrogen assisted diesel combustion resulted in a modest increase of NO_x emissions and a shift in NO/NO_2 ratio in which NO emissions decreased and NO_2 emissions increased, with NO_2 becoming the dominant NO_x component in some combustion modes. The results showed that substitution of diesel fuel with hydrogen can be realized with little or no detrimental effect. Compared with stationary application, the practicality of vehicle utilizing hydrogen substitution is limited by the equipment cost versus the cost benefit from the modest emission reduction.

Investigation on the effects of hydrogen addition on NO_x emissions and thermal efficiency under low-temperature and heavy-EGR condition has been reported by Shin, Cho, Han, Song, and Chun (2011). The brake thermal efficiency slightly improved due to hydrogen addition. It showed the relation of the thermal efficiency with changes in the CO_2 concentration. The increase in CO_2 indicated that diesel combustion was improved by the oxidation of the unburned hydrocarbon and CO due to hydrogen addition. Lower NO_x was achieved by introducing hydrogen at constant EGR ratio.

The examination of detailed effect of hydrogen addition on NO_2 has been conducted by S. Liu et al. (2011). The addition of small amounts of hydrogen increased the emissions of NO_2 and the NO_2/NO_x ratio. It was shown that the engine load and mixture temperature were not the main factor for the formation of NO_2 . A more detailed analysis showed the significant effect of unburned- H_2 on NO_2 emissions. When mixed with the hot combustion product, unburned- H_2 might further oxidized to increase the HO_2 concentration and enhanced the conversion of NO to NO_2 according to extended Zeldovich mechanism.

2.4.2 Gaseous Fuel Injection

Another way to introduce hydrogen into the combustion chamber is by injecting the hydrogen into the intake port, while diesel fuel was injected directly inside the cylinder. It was shown that using port-injected hydrogen there was an increase in brake thermal efficiency of the engine with a greater reduction in emissions (Saravanan, Nagarajan, et al., 2007b). Any decrease of emission, especially NO_x is likely due to enhancement of turbulent mixing in cylinder caused by the injection of pressurized hydrogen through the intake valve (Lilik et al., 2010).

Study on the exhaust emission characteristics of a diesel engine with small amounts of hydrogen added to the intake air has been conducted (Miyamoto, Kobayashi, Mikami, & Kojima, 2008). The results showed that hydrogen has contribution to heat release even if its concentration was lower than the lower flammability limit (4 % volume). At medium or high loads operation, NO increased with hydrogen addition when the diesel-fuel injection timing was earlier than TDC. NO decreased with hydrogen addition when the diesel-fuel injection timing was later than TDC. CO_2 emission decreased with the increase in the hydrogen percentage, while smoke emission decreased for high loads.

The use of electronically controlled timed port hydrogen injection in combination with EGR system has been reported (Bose & Maji, 2009). Hydrogen induction results in lowered emission level except NO_x and improved performance level compared to the case of neat diesel operation. The increase of NO_x was due to higher temperature when hydrogen was induced. EGR technique was useful in reducing NO_x concentration. Other emission such as CO , CO_2 , and HC increased with EGR addition. The use of low EGR percentage was preferred.

Comparison study on hydrogen induction method has been reported (Saravanan, Nagarajan, & Narayanasamy, 2007, 2008). Hydrogen was inducted by means of carburetion and timed port injection (TPI). Different results between the two methods were revealed. The specific energy consumption, NO_x emission and the exhaust gas temperature increased by certain per cent, and brake thermal efficiency and smoke level slightly reduced using carburetion technique compared to baseline diesel. But in the

TPI, the specific energy consumption, exhaust gas temperature and smoke level reduced by certain amount. The brake thermal efficiency and NO_x increased compared to diesel operation. The emissions such as HC, CO and CO_2 are low in both the techniques as compared to diesel. The reason for better performance given by TPI technique was not clearly described, but it may be due to the absence of gas “short circuiting” during the valve overlap.

In their other contribution, optimization of injection timing and injection duration to achieve dual fuel performance and emissions was conducted (Saravanan, Nagarajan, Dhanasekaran, & Kalaiselvan, 2007a). The diesel injection timing was kept constant at 23 °CA Before Ignition Top Dead Centre (BITDC). The optimized timing and duration for hydrogen injection was 5 °CA After Gas Exchange Top Dead Centre and 90 °CA respectively. Simultaneous reduction of smoke and NO_x was achieved in this optimized operating condition. The emissions of CO, CO_2 , and HC were reduced due to efficient combustion resulting from the hydrogen combustion. More variation in hydrogen injection timings investigated in their similar study (Saravanan & Nagarajan, 2008b, 2010). The results were similar except for NO_x emission, in which no NO_x reduction compared with that of diesel operation.

Although research on hydrogen combustion in internal combustion engine has intensified, the number of published papers in the field of hydrogen-diesel co-combustion is not as rich as for hydrogen used in spark ignited engines (Szwaja & Grab-Rogalinski, 2009). In this contribution, various hydrogen portions in the range from 0 % to 17 % with respect to energy sharing were investigated. Combustion knock occurrence was studied at the stoichiometric condition with hydrogen of 17 % sharing. It was shown that small amounts of hydrogen shortened the diesel ignition delay and decreased the rate of pressure rise.

Hydrogen addition to the intake air at late diesel fuel injection has been investigated (Miyamoto et al., 2011). Diesel injection timing and the hydrogen percentage were varied while maintaining the heat produced by diesel fuel and hydrogen. The NO emission was at minimum value at certain hydrogen fraction. EGR was applied to reduce further NO and smoke emissions. Low NO, low cyclic variation,

and smokeless operation were realized at the optimized values of diesel injection timing, fraction of hydrogen, and EGR rate.

Effect of hydrogen addition on engine performance and emissions has been reported (Deb et al., 2015). Hydrogen energy sharing was controlled via the injection timing and duration. The experiment was conducted at constant speed and load. The test results showed the improvement in brake thermal efficiency of the engine, reduction in brake specific energy consumption with an increasing hydrogen energy sharing. Furthermore, indicated specific CO, CO₂ and smoke emissions decrease with an increasing percentage of hydrogen energy content. Conversely, indicated specific NOx emissions increases with increase in hydrogen content. In addition to that, it was also observed that there was a sharp increase in peak in-cylinder pressure and the peak heat release rate values with the increasing hydrogen rate

2.4.3 Cyclic Variation

It is obvious that cycle-by-cycle variation occurred in spark ignition internal combustion engine. Cyclic variations in the combustion process are caused by variations of mixture motion within the cylinder, variations in the amounts of air and fuel fed to the cylinder each cycle, and variations in the mixing of fresh mixture and residual gases within the cylinder each cycle (Heywood, 1988). In contrast to spark ignition engines, the combustion process of compression ignition engine is regarded as being stable. However, more detailed investigations on combustion process reveal cyclic variability in diesel engine fuelled with pure diesel or diesel/biodiesel blending (Barboza, Yagnesh Sharma, & Sudhir, 2010; Bizon, Continillo, Leistner, Mancaruso, & Vaglieco, 2009; Sen, Longwic, Litak, & Górski, 2008; Tang, Ge, Duan, & Zhang, 2011).

There have been many studies concerning cycle-by-cycle variation and combustion stability of spark ignition engines fuelled with gaseous fuels, either single gas or blended gas (Huang et al., 2009; Ma et al., 2008; Wang, Chen, Liu, & Huang, 2008). The characteristics of mixture formation, ignition, and combustion process of the fuel-air mixture that greatly influences the cycle variation are well understood. However, in the dual fuel engine in which the diesel fuel ignites the hydrogen-air

mixture, the ignition characteristics of the gaseous fuel are not well understood. In addition to the cause of cyclic variations exist in diesel engine, dual fuel engines appear to be more prone to cyclic variability in combustion noise due to existence of gaseous fuel with compressed air (Selim, 2004). Therefore, it was considered necessary to study the cycle variation of the diesel-hydrogen dual fuel engine that was not covered before. The purpose is to investigate the effect of hydrogen addition and engine operating condition on cycle variation of the dual fuel engine.

2.5 DUAL FUEL MODELLING

To meet more stringent legislation, continuous improvements of internal combustion engines are needed. This complex task can be achieved by a combination of advanced experiments and computational studies. The modelling of combustion engine processes has some significant advantages as a complement to the experimental works. It is obvious that numerical simulations are suited to carry out extensive parametric studies that are more effective than construction of numerous prototypes (Stiesch, 2010).

Different types of engine combustion model have been developed. Three different model categories are typically distinguished. In an order of increasing complexity and increasing computer power, these are zero-dimensional thermodynamic models, quasi-dimensional phenomenological models, and multi-dimensional computational fluid dynamic (CFD) models (Lakshminarayanan & Aghav, 2010).

2.5.1 Thermodynamics Modelling

An attempt to model dual fuel combustion and NO_x using single-zone thermodynamic model coupled with detailed chemical kinetics has been conducted (Mansour, Bounif, Aris, & Gaillard, 2001). The estimation of ignition delay of diesel fuel was calculated by CHEMKIN code. The reaction of diesel fuel was taken from the quasi-global model with four step reactions. Detailed chemical kinetic reaction mechanism of NO_x consist of 79 reactions were applied. A reasonably good agreement with experimental results was achieved.

Computer simulation of hydrogen-diesel dual fuel has been developed to investigate the effect of hydrogen addition on exhaust gas emission (Masood & Ishrat, 2008). For the calculation of equilibrium constant, the data for constants was considered from JANAF tables. The molar-air fuel ratio was calculated from the number of carbon, hydrogen, nitrogen, and oxygen atoms presented in the fuel. The proportion of hydrogen in the hydrogen-diesel blend affecting the mole fraction of the exhaust gas species was also simulated. The simulation results were in good agreement with the experimental values.

2.5.2 Phenomenological Modelling

A quasi-two-zone analytical model was developed to investigate the effects of admission of hydrogen and its blend with methane on dual fuel engine (Liu & Karim, 1995). One of the problems associated with dual fuel conversion was the limitation of the maximum power output due to knock. Hydrogen or its blend with other gaseous fuel showed a notable different characteristic compared with other gaseous fuels. The reactivity of hydrogen in the engine tends to be low, but it is enhanced with the increase of hydrogen concentration in the cylinder.

Another contribution by Liu and Karim (1997) described a multizone model with detailed chemical kinetics to simulate the combustion process of dual fuel engines. The model consists of five zones as shown in Figure 2.4. The developed model can provide a description of the main features of the combustion process in dual-fuel engines. The performance of dual-fuel engines, such as the formation of exhaust emissions at light load and the onset of knock at high load, can be predicted by this model. The predicted values show good agreement with corresponding experimental values.

Another multi-zone model with detailed chemical kinetics was proposed by Pirouzpanah and Saray (2006). In this model, a quasi-dimensional multi-zone model was applied for combustion of diesel fuel. The combustion of natural gas was model with single zone couple with detailed chemical kinetics. It was assumed that the interaction between the two types of fuels to be primary thermal with no direct chemical

interaction between them. The predicted results showed good agreement with corresponding experimental values over the whole range of engine operating conditions

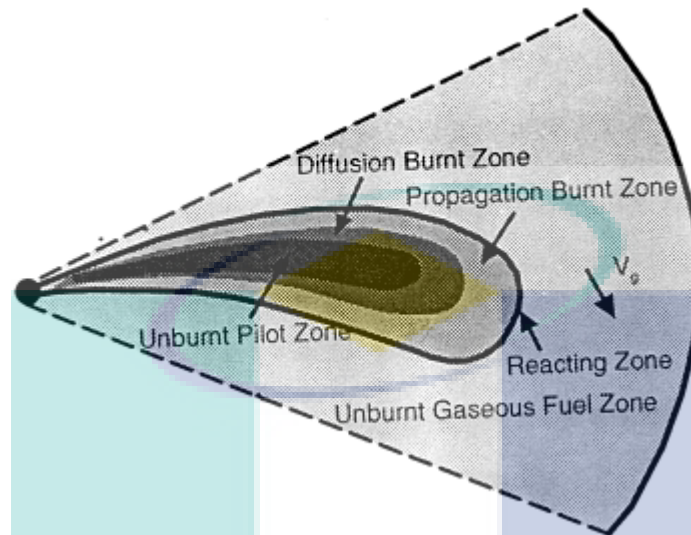


Figure 2.4. A schematic zone division during combustion process.

Source: (Liu & Karim, 1997)

Investigation by Papagiannakis, Hountalas, and Rakopoulos (2007) showed that the pilot diesel fuel quantity and injection advance influence significantly the combustion mechanism. In order to examine the effect of these two parameters on the performance and emissions, a comprehensive two-zone phenomenological model is employed and applied on a high-speed, pilot ignited, natural gas diesel engine. The model is shown in Figure 2.5. In this model, the cylinder charge during the compression phase is treated as a single zone (unburned zone), with assumed uniformity in space of pressure, temperature and composition. According to the results, the simultaneous increase of the pilot fuel quantity accompanied with an increase of its injection timing results to an improvement of the engine efficiency (increase) and of the emitted CO emissions (decrease) while it has a negative effect (increase) of NO emissions.

The mathematical models to predict combustion and performance for dual fuel diesel engine operated on hydrogen and its blend with LPG have been developed (Lata & Misra, 2010). In these models, spray mixing characteristics, flame propagation, equilibrium combustion products and in-cylinder processes were computed using empirical equations. To validate the models, experiments were conducted on a multi

cylinder turbocharged, intercooled gen-set diesel engine. The developed model predicts results which are in close agreement with the results of the experiments. The predictions are also in close agreement with the results on single cylinder diesel engine obtained by other researchers. A reasonable agreement between the predicted and experimental results reveals that the presented model gives quantitatively and qualitatively realistic prediction of in-cylinder processes and engine performances during combustion

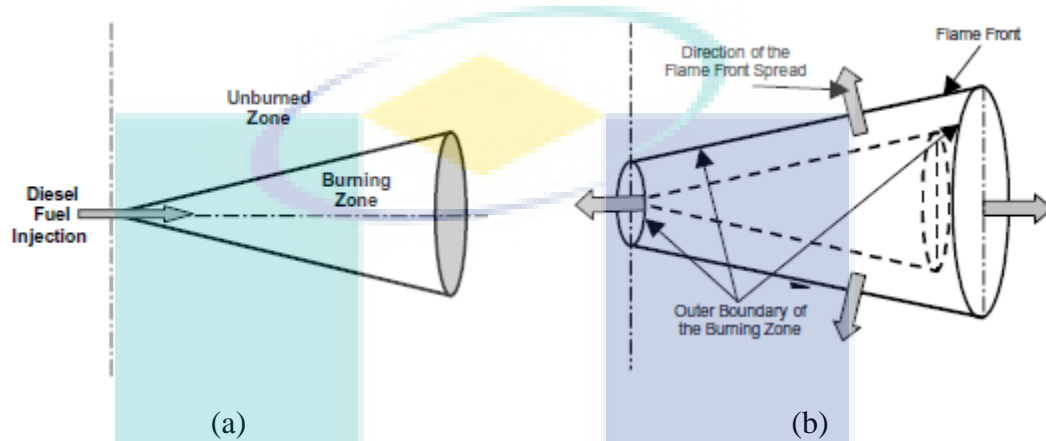


Figure 2.5. Definition of the burning zone before (a) and after (b) the initiation of combustion

Source: (Papagiannakis et al., 2007)

2.5.3 Multi-dimensional Modelling

A three-dimensional (3D) finite volume code has been developed to describe a constant volume, dual fuel diesel/methane combustion (Miao & Milton, 2002). Compared with their previous model (Choi & Milton, 1997), the distillate spray model, the spray parcel collision mechanism, and the characteristics for distillate combustion have been improved. An improved scheme for the multi-fuel (DF) combustion has also been implemented. The focus of the author's work was simulation factors of importance in engines such as the effect of swirl, the duration of the ignition delay, and the gaseous fuel characteristics on the DF combustion process.

In their other study, a three-dimensional, dual-fuel, in-cylinder model has been developed (Miao & Milton, 2005). This model was used to provide an improved understanding about the interaction between the gaseous fuel and the pilot fuel, the pre-

ignition processes, and subsequent combustion of the pilot fuel and gas during the piston movement. The complex engine in-cylinder process was simplified by the assumption that during each very short period (for example 0.05 ms), the control-volume working substance first undergoes an instantaneous isentropic compression or expansion process, where no heat and mass transfer can occur. The next process was a constant-volume, dual-fuel combustion process over a finite time period, with heat and mass transfer between the cells. The effects of liquid fuel injection and air movement (such as swirl) were considered during the combustion process. Based on this assumption, it was then possible to extend the existing constant-volume simulation to an engine combustion process. This assumption may produce small error, but its simplicity provided a rapidly calculated approach.

The effect of blending hydrogen with diesel in different proportions on combustion and emissions has been studied using a CFD code (Masood et al., 2007). Two injection methods for hydrogen introduction were compared: (1) directly injected the hydrogen into the combustion chamber, and (2) the induction of hydrogen through the inlet manifold. Percentage of hydrogen substitution was varied during the simulation. A modification of the turbulent mixing model constant was introduced to take into the account the hydrogen presence. The standard combustion and emission models were used for the analysis. The simulation results have a good agreement with the experimental ones. However, there exist many areas, which are unaddressed by the model. At low and high percentages of hydrogen and during transition between diesel and hydrogen, the model predictions are not very clear; this eventually shows the limitation of the model and opens the doors for further investigation.

A 3D computational fluid dynamics model with a reduced detailed chemical kinetic of the combustion of diesel and methane fuels was developed by Liu and Karim (2009). The model was applied to an indirect injection diesel engine. The turbulence during combustion was considered to simulate the mixture flow, formation, and combustion processes within diesel and diesel/methane dual fuel engines. The spatial and temporal distributions of the mixture temperature, pressure, and velocity under conditions with and without liquid fuel injection and combustion were validated with a set of experimental results. Investigation on the flow field under motoring condition found that the swirl centre is initially formed at the bottom-left of the swirl

chamber, and then moved up with continued compression in the top-right direction toward the highest point. The swirling motion within the swirl and main combustion chambers promotes the evaporation of the liquid pilot and the combustion processes of diesel and dual fuel engines. It was observed that the onset of auto-ignition can be adjusted by the injection strategy.

Effect of hydrogen addition on NO_x emissions in hydrogen diesel dual fuel has been explored using computational fluid dynamics analysis (Lilik et al., 2010; Zhang, Lilik, Boehman, & Haworth, 2009). It was shown by the experiment that engine-out NO tends to decrease while NO_2 increases with increasing level of H_2 addition. The CFD calculation using probability density function (PDF) for turbulence-chemistry interaction can capture these trends and reproduce the experimental results. The CFD results confirmed that temperature changes alone are not sufficient to explain the observed reduction in NO and increase in NO_2 with increasing H_2 . The CFD results are consistent with the hypothesis that in-cylinder HO_2 levels increase with increasing hydrogen, and that the increase in HO_2 enhances the conversion of NO to NO_2 .

Numerical study of the combustion and emissions of hydrogen diesel dual fuel using KIVA CFD code coupled with CHEMKIN has been reported (An et al., 2013). The model incorporated a detailed chemical kinetic of Diesel Surrogate Oil (DSO) and hydrogen. Simulation results showed that at low engine speeds, the indicated thermal efficiency, in-cylinder pressure and apparent heat release rate increased significantly with the increase of hydrogen percentage. On the other hand, at high engine speed and high load conditions, no significant changes in the engine performance, combustion characteristics were observed. In terms of emissions, CO and soot emissions were shown to be reduced under most of the engine operating conditions. In case of NO_x emissions, a slight increase was observed at low engine speed.

A comprehensive model for identifying knocking combustion has been developed (Maghbouli et al., 2014). Some critical local regions within the CFD computational domain were defined to identify the knock occurrence. Regional parameters such as local pressure rise rate, local heat release rate and local concentration change of specific chemical species were used for knock identification. Noticeable knocking combustion was detected by applying of hydrogen higher than 5 %

(by volume) in the intake charge of a compression ignition diesel engine. Regional parameters and chemical species concentration data showed that in such an operating condition, knock is occurring at start of combustion rather than end-gas auto-ignition of SI (spark ignition) engines

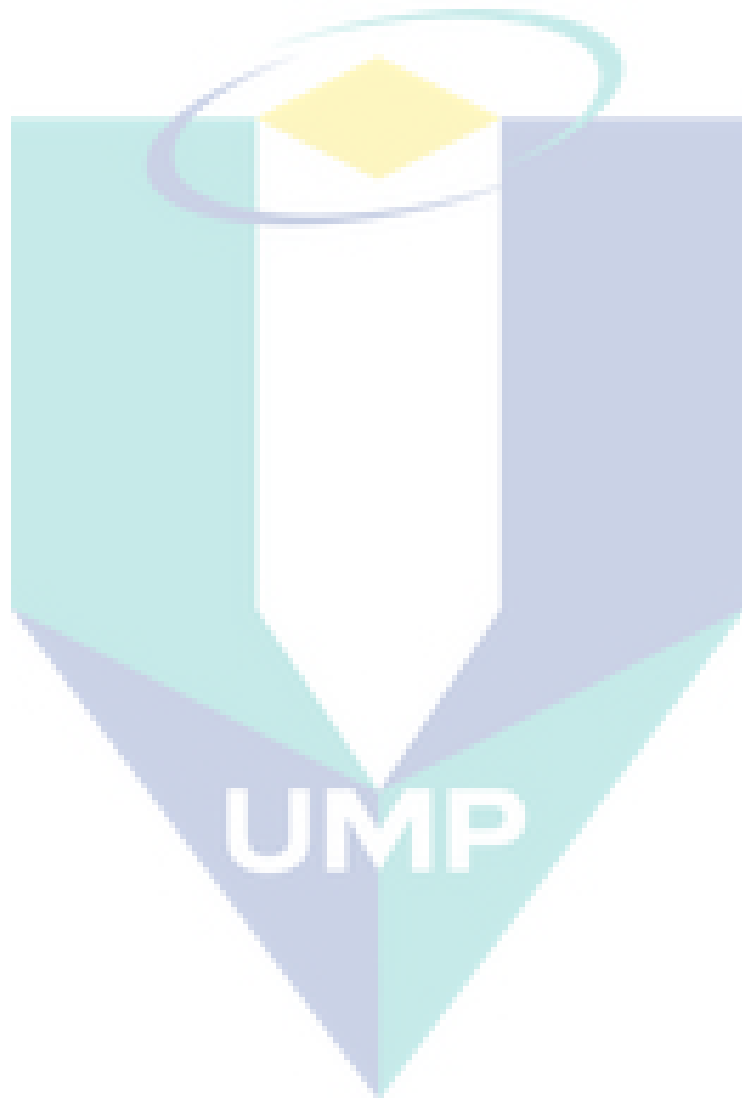
2.6 SUMMARY

This literature review has revealed the properties of hydrogen and the progress in the utilization of hydrogen as fuel for diesel engine in dual fuel mode. The apparent significant progress in the dual fuel research, both experimental works and simulation studies, has been achieved. There are still many areas that need further study due to the complexity of dual fuel combustion. The information on the combustion characteristics of dual fuel engine when hydrogen acts as the main fuel is still limited. An extensive review showed that most research was dealt with hydrogen as a fuel supplement/additive.

In general, there is an apparent lack of the study on the cyclic variability of dual fuel combustion. The characteristics of mixture formation, ignition, and combustion process of the fuel-air mixture that greatly influences the cycle variation in spark ignited engine are well understood. However, in the dual fuel engine in which the diesel fuel ignites the hydrogen-air mixture, the ignition characteristics of the gaseous fuel are not well understood.

Mixture formation plays an important role in the combustion process. The simulation study on the diesel spray interaction with hydrogen-air mixture inside the cylinder would be a good contribution to reveal the mixture formation of dual fuel engine. Some simulation results on combustion process have a good agreement with the experimental ones. However, there exist many areas, which are unaddressed by the model. At certain percentages of hydrogen, the model predictions are not very clear. This eventually shows the limitation of the model and opens the doors for further investigation. Combustion analysis using CFD tools combined with detailed chemical kinetics would give a better understanding of dual fuel combustion.

To fill these gaps, some experimental and simulation works will be conducted to identify the important parameters related to mixture formation and combustion characteristics of diesel hydrogen dual fuel engine. The experimental equipment and methods as well as the development of simulation models will be described and discussed in Chapter 3.



CHAPTER 3

EXPERIMENTAL DETAIL AND COMPUTATIONAL MODELLING

3.1 INTRODUCTION

In the previous chapter, a literature review on the background and history of diesel and dual fuel engine, the previous experiment, and the dual-fuel modelling has been discussed. The research gaps and their specific problems that will be solved have been outlined. This chapter provides the information on the engine experimental details and computational modelling that will be used to investigate the important parameters of dual fuel combustion. Detail of engine and test bed instrumentation, combustion analysis, and emission measurement are explained. Computational setup and governing equation are outlined.

3.2 EXPERIMENTAL DETAILS

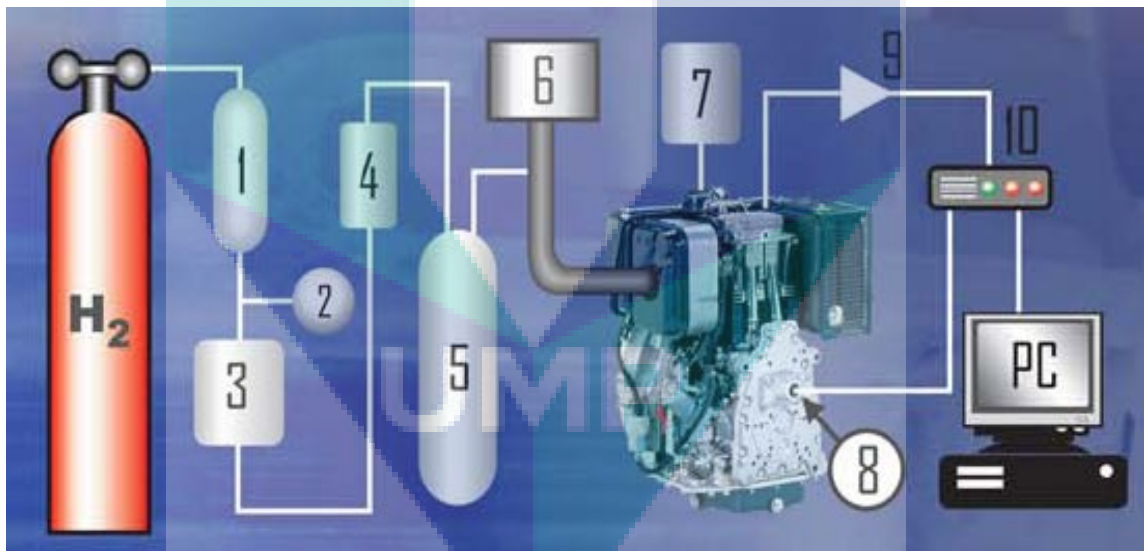
3.2.1 Experimental Setup

A single cylinder, air-cooled, direct injection (DI), 4-stroke HATZ D-series diesel engine was used in this study. This engine was equipped with a cylinder pressure transducer and crank angle sensor to investigate the combustion process. The main specifications of the engine are summarized in Table 3.1. The engine has 100 mm bore and 85 mm stroke yielding a displacement volume of 667 cc. The layout of engine and experimental arrangement are shown in Figure 3.1.

There are minor modifications applied to the engine in order to run in dual fuel mode. Hydrogen addition was realized by introducing the gas into the mixer in the intake manifold. The original diesel fuel injection system was used to control the flow rate of the diesel fuel.

Table 3.1
Engine Specification

Parameters	Description
Engine Type	Single cylinder air-cooled DI diesel engine
Rated power	10.3 kW @ 3000 rpm
Maximum torque	36 Nm @ 2000 rpm
Bore	100 mm
Stroke	85 mm
Conrod length	136.5 mm
Swept volume	0.667 liter
Compression ratio	20.5:1



- | | | |
|---------------------------|----------------------------|------------------------------|
| 1. Hydrogen surge tank | 5. Flame trap | 9. Signal conditioning |
| 2. Barometer | 6. Hot film air flow meter | 10. Engine indicating system |
| 3. Digital gas flow meter | 7. Gravimetric fuel meter | 11. PC |
| 4. Flash back arrestor | 8. Crank angle encoder | |

Figure 3.1. Schematic of experimental setup.

3.2.2 Dynamometer

In order to control the speed and load put on the engine, the engine was mounted on a SCHENCK W70 eddy-current dynamometer. The maximum capacity of the dynamometer is 150 Nm torque, 70 kW power, and 13 000 rpm speed. The engine was connected to the dynamometer by a flexible rubber coupling to isolate the dynamometer from any high frequency vibrations from the engine.

The dynamometer consists of a thin electrically conductive toothed disc mounted on a shaft. The disc rotates inside a magnetic field generated by a coil located on the casing of the dynamometer. The rotation normal to the magnetic field creates a resistive torque. To control the load applied to the engine, which is equivalent to the torque applied to the coupling shaft, the magnetic field can either be increased or decreased by adjusting the current from the dynamometer control panel. Water cooling was used to control the temperature generated within the dynamometer. The arrangement of engine and the dynamometer is shown in Figure 3.2

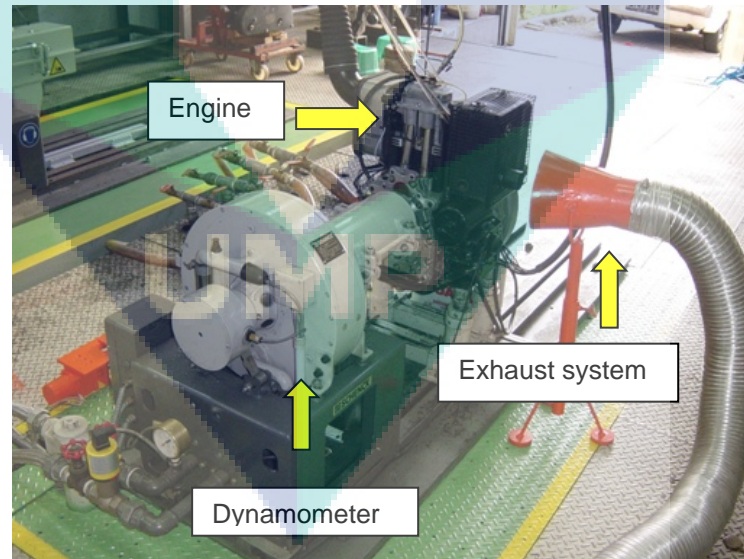


Figure 3.2. Arrangement of engine and dynamometer.

The engine load was measured by a load cell connected to the casing of the dynamometer. This load cell together with a speed sensor was used to accurately measure the speed and torque generated by the dynamometer. In order to remove any

interference generated by the engine vibration, the signal was low pass filtered. The load cell was calibrated by attaching calibration levers and calibrated weighing scales.

There are two main modes of engine control with this model of dynamometer: constant speed and constant torque. In the constant speed mode, the dynamometer maintains a constant rotational speed of the connecting shaft by increasing or decreasing the resistive torque as necessary depending on the force produced by the engine. The torque of the engine in this mode is therefore controlled by the level of fuelling. Similarly, in the constant torque mode, the dynamometer maintains a constant resistive torque, allowing the shaft, and therefore engine speed rise and fall depending on the fuelling level.

3.2.3 Pressure Transducer

A piezoelectric, water cooled pressure transducer as shown in Figure 3.3 was used to measure the in-cylinder pressure. It was mounted in the cylinder head and flushed into the combustion chamber. A Kistler type 6061B was used in this experiment. This transducer shows excellent thermal drift stability due to water cooling.



Figure 3.3. Kistler 6061B water cooled pressure transducer.

A piezoelectric pressure transducer contains a quartz crystal. The crystal is exposed to cylinder pressure through a diaphragm at one end. It produces an electrical charge proportional to the pressure exerted on the crystal when it is compressed. The signal was passed through a charge amplifier to boost it, and together with the crank angle signal provided from the shaft encoder, was used to log the change in cylinder pressure versus crank angle using a PC-based engine indicating system. The sensor was

regularly calibrated by an accredited laboratory. A stepwise calibration was conducted using a deadweight calibrator.

3.2.4 Crank Angle Encoder

In order to measure in-cylinder pressures at known crank angle positions, it is necessary to know the position of Top Dead Centre (TDC) and measure the rotation of the crank shaft. For that purpose, an optical crank angle encoder was mounted on the centre of the flywheel. The encoder consists of a slot mark disk and utilizes the reflection light principle. It is the most commonly used system in engine indicating technology due to the high precision in extreme operating conditions.

The angle mark resolution is 1 degree crank angle (up to 0.1 deg. CA by multiplication). The electronic components are mounted separately from the sensor (crank shaft) to minimize the influence of electric interference, temperature and vibration. There is one track on the marker disk with 360 pulses for the angle information which includes trigger pulse information per revolution for TDC synchronization purposes. The trigger pulse and the corresponding crank degree pulses were used together with the data-acquisition system to log the pressure traces from the cylinder. To correctly calibrate the position of TDC, the engine was run in motoring condition. TDC was found by counting the different between the peak cylinder pressure during motoring, and the trigger pulse generated by the disk marker. The complete shaft encoder fitted to the engine is shown in Figure 3.4.

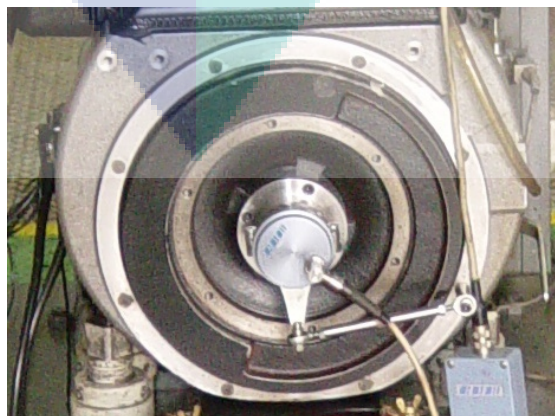


Figure 3.4. Arrangement of crank angle encoder.

3.2.5 Dynamometer Control and Engine Indicating System

The operation of the dynamometer, including testing mode setting, applied load and speed were conducted in the control room as shown in Figure 3.5. Other parameters, including engine speed and torque, fuel and air consumption, room and engine temperatures, exhaust gas emissions were monitored in this room. An engine indicating system, which recorded the cylinder pressure every degree crank angle was also located in this control room.



Figure 3.5. Instruments in the control room.

3.2.6 Air Intake and Fuel Supply System

Air flow rate is measured with a hot-film anemometer. To ensure the continuous air flow, a surge tank was installed at the upstream side of the engine. The actual temperature and relative humidity of intake air are measured to calculate its standard flow rate.

Hydrogen was introduced to the intake manifold by a mixer before entering the combustion chamber. It was supplied from a high-pressure cylinder (150 bar) and reduced to a pressure of 1.5 bar using a pressure regulator. Hydrogen was passed through a fine control valve to adjust the flow rate, and then a gas flow meter (Aalborg Gas Flow Meter) metered the flow of hydrogen. The hydrogen was passed through a flash back arrestor (WITT flame arrestor RF-53N) preventing a reverse flow of hydrogen into the system. Next, the hydrogen was allowed to pass through a flame trap, used to suppress flash-back into the intake manifold.

Diesel fuel was supplied with the original engine fuel system. There is no modification on diesel fuel supply. The mass flow rate of the diesel fuel was measured with an AVL 733S fuel balance. This fuel balance is based on the principle of gravimetric measurement. The amount of fuel consumption is determined directly by measuring the time-related weight decrease of the measuring vessel by a capacitive sensor.

The flow measuring units were calibrated by accredited laboratory. The indicated flow rates were compared to the traceable standard flow meters. The calibration processes were conducted under standard pressure and temperature condition.

3.2.7 Exhaust Emission Analysis System

The exhaust system was composed of two subsystems: exhaust ventilating and exhaust emission analysis. The tail pipe was simply inserted into a bell-mouth through which cell air is drawn (Martyr & Plint, 2007). The schematic of the system is shown in Figure 3.6. The emission measurement of exhaust was achieved through three main emission instruments.

Smoke intensity was measured with a Bosch-type smoke meter. Nitrogen oxides were measured with HORIBA 720 Diesel-NO_x meter. It has been engineered with a zirconia-ceramic sensor. This single unit provides fast-response measurements of NO_x concentrations from diesel or lean-burn engines and can simultaneously measure the

air/fuel ratio (A/F), excess air ratio (λ), and O_2 . The sensor can be directly inserted into the exhaust flow, eliminating the need for a sample-handling unit. This feature minimizes measurement time delays due to dead-volume sampling.

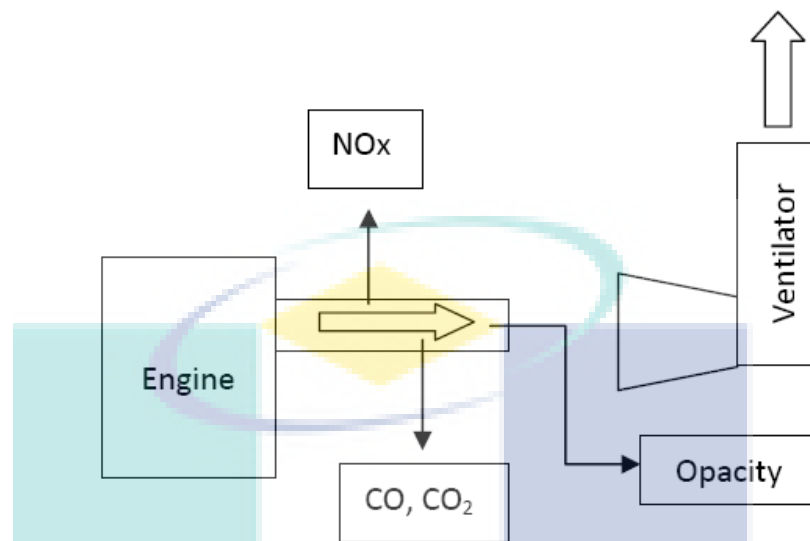


Figure 3.6. Schematic of the exhaust system.

An automotive gas analyser was used to measure carbon dioxide, carbon monoxide, and oxygen content in the exhaust gas. This analyser employs non-dispersive infra-red (NDIR) measurement technique. Exhaust gas analyser was calibrated with a certified gas standard.

3.2.8 Experimental Uncertainty

The uncertainty of measurement can be defined as "a parameter associated with the result of a measurement that characterizes the dispersion of the values that could reasonably be attributed to the measurand" (ISO, 1993). This parameter is usually a standard deviation or the width of a confidence interval. The evaluation of measurement uncertainty was conducted according to *Guide to the expression of uncertainty in measurement* (JCGM, 2008). In general, components of uncertainty may be categorized according to the method used to evaluate them. Experimental uncertainties that can be revealed by repeating measurements are called random uncertainty or Type A component of uncertainty. Systematic or Type B components of uncertainty are associated with errors that remain constant while a sample of measurements is taken.

Statistical methods can give reliable estimates of Type A uncertainties through analysis of a series of observations. In this case, the arithmetic mean or average of the results was calculated. For n repeated independent values x_1, x_2, \dots, x_n for quantity x , the mean value \bar{x} is given by:

$$\bar{x} = \frac{1}{n} \sum_{j=1}^n x_j \quad (3.1)$$

Standard deviation of a single sample of n measurements, termed the experimental standard deviation, $s(x)$ is given by:

$$s(x) = \sqrt{\frac{1}{n-1} \sum_{j=1}^n (x_j - \bar{x})^2} \quad (3.2)$$

If more samples are obtained, each will have a different value for the arithmetic mean and standard deviation. It follows from the central limit theorem that for large n , the sample mean approaches the normal distribution with the population mean. If samples of n measurements are taken after the estimation of the standard deviation of the population s , the standard deviation of the sample mean \bar{x} is given by:

$$s(\bar{x}) = s(x)/\sqrt{n} \quad (3.3)$$

which is also called standard uncertainty, u .

Type B components of uncertainty are usually determined on scientific judgment using all the available information. The pool of information may include manufacturer's specification, data provided in calibration reports, uncertainties assigned to reference data taken from handbooks, and knowledge of measurement process. While the normal distribution is used to describe random uncertainties, rectangular and triangular distributions are usually assumed for systematic uncertainties. If the upper and lower limits of an error are $\pm a$ without a confidence level and there is reason to

expect that all values within these bounds are equally probable, the rectangular distribution is considered to be the most appropriate. In case that extreme values are expected to be unlikely, the triangular distribution is usually assumed (Bean, 2001). The standard uncertainty values are equal to $\frac{a}{\sqrt{3}}$ for rectangular and $\frac{a}{\sqrt{6}}$ for the triangular distribution respectively.

All random or systematic sources of uncertainty associated with a measurement have to be quantified and then combined all together for the calculation of total uncertainty. Before combination all uncertainty contributions have to be expressed as standard uncertainties, which may involve conversion to the standard deviation from some other measure of dispersion (JCGM, 2008). Once the uncertainty components have been identified, estimated and expressed as standard deviations, the next stage involves calculation of the combined standard uncertainty $u_c(y)$. The relationship between $u_c(y)$ of a value y and the uncertainty of the independent parameters x_1, x_2, \dots, x_n is given by:

$$u_c(y) = \sqrt{\sum_{i=1}^n c_i^2 u(x_i)^2} \quad (3.4)$$

where c_i is a sensitivity coefficient calculated as $c_i = \partial y / \partial x_i$, the partial derivative of y with respect to each of standard uncertainty component x_i .

Usually a statement of confidence associated with a calculated total uncertainty is required. The combined standard uncertainty is in the form of one standard deviation and therefore may not provide sufficient confidence. For this reason the expanded uncertainty U is calculated by multiplying the standard uncertainty by a coverage factor k as follows:

$$U = k u_c(y) \quad (3.5)$$

Expanded uncertainties provide intervals that encompass a larger fraction of the measurand value distribution, compared to that of the combined uncertainty. The result

of a measurement is then reported in the form $\pm U$ along with the confidence level, which depends on the coverage factor. According to the requirements of dominant accreditation bodies, the expanded uncertainty should provide an interval with a level of confidence close to 95 % (ISO, 2005)

There are cases that combined standard uncertainty is dominated by single contribution with fewer than six degrees of freedom. It is probable that the probability distribution will not be normal and the value of coverage factor k will result in a confidence level that is smaller than the expected one. In this case, the value of coverage factor has to be derived by considering the effective degrees of freedom v_{eff} of the combined standard uncertainty. These can be evaluated using Eq. (3.6).

$$v_{eff} = \frac{u^4(y)}{\sum_{j=1}^n \frac{c_j^4 u_j^4(y)}{v_j}} \quad (3.6)$$

The effective degrees of freedom are based on the degrees of freedom v_j , which are equal to the number of measurement taken n , less 1. The coverage factor is then determined based on a t-distribution rather than a normal distribution. The results of uncertainty calculation are listed in Table 3.2.

Table 3.2
List of Measured Parameters and Their Related Uncertainties

Parameter	Measuring range	Accuracy	Uncertainty
CO	0 ... 10 % vol	± 0.03 % vol	± 0.12 % vol
CO ₂	0 ... 20 % vol	± 0.5 % vol	± 0.12 % vol
O ₂	0 ... 25 vol %	± 0.5 % vol	± 0.12 % vol
NO _x	0 ... 3000ppm	± 30 ppm	± 17 ppm
Air flow	0 ... 400 kg/h	± 0.3 kg/h	± 0.18 kg/h
Fuel flow	0 ... 125 kg/h	± 0.12 % of reading	± 0.18 % of reading
H ₂ flow	0 ... 80 l/min	± 0.8 l/min	± 0.5 l/min
Dyno speed	0 ... 13,000 rpm	± 1 rpm	± 1 rpm
Dyno load	0 ... 150 Nm	± 0.2 % of reading	± 0.1 Nm
Crank angle	1 ... 20,000 rpm	± 0.02 rpm	± 0.3 rpm
Cylinder pressure	0 ... 250 bar	± 1 % of FS	± 1.61 bar

3.2.9 Experimental Procedure

The experiment was conducted at speed of 1500, 2000, and 2500 rpm; variable loads of 5, 10, 15, 20, and 25 Nm were applied for each speed. At each load, the hydrogen was introduced at the flow rate of 21.4, 28.5, 36.2, 42.8, and 49.6 litre/minute. The experimental matrix is depicted in Table 3.3. The engine was started with diesel fuel at 1500 rpm and 5 Nm load. After allowing the engine to reach the steady-state conditions, the following parameters were measured and recorded: fuel and air consumption, exhaust gas temperature, exhaust emissions, needle lift, and cylinder pressure. Hydrogen was introduced at the flow rate of 21.4 litre/minute; engine speed was kept constant by adjusting the position of the injection pump lever. The above parameters were measured and recorded again. This procedure was repeated for different loads and hydrogen flow rates. After completing the measurement at this speed, the engine was shut down for a cooling purpose. Other sets of experiment were then conducted for the speed of 2000 and 2500 rpm with the same procedure.

Table 3.3
Experimental Matrix

Parameters	Value
Engine speed	1500, 2000, 2500 rpm
Engine load	5, 10, 15, 20, 25 Nm
Hydrogen flow rate	21.4, 28.5, 36.2, 42.8, 49.6 litre/minute

3.2.10 Parameters of Engine Performance

The engine performance tests were carried out in accordance with the SAE standard for measuring diesel engines' performance and emissions. The following are some of main parameters to be calculated for analysing engine performance. The stoichiometric air/fuel mass ratios for the hydrogen and diesel fuel are 34.33 and 14.5 respectively. Therefore for diesel-hydrogen dual fuel engine operation the total equivalence ratio is given as in Eq. (3.7):

$$\phi_{tot} = \frac{34.33\dot{m}_{H_2} + 14.5\dot{m}_{diesel}}{\dot{m}_{air}} \quad (3.7)$$

where ϕ_{tot} is the total equivalence ratio, and \dot{m}_{H_2} , \dot{m}_{diesel} , and \dot{m}_{air} are the mass flow rates in kg/h of hydrogen, diesel, and air, respectively.

Eq. (3.8) and (3.9) show the equivalence ratio of hydrogen and diesel respectively

$$\phi_{H_2} = \frac{34.33\dot{m}_{H_2}}{\dot{m}_{air}} \quad (3.8)$$

$$\phi_{diesel} = \frac{14.5\dot{m}_{diesel}}{\dot{m}_{air}} \quad (3.9)$$

where ϕ_{H_2} and ϕ_{diesel} are the equivalence ratios of hydrogen and diesel respectively.

Other engine parameters that will be part of interest in this study are power, specific fuel consumption, and specific energy consumption. These parameters are calculated according to Eq. (3.10), Eq. (3.11), and Eq. (3.12) respectively. The diesel energy sharing is shown in Eq. (3.13)

$$Pe = \frac{Me \times n}{9550} \quad (3.10)$$

where, Pe is the brake power in kW, Me is the brake torque in N.m, and n is the engine speed in rev/min.

$$BSFC = \frac{\dot{m}_{diesel} \times 1000}{Pe} \quad (3.11)$$

$$BSEC = \frac{\dot{m}_{diesel} \times LHV_{diesel} + \dot{m}_{H_2} \times LHV_{H_2}}{Pe} \quad (3.12)$$

$$\% Diesel = \frac{\dot{m}_{diesel} \times LHV_{diesel}}{\dot{m}_{diesel} \times LHV_{diesel} + \dot{m}_{H_2} \times LHV_{H_2}} \times 100 \quad (3.13)$$

where $BSFC$ is Brake Specific Fuel Consumption (g/kW.h), $BSEC$ is Brake Specific Energy Consumption (MJ/kW.h). LHV_{diesel} is the heating value of diesel fuel, considered constant with a value of 42.8 MJ/kg, and LHV_{H_2} is the heating value of hydrogen of 120 MJ/kg.

3.3 MODEL DEVELOPMENT

Currently CFD has been successfully an important tool for the calculation of fluid flow, mixture formation and combustion in internal combustion engines. It becomes a complementary tool to in-cylinder pressure analysis and optical diagnostics. There are three major steps in the CFD calculation for internal combustion engine, i.e. the generation of the computational meshes, the specification of the initial and boundary conditions, the flow solver settings and the physical and chemical models adopted to simulate the governing in-cylinder processes and finally, the post-processing and interpretation of the simulation results (Merker, Schwarz, & Teichmann, 2012).

3.3.1 Generation of Computational Mesh

In the case of diesel engine, the calculation of the intake stroke is usually not performed in order to reduce calculation time. It is quite common to start the calculation of the in-cylinder process (mixture formation and combustion) at the closing of the intake valves assuming an ideal cylinder-shaped swirl structure (Merker, Schwarz, Stiesch, & Otto, 2006). A simplified geometry is used to reduce the effort for mesh generation. Details like intake ports and valves (valve reliefs) are not considered.

In a symmetric arrangement of IC-engine injector/piston bowl configurations and if the fuel mass flow is the same for all holes of the injector, the analysis and optimization of the spray injection and combustion processes is usually done by simulating an engine segment model only. The angle of the segment is given by the number of holes in the injection nozzle (angle = $360^\circ/\text{number of nozzle holes}$).

Commercial CFD software namely AVL FIRE owned by LIPI was used throughout this study. The feature of automatic mesh generation was used to generate the mesh used in this simulation work. The meshing process also takes into account the

generation of a piston position, independent mesh topology for the spray domain, a defined number and thickness of boundary layers, and matching of the compression ratio.

During a mesh generation, a 2D model of a piston bowl along with the engine data (bore, compression ratio, crank radius, connecting rod length, and piston pin offset) were used to generate a mesh. The model was then imported into the CFD mesh generator to start the meshing process. The model of piston bowl and the injector spray angle is shown in Figure 3.7(a). Injector modelling including nozzle position, number of injection holes, spray axis, and injection spray angle were defined during this phase. The number and the thickness of boundary layers were specified. Based on the geometry description made above, a set of computational meshes covering 360 °CA is created. The 2D computational meshes consist of unstructured, quadrilateral mesh with wall adaptation.

A three-dimensional set of computational meshes is created based on the two-dimensional grids. The number of computational cells in circumferential (angular) direction was defined. Due to an unsymmetrical arrangement of injector/piston bowl configuration of the engine used in this work, an X and Y offset relative to the cylinder axis has to be specified. Mesh processing is shown in Figure 3.7.

Mesh generation is critical to multi-dimensional CFD engine modelling due to the fact that the mesh quality has a large impact on the numerical stability of CFD solvers and the mesh density can influence the simulation results, depending on the mesh-dependence of the numerical models (Lakshminarayanan & Aghav, 2010). Mesh quality is one of the important aspects for successful CFD calculation. It is usually required to check the following: negative volume, negative normal distance, partially negative volume, duplicate cell, identical vortex, and irregular connection. Checking the aspect ratio, skewness, edge angle, and twisted face are recommended. Additional check could be performed on the face area and face area ratio.

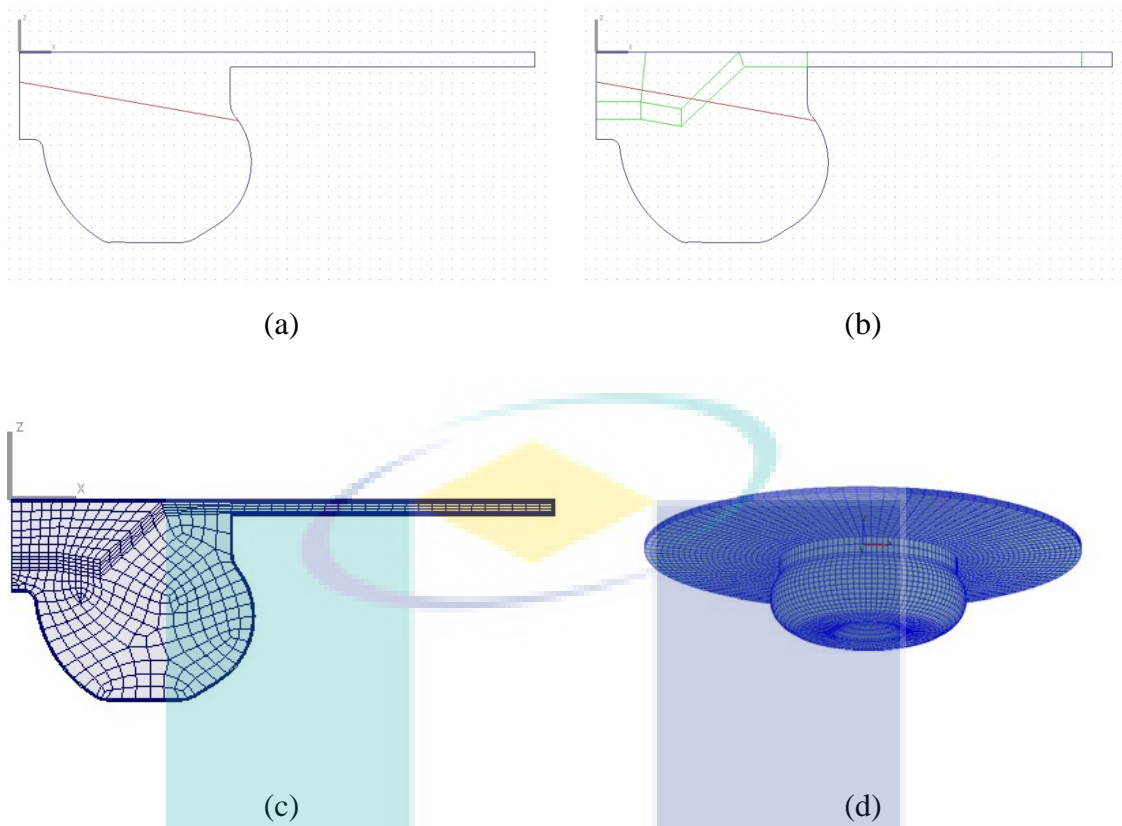


Figure 3.7. Generation of computational model: (a) 2D piston bowl and spray target, (b) definition of block structure, (c) 2D mesh, (d) final 3D mesh.

3.3.2 Setting the Boundary and Initial Conditions

Defining accurate boundary conditions are essential for IC engine simulation. For instance, heat loss on the solid wall, is very sensitive to the corresponding boundary conditions used in the simulation. Generally, there are four types of boundary conditions in CFD simulation: inflow boundary; outflow boundary; rigid/fixed wall boundary; periodic/cyclic boundary (Shi, Ge, & Reitz, 2011).

The boundary conditions for the model are shown in Figure 3.8. Three boundaries were defined in the model, i.e. cylinder head, liner, and piston. Cylinder head and liner are fixed wall, and hence they have velocity components of zero, while the piston is moving mesh. The walls are assumed smooth and impermeable. For real flows, the velocity of fluid, which is in contact with the wall, is equal to the wall velocity. This is known as a no-slip condition. Temperatures for all boundaries were

assumed constant. The movement of the piston is according to the crank-piston mechanism.

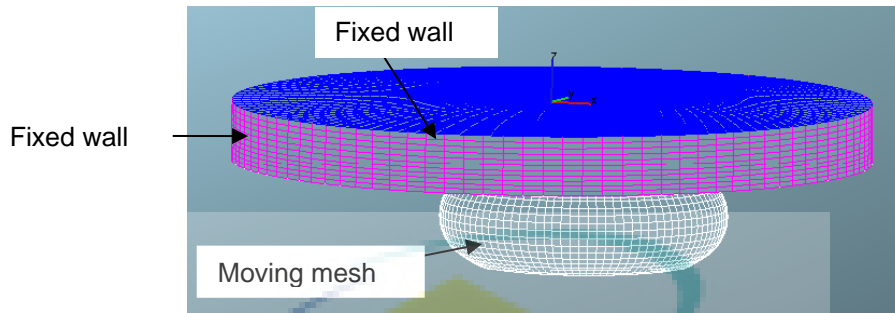


Figure 3.8. Boundary conditions.

The initial conditions state the introductory value of pressure, temperature, turbulence kinetic energy, turbulence length scale, and turbulence dissipation rate. The gas pressure and temperature at inlet valve closure results from thermodynamic computation or experimental work. The boundary and initial conditions is shown in Table 3.4

Table 3.4
Boundary and Initial Conditions

Boundary Condition	
Name and type of boundary	Temperature (K)
Cylinder head (fixed wall)	520
Cylinder liner (fixed wall)	450
Piston (moving mesh)	550
Initial Value	
Parameter	Initial value
Pressure	222235 Pa
Temperature	488.41 K
Turbulence kinetic energy	23.6 m ² /s ²
Turbulence length scale	0.0475 m

A recommendation for the global values for turbulence kinetic energy (TKE) and turbulence length scale (TLS) are given in the Eq. (3.14) and (3.15)(AVL, 2011).

$$TKE = \frac{3}{2} u'^2 \quad (3.14)$$

$$c_m = 2 \times h \times \frac{n}{60} \quad (3.15)$$

where u' and c_m are the turbulence fluctuation velocity and mean piston velocity respectively. For high speed diesel engine, these two velocities are correlated according to Eq. (3.16) and (3.17)

$$u' = 0.7 \times c_m \quad (3.16)$$

The turbulence length scale was calculated from the valve lift according to Eq. (3.17):

$$TLS = h_v/2 \quad (3.17)$$

where h_v is the maximum valve lift.

Another parameter that was defined in the initial condition is the amount of each species involved in the simulation. Intake air was assumed to consist of oxygen (O₂) and nitrogen (N₂). The surrogate diesel fuel was a blended of primary reference fuels n-heptane (nC₇H₁₆) and iso-octane (iC₈H₁₈). The mass fraction of hydrogen (H₂) was defined as initial value during dual fuel simulation.

3.3.3 Governing Equations

In the following, the basic equations used for gas phase is presented (AVL, 2011; Merker et al., 2006). The basic equations of continuity, momentum, and energy calculated for a closed cycle are shown in Eq. (3.18) – (3.20). The momentum and continuity equations are related to the calculation of velocity and pressure fields and the energy equation calculates the enthalpy.

$$\frac{\partial}{\partial t} \rho = \frac{\partial}{\partial x_j} (\rho U_j) \quad (3.18)$$

$$\begin{aligned}\frac{DU_i}{Dt} &= \rho \frac{\partial U_i}{\partial t} + \rho \frac{\partial U_i}{\partial x_j} = \rho g_i + \frac{\partial \sigma_{ij}}{\partial x_j} \\ &= \rho g_i - \frac{\partial P}{\partial x_i} + \frac{\partial}{\partial x_j} \left[\mu \left(\frac{\partial U_i}{\partial x_j} + \frac{\partial U_j}{\partial x_i} \right) - \frac{2}{3} \frac{\partial U_k}{\partial x_k} \delta_{ij} \right]\end{aligned}\quad (3.19)$$

$$\begin{aligned}\rho \frac{DH}{Dt} &= \rho \left(\frac{\partial H}{\partial t} + U_j \frac{\partial H}{\partial x_j} \right) \\ &= \rho g_j + \frac{\partial P}{\partial t} + \frac{\partial}{\partial x_i} (\tau_{ij} U_j) + \frac{\partial}{\partial x_j} \left(\lambda \frac{\partial T}{\partial x_j} \right)\end{aligned}\quad (3.20)$$

where ρ is fluid density, U is velocity, g is gravity acceleration, σ is the stress tensor, P is pressure, μ is viscosity, δ is the unit tensor, H is stagnation enthalpy, \dot{q} is any thermal source, τ is the shear tensor and λ is the coefficient of heat conductivity

3.3.4 Turbulence Model

Simulating the fluid flow in the internal combustion engine is mostly related to turbulent flows. Hence, the accurate model of turbulence is a basis for precisely simulating the real flows. Turbulence not only determines the details of the fluid flow itself, but also strongly influences the physical and chemical processes taking place during mixture formation and combustion. For example, in internal combustion engines the turbulent kinetic energy is a major influencing factor on the propagation and evaporation of liquid fuel spray droplets and the subsequent combustion of the air/fuel mixture (Merker et al., 2012). In addition to the well-known, standard turbulence models, such as k- ϵ , Spalart-Allmaras, and Reynolds Stress, the CFD code used in this study offers the k- ζ -f turbulence model, recently developed and validated for engine related flow, heat transfer and combustion processes (Basara, 2006).

For internal combustion engine flows, the k- ζ -f model (Hanjalić, Popovac, & Hadžiabdić, 2004) gives more accurate results than the much simpler two-equation eddy viscosity models of the k- ϵ type by simultaneously exhibiting a high degree of numerical robustness. In combination with a hybrid wall treatment, combining the integration up to the wall with standard wall functions, the k- ζ -f turbulence model is

universally applicable to computational meshes and flow situations of any reasonable y^+ value near the wall (Popovac & Hanjalic, 2007).

This turbulence model is aimed to improve numerical stability of the original $\overline{v^2} - f$ model by solving a transport equation for the velocity scale ratio instead of - velocity scale $\overline{v^2}$ as shown in Eq. (3.21).

$$\zeta = \frac{\overline{v^2}}{k} \quad (3.21)$$

The eddy-viscosity ν_t is defined according to Eq. (3.22)

$$\nu_t = C_\mu \zeta k \tau \quad (3.22)$$

The transport equation for ζ is shown in Eq. (3.23), while the equation for the relaxation factor f is shown in Eq. (3.24)

$$\frac{D\zeta}{Dt} = f - \frac{\zeta}{k} P_k + \frac{\partial}{\partial x_j} \left[\left(\nu + \frac{\nu_t}{\sigma_\zeta} \right) \frac{\partial \zeta}{\partial x_j} \right] \quad (3.23)$$

$$L^2 \nabla^2 f - f = \frac{1}{\tau} \left(C_1 - 1 + C_2 \frac{P_k}{\varepsilon} \right) \left(\zeta - \frac{2}{3} \right) \quad (3.24)$$

The value of turbulent time scale τ and length scale L are given by Eq. (3.25) and Eq. (3.26). The constant coefficients are given in Table 3.5.

$$\tau = \max \left[\min \left(\frac{k}{\varepsilon}, \frac{0.6}{\sqrt{6} C_\mu |S| \zeta} \right), C_\tau \left(\frac{\nu}{\varepsilon} \right)^{1/2} \right] \quad (3.25)$$

$$L = C_L \max \left[\min \left(\frac{k^{2/3}}{\varepsilon}, \frac{k^{1/2}}{\sqrt{6} C_\mu |S| \zeta} \right), C_\eta \left(\frac{\nu^3}{\varepsilon} \right)^{1/4} \right] \quad (3.26)$$

Table 3.5
Coefficient Value for Turbulence Model

Constant	C_μ	σ_ζ	C_1	C_2	C_τ	C_L	C_η
Value	0.22	1.2	0.4	0.65	6	0.36	85

3.3.5 Spray and Atomization Model

The Kelvin-Helmholtz (KH) model (Reitz & Diwakar, 1987) was used in the simulation study. The model is based on a first order linear analysis of a Kelvin-Helmholtz instability growing on the surface of a cylindrical liquid jet with initial diameter r_0 that is penetrating into a stationary incompressible gas with a relative velocity u_{rel} . Both the liquid and the gas are assumed to be incompressible, and the gas is assumed to be inviscid.

This theory is applied to break-up modelling of liquid droplets with radius, r . Waves grow on the drop surface with growth rate Ω and wavelength Λ . In the KH model, a parent parcel with radius r breaks up to form new droplets with radius r_{new} such that

$$r_{new} = C_1 \cdot \Lambda \quad (3.27)$$

where $C_1 = 0.61$ is a constant. A new parcel containing product drops of size r_{new} is created and added to the computation. The growth rate Ω of the fastest growing and thus most unstable surface wave is:

$$\Omega = \frac{0.34 + 0.38 \cdot We_g^{1.5}}{(1 + Z)(1 + 1.4 \cdot T^{0.6})} \sqrt{\frac{\sigma}{\rho_l r_0^3}} \quad (3.28)$$

and the corresponding wavelength Λ ,

$$\Lambda = \frac{9.02 \cdot r_0 (1 + 0.45 \cdot Z^{0.5})(1 + 0.4 \cdot T^{0.7})}{(1 + 0.865 \cdot We_g^{1.67})^{0.6}} \quad (3.29)$$

where

$$Z = \frac{\sqrt{We_l}}{Re_l}, T = Z \sqrt{We_g}, We_g = \frac{\rho_g r_0 u_{rel}^2}{\sigma}, We_l = \frac{\rho_l r_0 u_{rel}^2}{\sigma}, Re_l = \frac{\rho_l r_0 u_{rel}}{\eta_l}$$

Z and T are the Ohnesorge number and the Taylor number, and r_0 is the radius of the undisturbed jet. We is the Webber number and Re is the Reynold number.

The droplet radius rates of reduction at a certain time t depends on the difference between the actual value of the droplet radius r and an equilibrium droplet size (which is equal to the child droplet radius r_{new} as well as on the value of a characteristic time span τ_{bu}

$$\frac{dr}{dt} = -\frac{r - r_{new}}{\tau_{bu}}, \tau_{bu} = 3.788 \cdot C_2 \frac{r}{\Omega\Lambda} \quad (3.30)$$

C_2 is a constant that can have values ranging between 10 and 60, and it is usually calibrated with experiments (Lakshminarayanan & Aghav, 2010).

The multi-component droplet evaporation is based on the approach of Abramzon and Sirignano (1989), which has been extended by Brenn, Deviprasath, Durst, and Fink (2007). The main difference to the single-component case is that mass transfer of every component is taken into account separately, whereas heat transfer remains a global mechanism. The droplet collision was modelled according to the algorithm proposed by Schmidt and Rutland (2000). The method of looping in this model uses a pre-sorting algorithm which is much more efficient for most cases. The higher the average numbers of parcels per cell the greater the advantage.

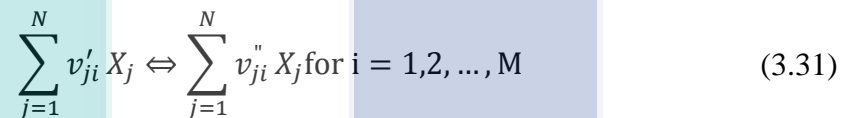
3.3.6 Integration of Chemical Kinetics

In diesel engine simulations, combustion modelling mainly deals with two processes: first, low-temperature chemistry, which leads to auto ignition and produces intermediate species, and second, these intermediate species trigger high-temperature reactions that contribute the main heat release, as well as further complete and incomplete combustion products (Lakshminarayanan & Aghav, 2010). Another

important task for combustion models is to properly account for the significance of the effect of turbulence on the combustion processes

Direct integration of the chemical kinetics resolves the species conversion rates by considering detailed chemistry for modelling engine combustion processes. The solutions provide the combustion source terms in the energy and species transport equations. Turbulence may or may not play a role at the sub-grid scale in the model, depending on if the computational cells are treated as well stirred reactors (WSR) or partially stirred reactors (PaSR) (Shi & Reitz, 2010)

In a combustion system a chemical kinetics mechanism is used to define the reaction pathways and the associated reaction rates leading to the change of species concentrations and heat release. An elementary chemical reaction of arbitrary complexity can be represented by



Where v'_i and v''_i are the stoichiometric coefficient of the reactant and products, respectively, and X is the arbitrary specification of all chemical species for the M reaction. A species usually involved in multiple reactions in a chemical kinetic mechanism. Its production rate is the sum of its consumption and generation rate. It is defined that:

$$v_{ji} = v''_{ji} - v'_{ji} \quad (3.32)$$

The production rate of species j is expressed as:

$$\dot{r}_j = \sum_{i=1}^M v_{ji} \cdot \dot{q}_i \quad (3.33)$$

Where \dot{q}_i is the reaction rate of reaction i , defined by the difference of forward and reverse reaction rate

$$\dot{q}_i = k_f \prod_{j=1}^N [X_j]^{v'_{ji}} - k_r \prod_{j=1}^N [X_j]^{v''_{ji}} \text{ for } i = 1, 2, \dots, M \quad (3.34)$$

k_f and k_r are the forward and reverse rate coefficient for the i th elementary reaction, which are a function of temperature T and take the Arrhenius form as follows:

$$k = AT^{-b}e^{(-E/RT)} \quad (3.35)$$

The constant A , b , and E are the pre-exponential factor, temperature-dependence factor, and activation energy respectively. R is the universal gas constant.

A reduced chemical kinetic model of primary reference fuel developed by Ra and Reitz (2008) was used in this study. The mechanism consists of 41 species and 130 reactions. Some of reaction rate constants were modified to meet the experimental results. The mechanism was constructed in CHEMKIN format and integrated into the CFD using the internal chemistry interpreter.

To take into account the effect of both chemical kinetics and mixing, the approach of Kong, Marriot, Reitz, and Christensen (2001) is used. It is assumed that the computational cell to be just partially stirred. The role of turbulence in the combustion is introduced through the turbulence timescale τ_t . The turbulence timescale is expressed as:

$$\tau_t = C_{mix} \frac{k}{\varepsilon} \quad (3.36)$$

where C_{mix} is a model constant of an order of 0.1, which is tuneable in order to match measured engine pressure traces and heat release data (Shi & Reitz, 2010). The influence of both chemical kinetic and turbulence on source terms for species transport equations reaction rate of the species are calculated as:

$$S_k = \frac{\tau_{kin}}{\tau_{kin} + f \cdot \tau_t} \frac{\rho^{n+1} w_i^{n+1} - \rho^n w_i^n}{\Delta t} \quad (3.37)$$

The delay coefficient f was adopted from Kong, Han, and Reitz (1995)

$$f = \frac{1 - e^{-r}}{0.632} \quad (3.38)$$

$$r = \frac{w_{CO_2} - w_{H_2O} - w_{CO} - w_{H_2}}{1 - w_{N_2}} \quad (3.39)$$

3.3.7 Numerical Solution

The CFD Solver employs the finite volume discretization method which rests on the integral conservation statements applied to a general control volume (CV). Therefore, the finite volume method has the ability to preserve conservation properties which are inherent in the integral equations. Obviously, the physical domain (space) has to be divided into a number of non-overlapping control volumes which constitute a *numerical grid*. A general *convex* polyhedron, i.e. a control volume bounded by an arbitrary number of planar or even non-planar surfaces (faces) can be used:

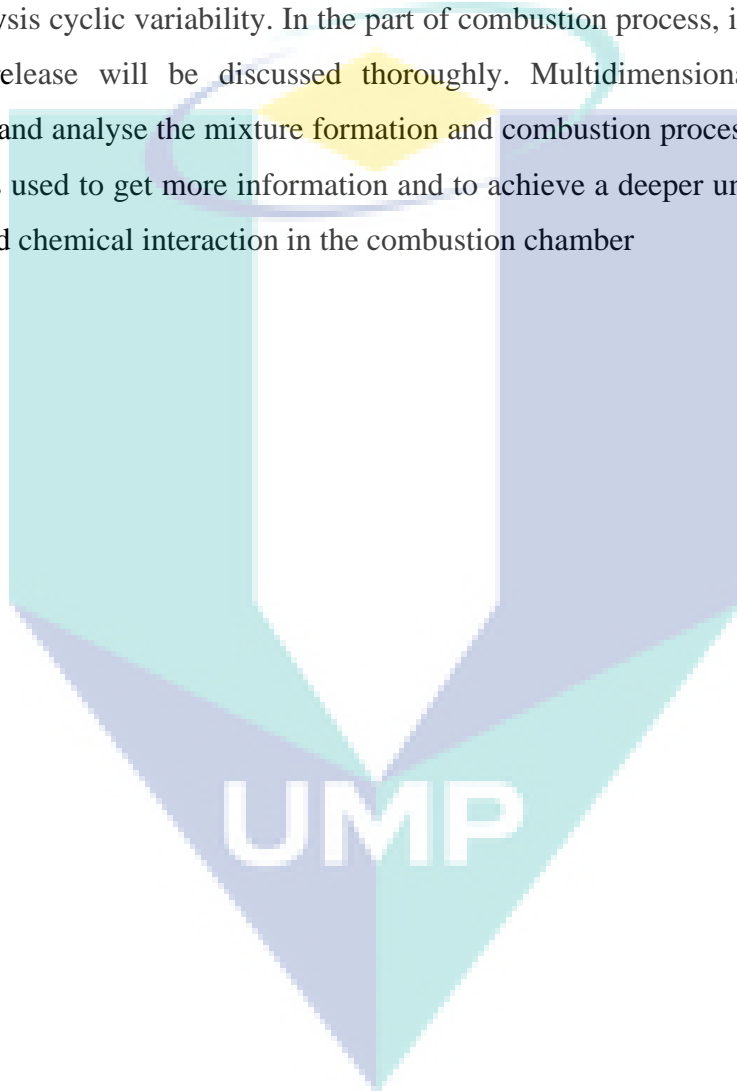
The rate of change is discretized by using implicit schemes, namely an Euler implicit scheme and a three time level implicit scheme of second order accuracy. The overall solution procedure is iterative and is based on the Semi-Implicit Method for Pressure-Linked Equations algorithm (SIMPLE) applicable to turbulent flows at all speeds.

3.4 SUMMARY

This chapter has explained the detail step of the research work. The first step in conducting this research was the experimental works on a diesel engine that has been converted to accommodate hydrogen as fuel in dual fuel mode. Experimental setups, detail of instrumentation, and measurement method have been outlined. The uncertainty of the instruments and measurement was thoroughly described. The second step was the development of the model for computational works. Model developments consist of

mesh generation, setting of initial and boundary conditions, and setting of constants for turbulence and spray models. The governing equations and the numerical solution of CFD tools were briefly outlined.

Based on the experimental and simulation works explained in this chapter, the results will be presented and discussed in Chapter 4. The first part will show and discuss the performance and emissions of this dual fuel engine. Second part will mainly focus on the analysis cyclic variability. In the part of combustion process, in-cylinder pressure and heat release will be discussed thoroughly. Multidimensional simulation will investigate and analyse the mixture formation and combustion process in more detail. A CFD tool is used to get more information and to achieve a deeper understanding on the physical and chemical interaction in the combustion chamber



CHAPTER 4

RESULTS AND DISCUSSION

4.1 INTRODUCTION

This chapter explains and discusses the effect of hydrogen addition on engine performance, combustion, and exhaust emission. Engine performance is focused on brake specific energy consumption and thermal efficiency. Exhaust emissions of NO_x , smoke, CO and CO_2 are outlined. The cycle-by-cycle of the combustion process is discussed in the next part. Comparison on cylinder pressure and heat release is discussed to explore the combustion process of both diesel and dual fuel engine.

The mesh independent test, model validation, mixture formation, and combustion characteristics of the engines are numerical investigation of mixture formation and combustion processes. The last part of this chapter is aimed at providing the results of the CFD simulation of the in-cylinder physical and chemical processes governing performance and emission characteristics of diesel and dual fuel engine with wide ranges of hydrogen percentages.

4.2 ENGINE PERFORMANCE

4.2.1 Diesel-Hydrogen Energy Sharing

The engine speed and load were kept constant during the hydrogen addition to the intake manifold. This mode can be realized by setting the dynamometer at fixed

load. The engine speed was kept constant by controlling the diesel fuel governor. When hydrogen was introduced, the total energy input increased. Due to constant load setting at the dynamometer side, the engine speed tended to increase. The injection pump lever was then moved to reduce the engine speed until the defined speed achieved.

The percentage of diesel energy at each load condition when hydrogen was introduced is depicted in Figure 4.1. This energy percentage was calculated according to Eq. (3.14). When hydrogen was introduced into the intake port, part of diesel fuel was replaced by hydrogen for all speed and load condition. It is shown that the percentage of diesel fuel is higher when the engine was operated at higher load. This happens since when the load was increased, more diesel fuel was introduced. It means that at the same hydrogen flow rate, the percentage of diesel fuel is higher.

Overall, the trend of energy sharing is almost the same for all speed. At the speed of 1500 rpm and load of 5 and 10 Nm, hydrogen can be added until 49.6 l/min, the maximum hydrogen flow rate in this study. Hydrogen addition at higher loads was limited by knock occurrence as shown in Figure 4.1(a). The maximum hydrogen flow rate for engine operation with the load of 15 Nm was 42.8 l/min. Further increase in engine load reduced the maximum hydrogen flow rate. Engine speed of 2000 rpm shows a better knock resistance as it can be operated at higher loads with higher hydrogen flow rates. Knock occurrence was not detected until the engine load of 20 Nm. The maximum hydrogen enrichment can be achieved until the load of 20 Nm as depicted in Figure 4.1(b). At the engine speed of 2500 rpm, maximum hydrogen flow rate at highest load was 48.2 l/min. The knock occurred at higher load limited the maximum portion of gaseous fuel added to the dual fuel engine. This is due to high compression ratio of CI engine and the quick burning of gaseous fuel benefiting from the multi-point fuel process of the pilot diesel fuel (Ganesan, 2012). As the mass of hydrogen introduced with air increases and leads to higher combustion temperature, hydrogen mixture in the combustion chamber would be more susceptible to self-ignition (Liu & Karim, 1995; Selim, 2004).

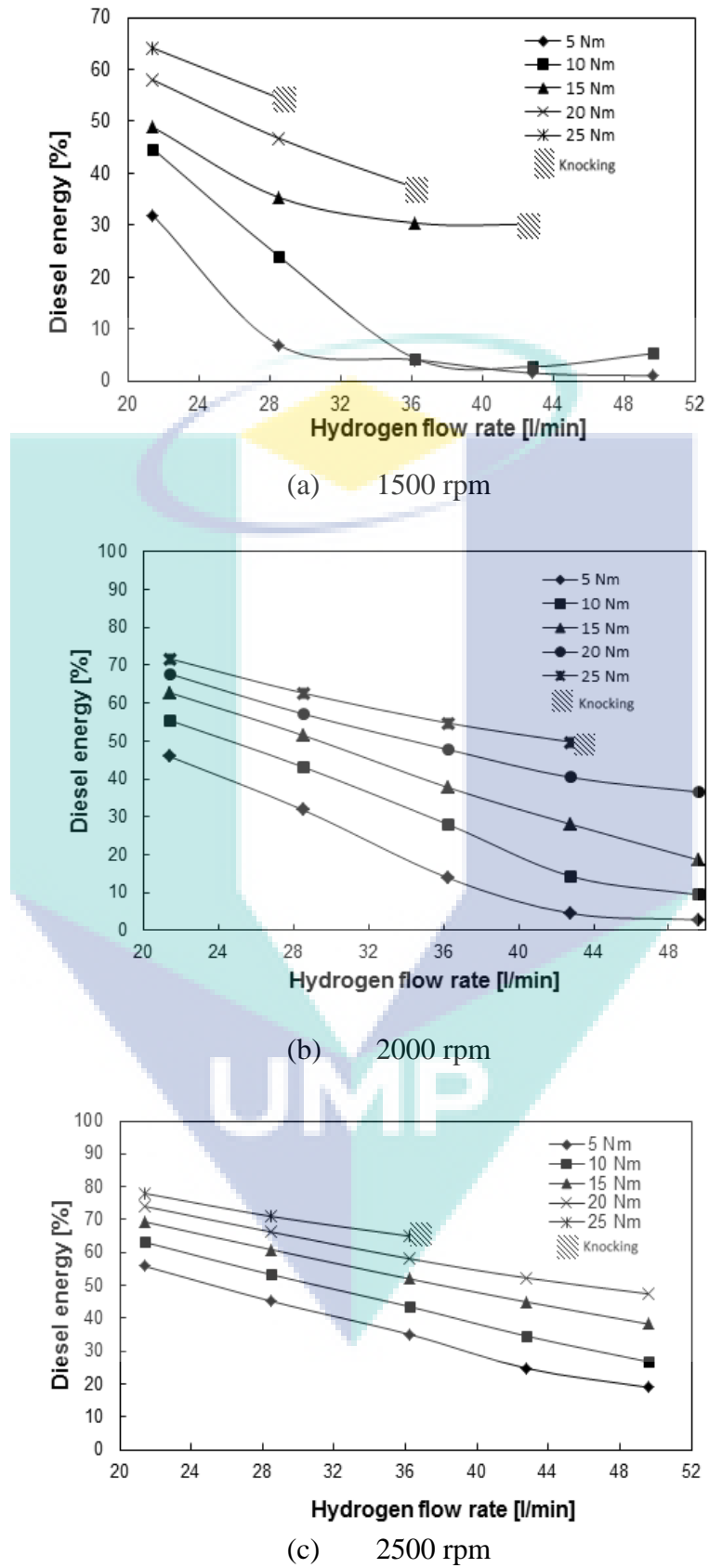


Figure 4.1. Diesel energy sharing at various speeds.

Figure 4.2 illustrates the response of diesel injector when the engine was operated at 2000 rpm and 5 Nm. The reduction of diesel fuel was represented by the injector needle lift over the crank angle. It can be noted that the start of diesel injection is almost the same for all condition because there is no SOI controller in the engine used for this study. The injector governor reduced the amount of diesel fuel to maintain the engine speed when hydrogen was introduced. Diesel fuel reduction is shown by a smaller distance of needle lift and the earlier end of injection.

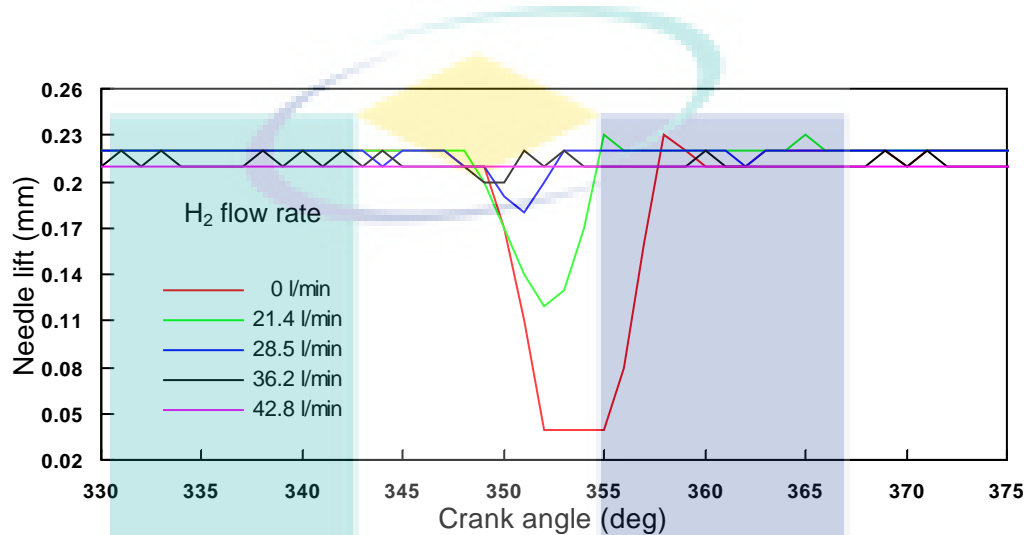


Figure 4.2. Effect on hydrogen addition on needle lift, engine operation at 2000 rpm and 5 Nm.

4.2.2 Brake Specific Energy Consumption

Figure 4.3 depicts the variation of BSEC over the level of hydrogen enrichment. BSEC indicates the amount of total fuel energy (diesel and hydrogen) needed to produce power for an hour engine operation. Specific energy consumption is calculated from the fuel consumption of individual fuels (diesel and hydrogen) multiplied by their respective calorific value divided by the power output as stated in Eq. (3.6).

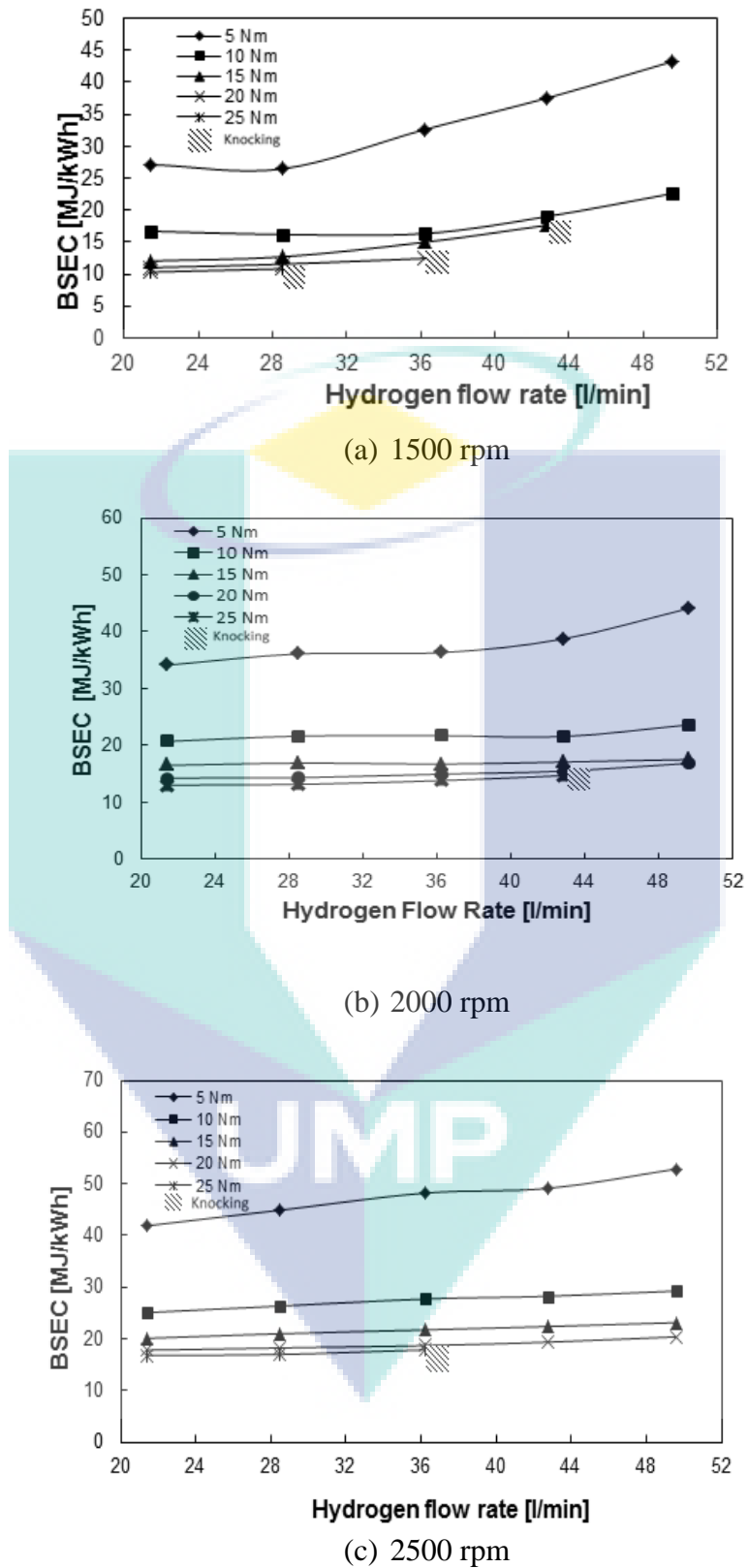


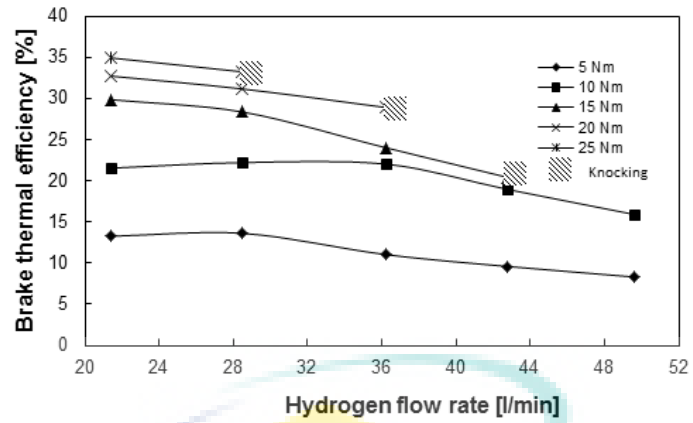
Figure 4.3. Variation of BSEC with hydrogen enrichment.

BSEC tends to increase slightly with hydrogen addition for all speed. As seen in Figure 4.3, internal combustion engines are most efficient at high loads. Hydrogen addition increases the overall equivalence ratio as calculated by Eq. (3.1). Brake specific energy consumption follows the trend in overall equivalence ratio, such that both increase with hydrogen substitution. The highest specific energy consumption of the entire experimental mode is observed at 2500 rpm and 5 Nm loads. This is due to the large amount of incomplete combustion which occurs in this engine operation (Lilik et al., 2010). Addition of hydrogen into the air intake displaces air with hydrogen and reduces the mass of the intake charge. Air is the working fluid of an internal combustion engine, and thus a reduction in air induction will reduce the output of an engine.

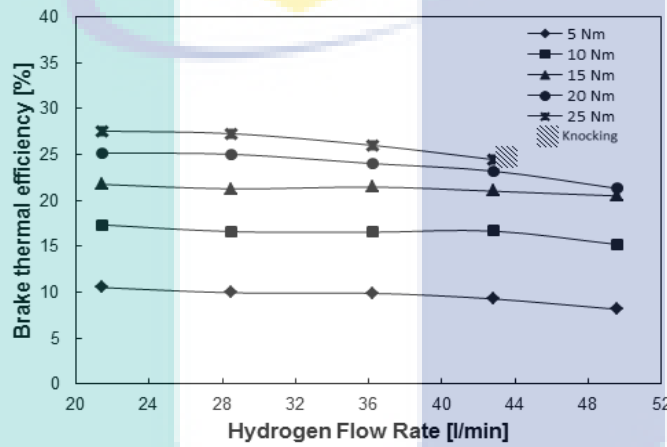
4.2.3 Brake Thermal Efficiency

Figure 4.4 shows the variation of brake thermal efficiency at all operating conditions when hydrogen was introduced. The brake thermal efficiency relates the effective brake power to the supplied fuel energy. It is seen that the most efficient operation for all the engine speed is achieved at high loads. Hydrogen enrichment at the flow rate of 21.4 l/min, 25 Nm load, and 1500 rpm gave the best efficiency of 34.9 %. The brake thermal efficiency for the same load and hydrogen flow rate at 2000 and 2500 rpm are 30.8 and 21.5 % respectively.

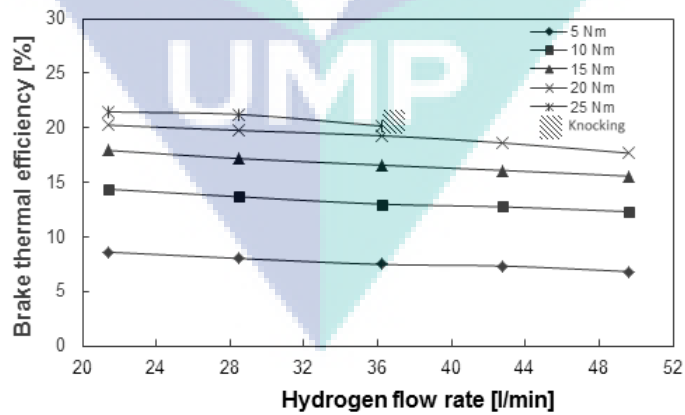
Hydrogen substitution decreased the brake thermal efficiency due to the reduction of volumetric efficiency. The existence of gaseous fuel in the intake mixture reduced the volumetric efficiency significantly. At higher engine speeds, the flow into the engine during the least part of the intake process becomes choked. Further increases in speed do not increase the flow rate significantly so volumetric efficiency decreases (Heywood, 1988). The amount of air induced reduces and so does the engine output. The brake thermal efficiency becomes lower with the increasing speed.



(a) 1500 rpm



(b) 2000 rpm



(c) 2500 rpm

Figure 4.4. Variation of brake thermal efficiency.

4.2.4 Emissions Analysis

Effect of hydrogen enrichment on engine emissions when the engine was operated at 2000 rpm is presented in the following section. Diesel main emissions are NO_x and smoke, but due to hydrogen enrichment, CO and CO_2 are taken into consideration during the investigation.

Figure 4.5 shows the NO_x variation at different loads applied when hydrogen was introduced. It is shown that NO_x was increased at higher loads. NO_x formed in the near stoichiometric mixture with a high temperature (Heywood, 1988). Higher load resulted in higher temperature. This leads to higher NO_x emission. At low temperature, nitrogen exists as a stable diatomic molecule (N_2). However, at very high temperature such as in the combustion chamber, some diatomic molecule of nitrogen breaks down to reactive monoatomic nitrogen (N). The chemical equilibrium constant of the reaction is highly dependent on temperature (Ganesan, 2012). The monoatomic nitrogen can react with oxygen or oxide of hydrogen to form nitrogen oxides. It is noted for the lower loads (5 and 10 Nm), hydrogen enrichment tends to decrease the NO_x emission. In these loads condition, hydrogen enrichment decreases the cylinder peak pressure and temperature. The diesel fuel percentage on energy basis reduced significantly with an increase in hydrogen. The amount of diesel fuel to ignite the premixing of hydrogen with air was reduced and resulted in a late start of combustion. The production of NO_x is also associated primarily with the pilot diffusion combustion zone, where very high local temperatures are produced and longer reaction times are possible (Karim, 2015). The small amount of pilot fuel in these low loads operation will reduce the high temperature combustion zones.

NO_x emission was relatively constant at the engine load of 15 Nm. Hydrogen enrichment did not change significantly the cylinder pressure. The availability of diesel portion is sufficient to achieve the efficient combustion. Higher loads (20 and 25 Nm) resulted in the increase of NO_x emission with hydrogen addition. In these loads, diesel portion was sufficient to achieve more efficient combustion. Cylinder peak pressure was increased. At the engine load of 25 Nm, the maximum hydrogen flow rate was 42.8 l/min. More hydrogen enrichment resulted in knocking, which limits the engine operation. An increase in the amount of hydrogen beyond a limit can increase the

number of active radicals and speed up the reaction. A sudden rise in the temperature of hydrogen mixture in the neighbourhood of the sprays ignited the pilot fuel and the flame fronts spread from these ignition points (Ganesan, 2012). A flame starting from ignition point would have to propagate through the adjacent mixture before it meets flames from similar neighbouring regions (Karim, 2015). This flame fronts consumes gas in its surrounding and more thermal energy is released. This process speeds up reaction everywhere and knocking occurred.

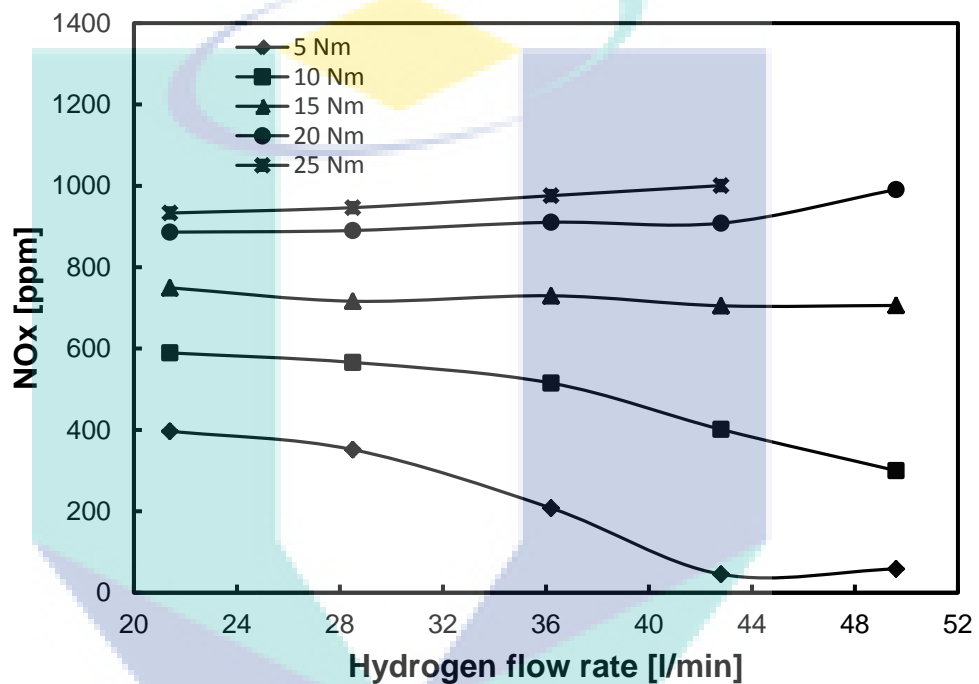


Figure 4.5. Variation of NO_x with load and hydrogen flow rate.

The variation of smoke level with load and hydrogen flow rates is shown in Figure 4.6. Smoke is a visible product of combustion, formed due to poor combustion (Saravanan & Nagarajan, 2008a). Soot emission is the major constituent of diesel smoke and a main problem of diesel engine. It originates at high temperatures of more than 1500 K with local lack of oxygen (Pischinger, 2002). Smokeless operations were achieved except for the load of 25 Nm. When hydrogen was mixed with air, smoke was not exhausted because hydrogen does not include carbon atoms in its molecular structure (Tomita et al., 2001). The smoke meter was calibrated at 50.8 % of smoke value. Negative value was achieved at no smoke condition. The small amount of smoke

at high load is considered to be formed from the combustion of the diesel fuel. The portion of diesel fuel at this load is more than 49.7 %.

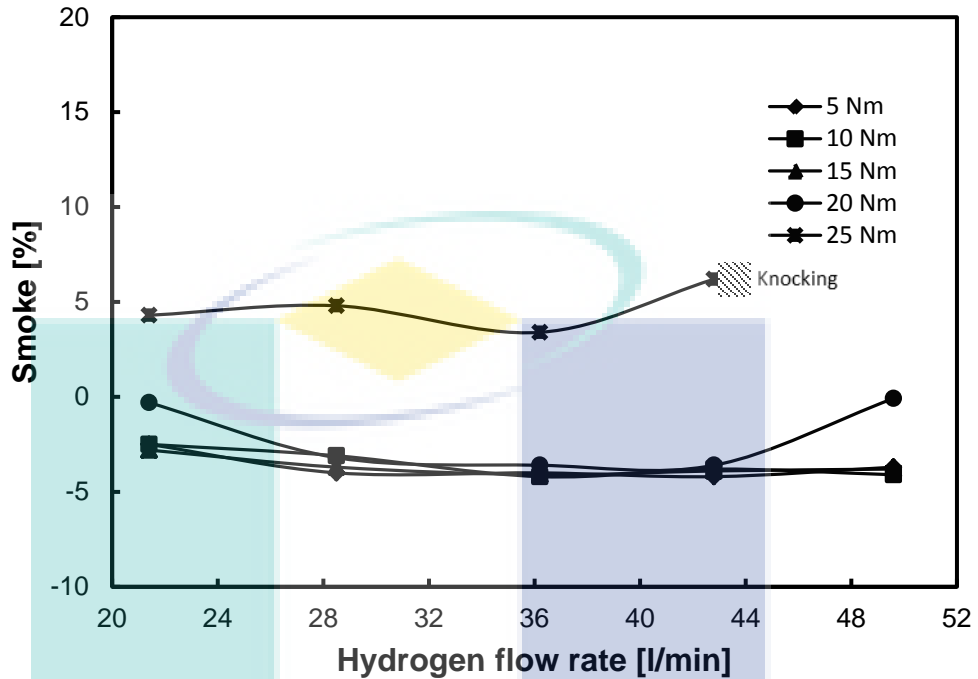


Figure 4.6. Variation of smoke number with load and hydrogen flow rate.

CO emission was not detected due to lean combustion. Carbon monoxide is generated in an engine when it is operated in fuel-rich mixture. CO is not only considered an emission, but it also represent lost chemical energy (Ganesan, 2012). The overall equivalence ratio for all cases in this study was in the range of 0.20-0.65 which was a lean mixture. The leanest mixture was diesel operation at low load of 5 Nm. A traceable amount of 0.06 % CO was detected in this operation condition of diesel fuel alone. Addition of hydrogen can condense CO emissions to a smaller value than the exactitude of the measurement device (Deb et al., 2015). In addition, the higher diffusivity of hydrogen in comparison to other fuels provides better homogeneity of the combustible mixture which boost the combustion (Ghazal, 2013).

The variation of carbon dioxide with load for different value of hydrogen enrichment is shown in Figure 4.7. This figure reveals that the formation of carbon dioxide is reduced by the increase of hydrogen flow rate. The reduction in carbon dioxide emission is due to the absence of carbon in hydrogen fuel (Bari & Mohammad

Esmail, 2010). Small amount of 0.3 % CO₂ during pure diesel operation at 5 Nm load. CO₂ was not traced on the dual fuel mode. Higher loads increase the production of CO₂. Hydrogen additions reduce the CO₂ emission. In all cases, hydrogen additions reduce the amount of CO₂ emissions. Hydrogen addition to diesel fuel could decrease the heterogeneity of diesel fuel spray since the high diffusivity of hydrogen results in a superior premixed and more uniform combustible mixture (Szwaja & Grab-Rogalinski, 2009). Enhancement in the premixing of the combustible mixture will facilitate higher efficiency for complete combustion (Ghazal, 2013).

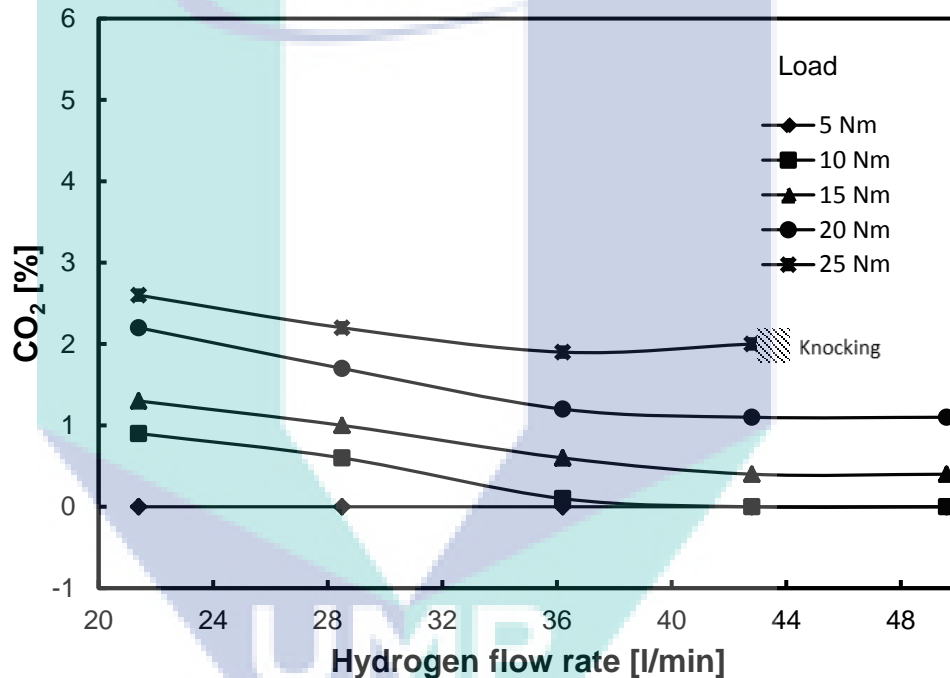


Figure 4.7. Variation of CO₂ emissions with load and hydrogen flow rate.

4.3 CYCLIC VARIABILITY OF DUAL FUEL COMBUSTION

There have been many studies concerning cycle-by-cycle variation and combustion stability of spark ignition engines fuelled with gaseous fuels, either single gas or blended gas (Huang et al., 2009; Ma et al., 2008; Wang et al., 2008). The characteristics of mixture formation, ignition, and combustion process of the fuel-air mixture that greatly influences the cycle variation are well understood. However, in the

dual fuel engine that used the diesel fuel to ignite the hydrogen-air mixture, the ignition characteristics of the gaseous fuel are not well understood. The combustion process in the dual fuel engine is quite complex. It combines some of features and associated problem of compression ignition engine , as well as those of premixed spark ignition type (Karim, 2015). In addition to the cause of cyclic variations exist in diesel engine, dual fuel engines appear to be more prone to cyclic variability in combustion noise due to existence of gaseous fuel with compressed air (Selim, 2005).

Figure 4.8 shows the cylinder pressure variation for 36 consecutive cycles in diesel and dual fuel operation at engine speed 2000 rpm and loads of 5 and 20 Nm. Hydrogen was added at 49.6 l/min for dual fuel operation. Hydrogen enrichment resulted in lower cylinder pressure when operate at 5 Nm. The average of maximum cylinder pressure for 160 cycles in diesel operation was 71.10 bar, compared to that of 55.94 bar in dual fuel operation. The combustion process was promoted by the auto-ignition of diesel fuel. In such a lower load, diesel percentage on energy basis reduced significantly with an increase in hydrogen. The amount of diesel fuel to ignite the premixing of hydrogen with air was reduced and resulted in a late start of combustion and the combustion instability.

In contrast to low load operation, the cyclic variability at high load operation was not so obvious, as depicted in Figure 4.8(c) and (d). It is noted that the cylinder peak pressures resulted from dual fuel combustion are higher than that of diesel combustion. In this operating condition, the percentage of diesel fuel is more than 30 % and indicated efficiency is slightly increased at higher hydrogen flow rate. This portion of diesel fuel is sufficient to produce efficient dual fuel combustion (Ganesan, 2012). The cyclic variations are usually related to the occurrence of substantial combustion instabilities, such as when operating at very lean gaseous mixture or employing excessive EGR. In such conditions, the injection characteristics, the pilot fuel quantity, and mixing processes significantly influence the variation. Larger pilot fuel and less lean gaseous fuel-air mixtures produce stability engine operation (Karim, 2015).

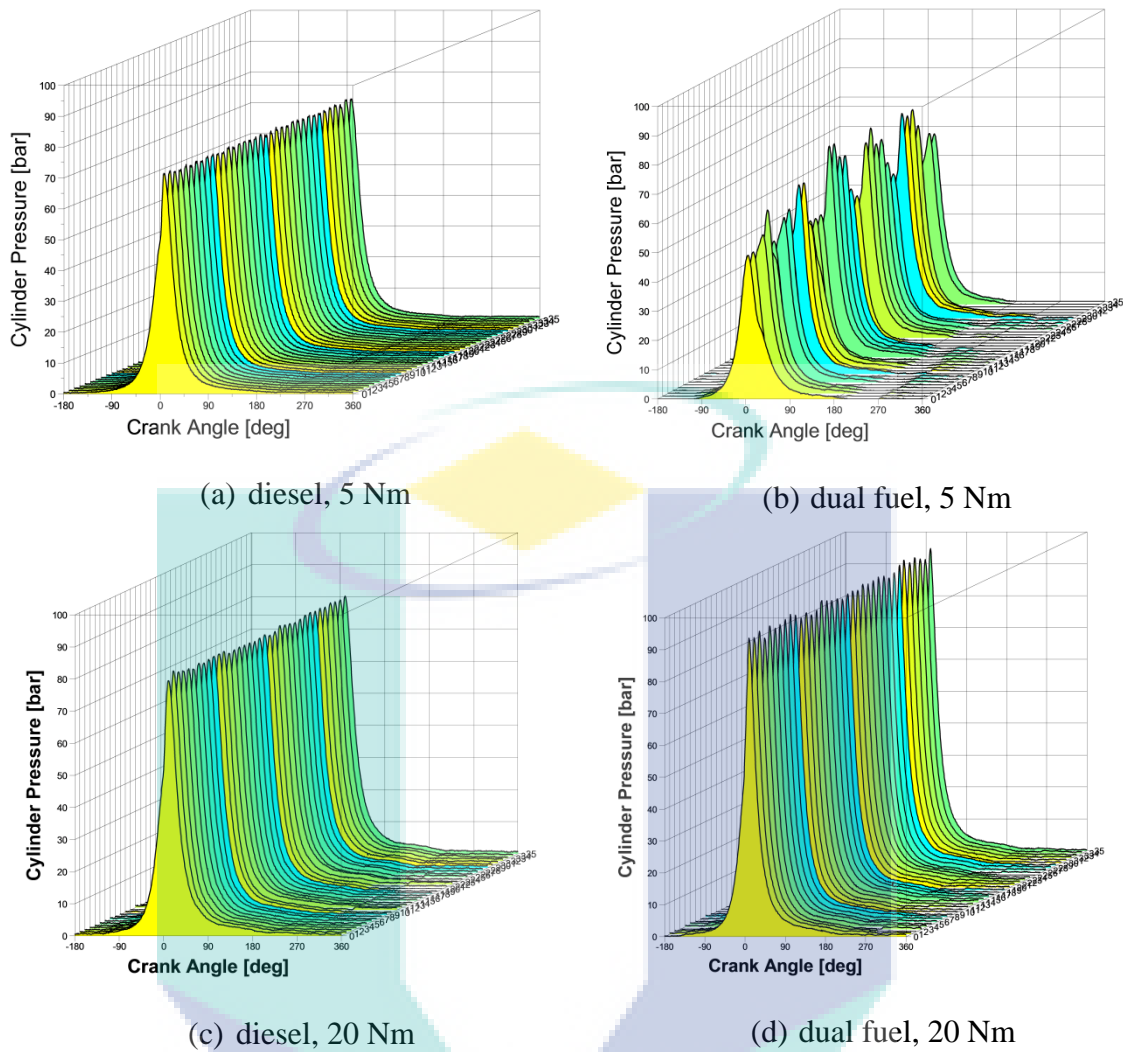
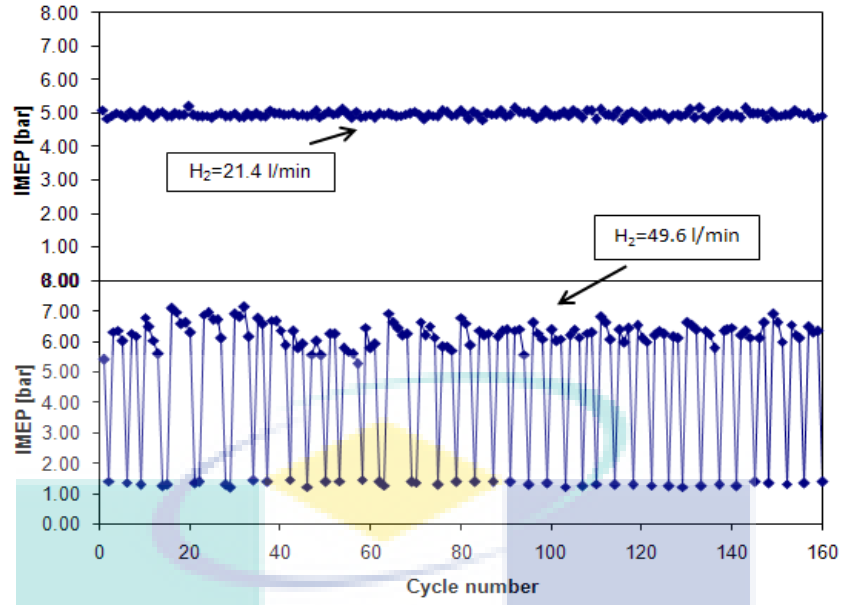


Figure 4.8. Cylinder pressure variation in diesel dual fuel engine operation.

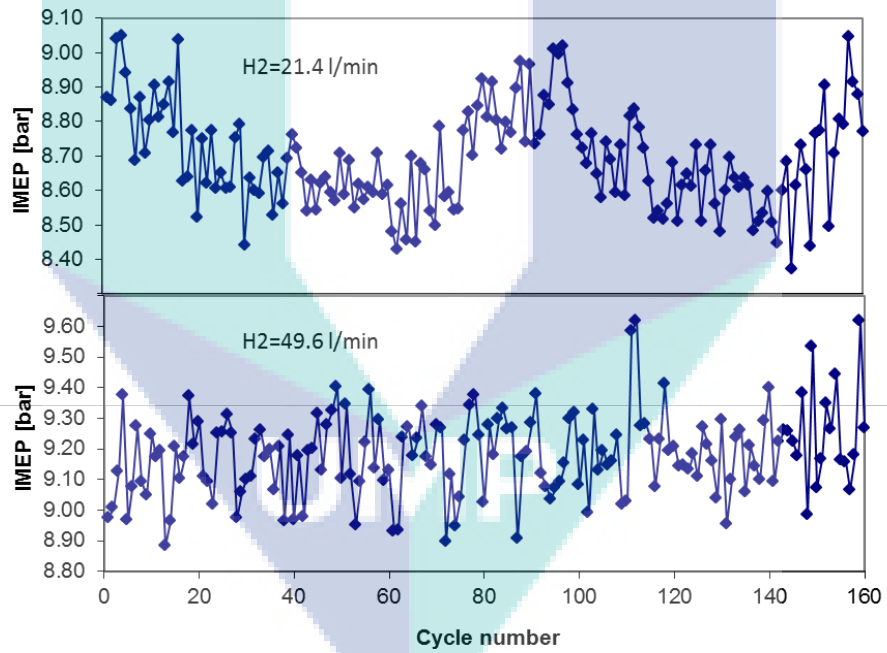
Figure 4.9(a) depicts IMEP variation when hydrogen was introduced at the flow rate of 21.4 l/min and 49.6 l/min. The engine operated at 5 Nm load and 2000 rpm. There is a significant variability between these two cases but the mean values are almost the same. The availability of diesel fuel needed to ignite the premixing of hydrogen with air resulted in combustion instability. On energy basis, the percentage of diesel fuel at 21.4 l/min hydrogen enrichment was around 46 %. A further increase in hydrogen enrichment at 49.6 l/min reduced the percentage of diesel fuel to 3 %. This portion of diesel is not sufficient to produce an efficient and stable combustion. The minimum amount of the pilot fuel to sustain the load is 5-7 % (Ganesan, 2012).

Cyclic variability of IMEP when the engine is operated at 20 Nm load is shown in Figure 4.9(b). Hydrogen addition slightly increased the average value of IMEP from 8.69 to 9.18 bar due to the increase of the cylinder peak pressure. The amount heat released is slightly increased with hydrogen addition as shown in Figure 4.10. In this higher load, the amount of diesel pilot fuel was 40.4 % of the total input energy. Hydrogen addition reduced the percentage of diesel fuel, but it is sufficient to produce the efficient and stable combustion (Ganesan, 2012). It is noted that cyclic variability was slightly reduced with COV of 0.015 compared to that of 0.071 for lower hydrogen flow rate. The hydrogen-air mixture was richer, but the amount of diesel pilot could sustain the load and result in a stable combustion.

Figure 4.11 depicts the coefficient of variation of indicated mean effective pressure for all loads applied and hydrogen enrichment. As stated above, the cyclic variability tends to increase with an increase in hydrogen addition for the engine operation at low load. Hydrogen addition until 36.2 l/min reduced the diesel pilot fuel up to 13.9 % on energy basis. The percentage of diesel fuel when hydrogen was introduced at 42.8 and 49.6 l/min was 4.5 and 2.9 % respectively. These small amounts of pilot fuel are below the minimum percentage of pilot fuel to sustain the load (Ganesan, 2012). The combustion become unstable and significantly increased the coefficient of variance. Combination of small amount of diesel pilot fuel and lean gaseous-air mixture may produce long delays that lead to slow post-ignition energy releases. Flame propagation becomes more prone to variations (Karim, 2015). For the same hydrogen flow rates and engine operation at higher loads of 10 and 15 Nm, it is noticed that the coefficient of variances are slightly increase. The percentage of diesel energy for the load of 10 Nm was 14.3 and 9.4 %, while for the load of 15 Nm it was 28 and 18.6 % respectively. More stable combustion was achieved compared with that of engine load of 5 Nm.



(a) 5 Nm



(b) 20 Nm

Figure 4.9. IMEP variation due to hydrogen addition at 5 and 20 Nm load.

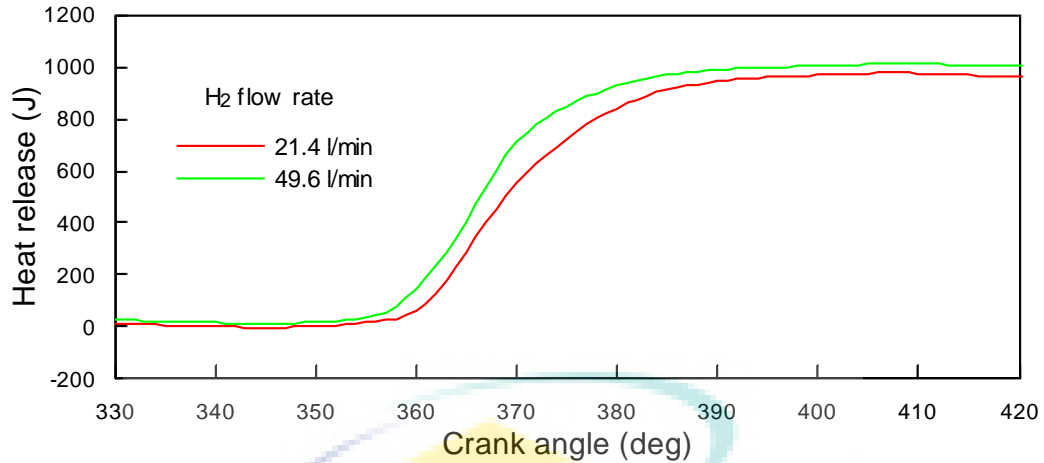


Figure 4.10. Accumulative heat release at 20 Nm load engine operation.

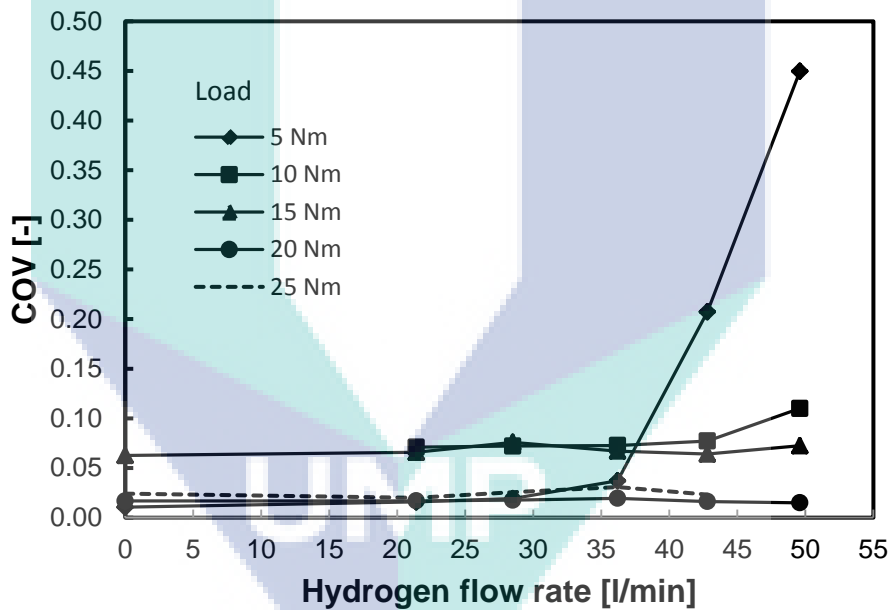


Figure 4.11. Coefficient of variation of IMEP at variable load and hydrogen flow rate.

It is noted that combustion stability was achieved at higher loads. The combustion process was promoted by the auto-ignition of diesel fuel. At higher load and the same hydrogen flow rate, diesel percentage on energy basis increased compared with that of lower load operation. The minimum diesel energy sharing for the load of 20 and 25 Nm was 36.6 and 49.7 % respectively. The amount of diesel fuel to ignite the premixing of hydrogen with air was high and resulted in more stable combustion.

4.4 COMBUSTION CHARACTERISTICS

Analysis of combustion characteristics of the dual fuel engine in the experimental works is based on cylinder pressure trace and its derivative parameters, i.e. rate of pressure rise and rate of heat release. The variation of cylinder pressure traces at engine speed of 2000 rpm and varied loads of 5-25 Nm load for different hydrogen flow rates is shown in Figure 4.12. It is noted that hydrogen additions has a different impact on the cylinder peak pressure. Hydrogen addition on the low load engine operation (5 and 10 Nm) reduced the peak cylinder pressure. On the other hand, the addition of hydrogen at higher load operation increased the peak cylinder pressures.

Figure 4.12(a) shows the effect of hydrogen addition on the cylinder pressure at 5 Nm load. The addition of hydrogen substantially reduced the cylinder pressure after the combustion was initiated. The combustion process was promoted by the auto-ignition of diesel fuel. In such a lower load, diesel percentage on energy basis reduced significantly with an increase in hydrogen as has been previously shown by diesel energy sharing in Figure 4.1(b). The amount of diesel fuel to ignite the premixing of hydrogen with air was reduced and resulted in a late start of combustion. Part of diesel-type premixed combustion was also reduced as shown in rate of heat release diagram in Figure 4.13. The deteriorated premixed combustion and elongated diffusion combustion made the combustion process lasted for a longer time and correspondingly deteriorated the engine performance (Liew et al., 2010)

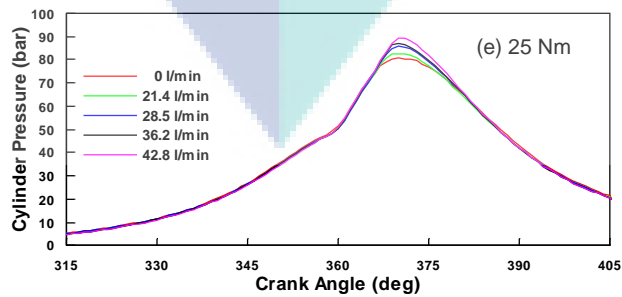
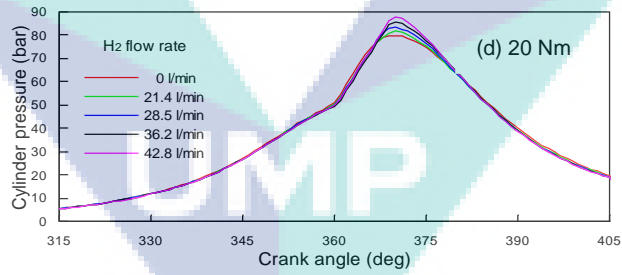
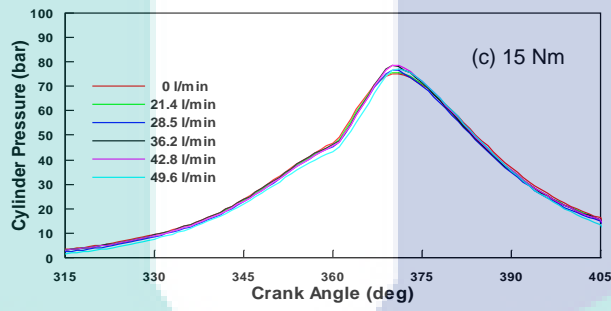
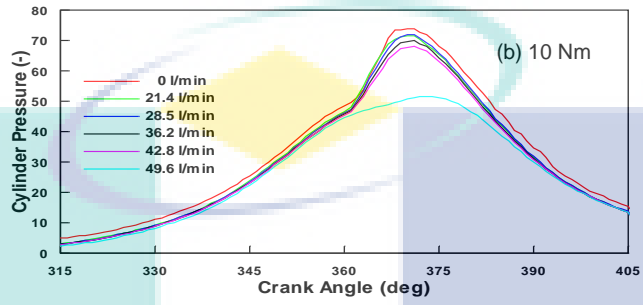
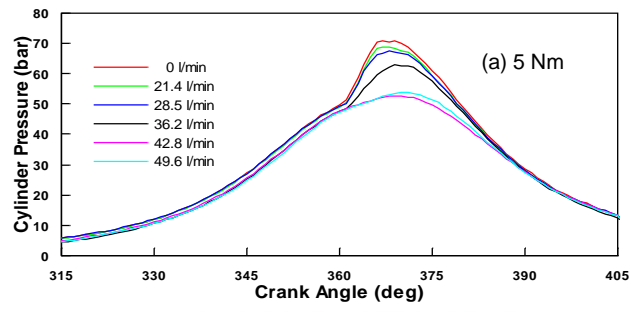


Figure 4.12. Cylinder pressure at various load and hydrogen flow rate at 2000 rpm.

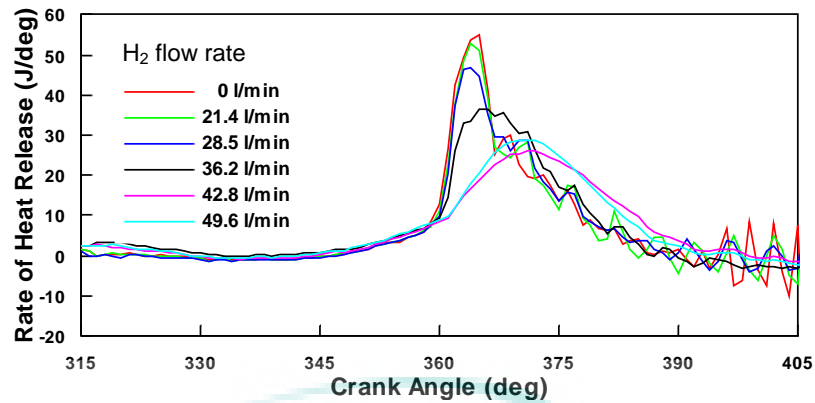


Figure 4.13. Rate of heat release at 2000 rpm, 5 Nm.

Figure 4.12(b) depicts the pressure traces at engine operating condition of 2000 rpm and 10 Nm. The cylinder peak pressures when hydrogen was introduced are lower than that of diesel operation. The peak pressure for diesel operation is found to be 74.07 bar. There is insignificant peak pressure reduction when hydrogen was introduced at 21.4 and 28.5 l/min. The peak pressure is found to be 71.81 and 71.92 bar respectively. Further increase in hydrogen flow rate of 36.2 and 49.6 l/min reduces the cylinder peak pressure to 69.94 and 51.67 bar respectively. The rate of pressure rise is shown in Figure 4.14. The peak value of the rise shifted a few degree crank angle when the hydrogen flow rate increased. This indicates a slower combustion reaction rate. The pressure rise is almost the same with that of diesel combustion for hydrogen flow rate of 21.4 and 28.5 l/min. Further increasing hydrogen flow rate reduced both peak cylinder pressure and pressure rise significantly. This may be due to the availability of diesel fuel needed to ignite the premixing of hydrogen with air (Saravanan & Nagarajan, 2010). The percentage of diesel fuel at 21.4 l/min and 28.5 l/min hydrogen enrichments were 45.9 % and 31.8 % respectively. A further increase in hydrogen enrichment reduced the percentage of diesel fuel to 13.9 %, 4.5 %, and 2.9 %. These portions of diesel may not be adequate to produce an efficient combustion and sustain the load (Ganesan, 2012). Furthermore, the combustion starts a little bit later as shown in Figure 4.15. When hydrogen was added at 49.6 l/min, slow heat release was noticed. The peak heat release was at 15 °CA after TDC, resulted in a lower cylinder pressure.

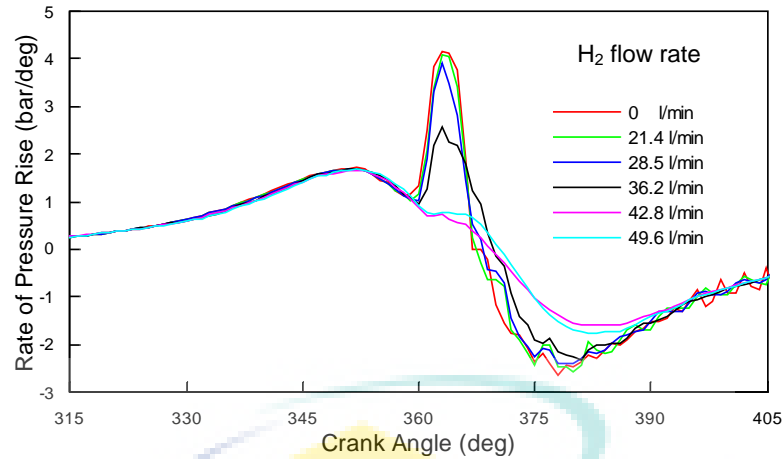


Figure 4.14. Rate of pressure rise under hydrogen enrichment at 2000 rpm, 10 Nm.

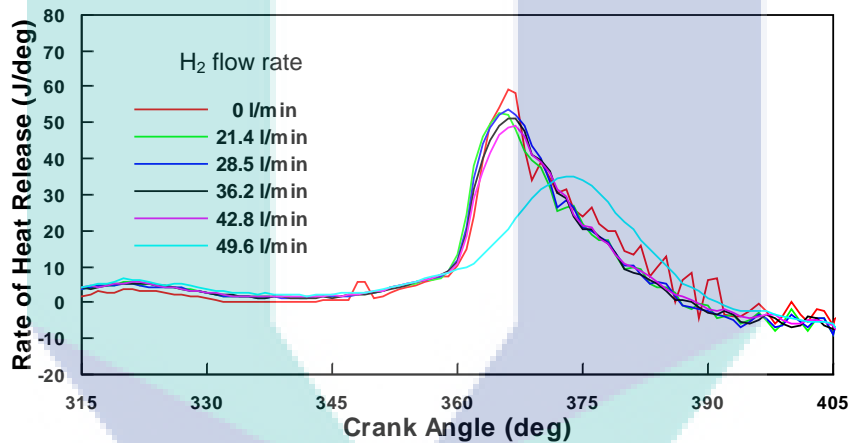


Figure 4.15. Rate of heat release at 2000 rpm, 10 Nm.

Figure 4.12(c) shows the variation of cylinder pressure for different level of hydrogen enrichment at engine speed 2000 rpm and 15 Nm load. It is noted that the cylinder peak pressures resulted from dual fuel combustion are slightly higher than that of diesel combustion with its peak value observed at retarded phasing. As shown in Figure 4.16, the peak heat release rate was observed at the premixed combustion stage. Hydrogen addition was shown to retard the start of combustion and enhanced the premixed combustion. Combustion was observed to be faster compared to that of diesel engine operation.

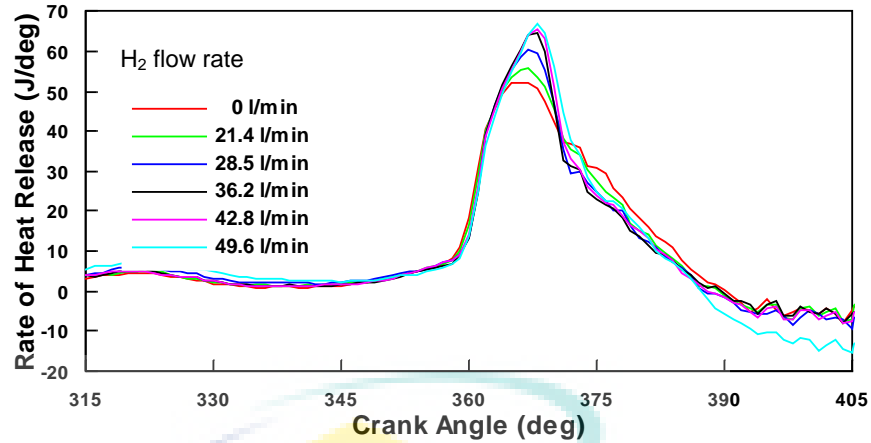
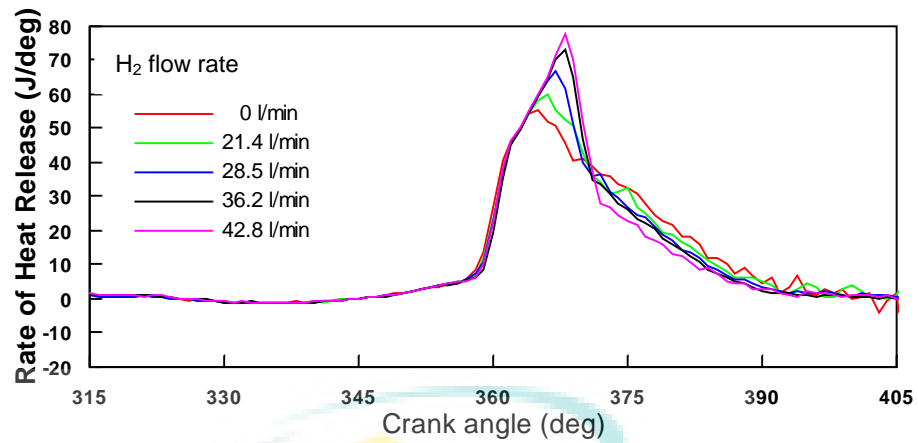
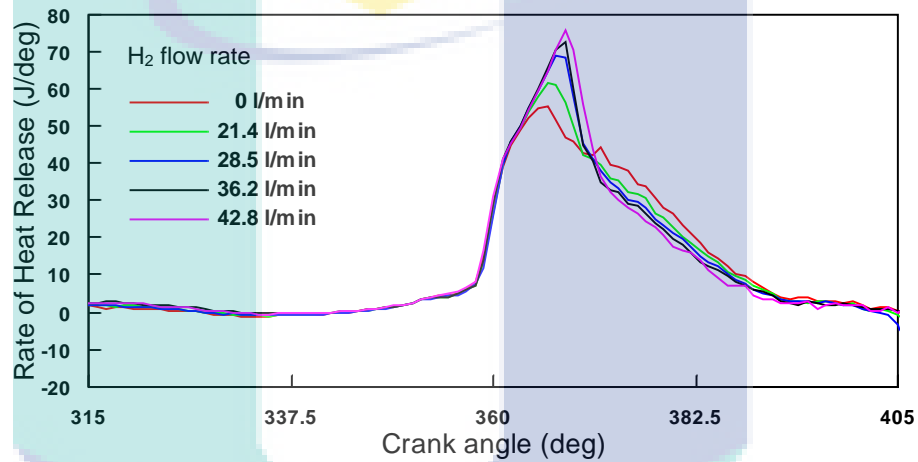


Figure 4.16. Rate of heat release at 2000 rpm, 15 Nm.

The cylinder pressures when operating at higher loads (20 and 25 Nm) are shown in Figure 4.12(d) and (e). The hydrogen enrichment at these higher load engine operations increased the cylinder pressures. The peak cylinder pressures were observed at retarded phasing. It is observed from rate of heat release diagram as depicted in Figure 4.17, hydrogen addition increased the peak value of heat release with retarded phasing. The combustion duration was shorter with the increase of hydrogen. The minimum diesel fuel portions at 20 and 25 Nm load were 36.6 % and 49.7 % respectively. This diesel sharing seems to be sufficient to achieve the efficient and sustain combustion with this hydrogen flow rate (Ganesan, 2012). As the amount of hydrogen is increased, the gas air mixture in the vicinity of the spray plume also gets oxidized and the ignition started at a number of points. The featured multiple turbulent flames enhanced the heat release process of the hydrogen diesel dual fuel engine and might have accelerated the combustion process of the diesel fuel (Liew et al., 2010).



(a) 20 Nm



(b) 25 Nm

Figure 4.17. Rate of heat release of engine operation at high load.

4.5 NUMERICAL INVESTIGATION OF DUAL FUEL COMBUSTION

4.5.1 Mesh Independence Test

Three meshes with different cell size namely fine, medium, and coarse mesh were created. The total numbers of cells at TDC position are 75 500, 50 200, and 43 500 respectively. To validate the mesh independence, the calculation was run with the three meshes with the same operating conditions. The cylinder pressure curves were compared at the condition of 2000 rpm and 10 Nm load (see Figure 4.19). It can be seen that there is no significant difference on the predicted cylinder pressure. By considering the computational time, the coarse mesh was used for all the simulation.

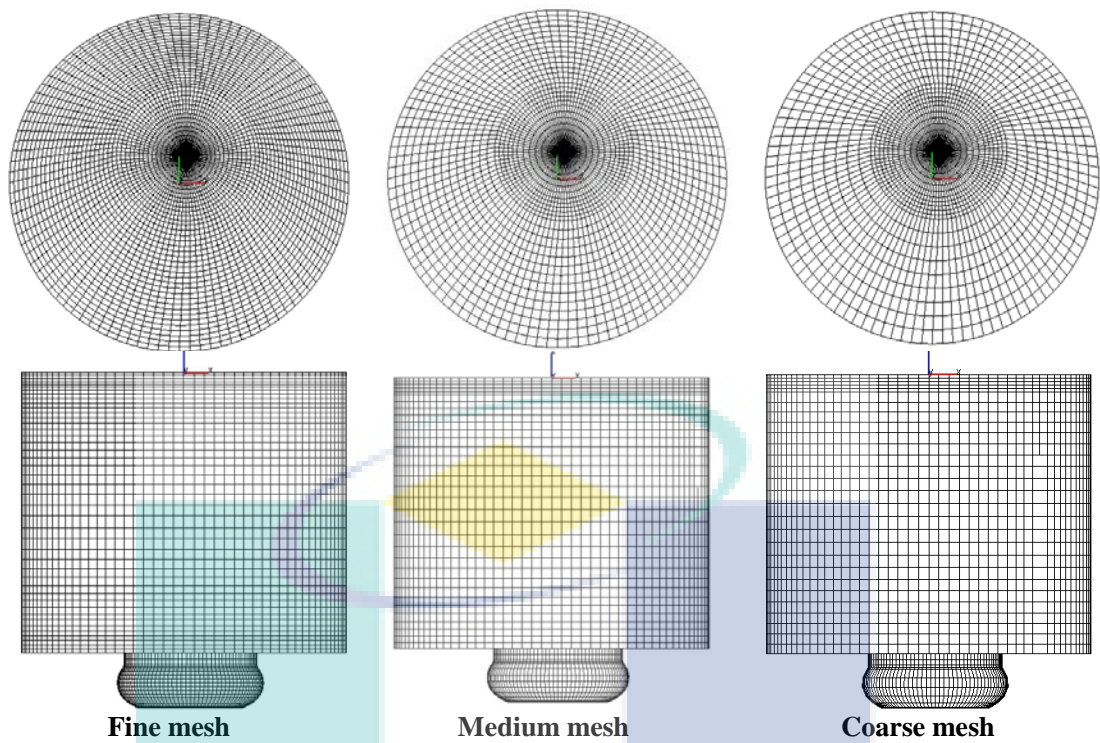


Figure 4.18. CFD meshes for study of mesh sensitivity.

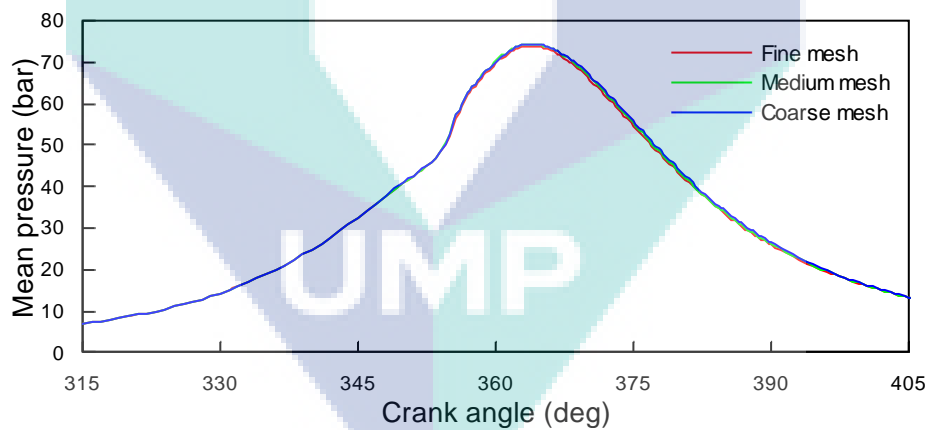


Figure 4.19. Mesh independence test; engine operating at 2000 rpm, 10 Nm.

4.5.2 Validation of Diesel Simulation

The developed computational model was validated by comparing the in-cylinder pressure between the experimental results and simulation results for engine operating conditions with diesel fuel only. The validation of cylinder pressures for all cases in this investigation are shown in Figure 4.20.

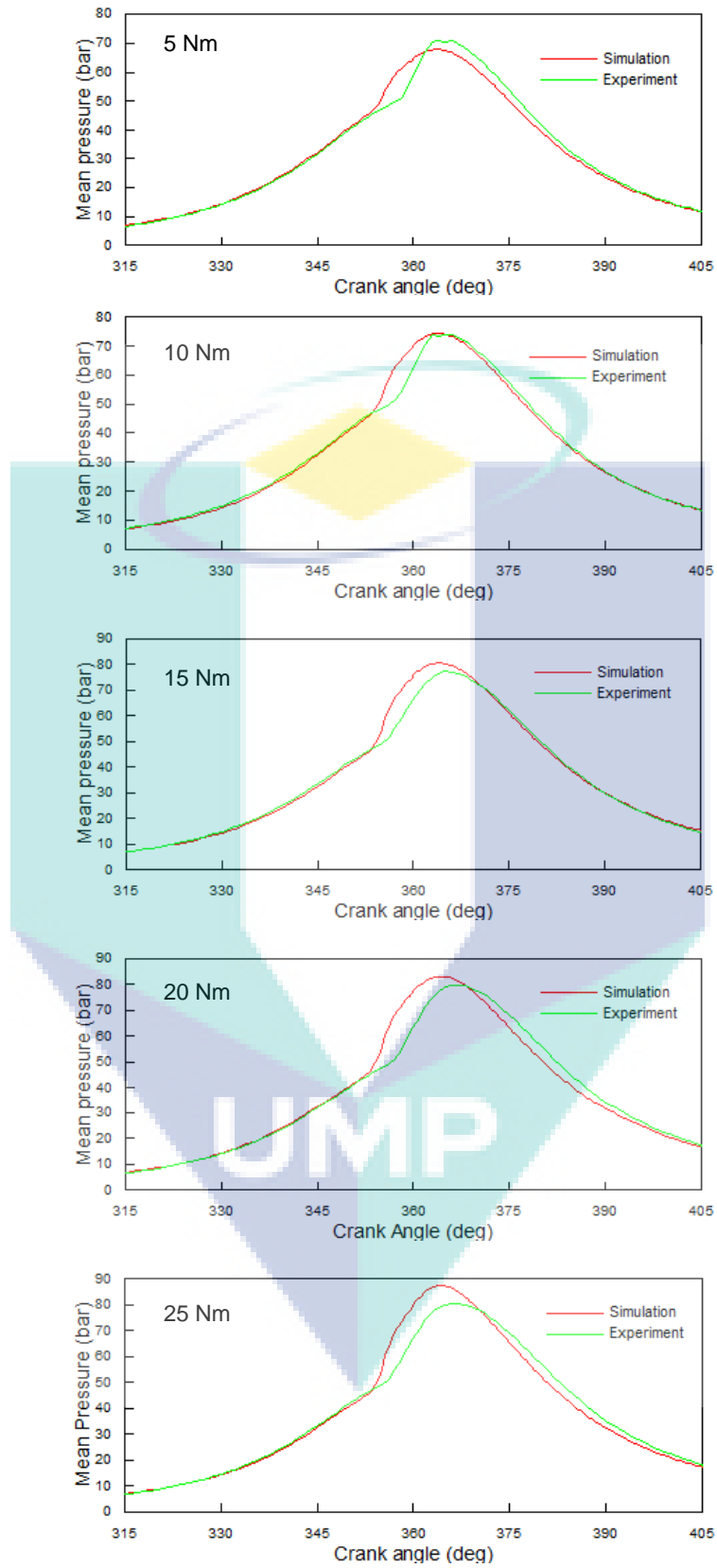


Figure 4.20. Validation of simulation result of diesel combustion at 2000 rpm.

In general, the simulation's results seem to have a good agreement with the experimental data during the compression stroke and at the end of expansion stroke. The pressure during the combustion stroke can be simulated very well for all loads applied. It was observed that the start of combustion of the simulation results occurred earlier compared to that of experimental results. The pressure rise was faster, and the peak pressures were slightly higher at advanced phasing. The reason behind the advanced ignition timing is uncertain as it depends on various parameters both physical and chemical (Xiao & Karim, 2011). as can be seen in Figure 4.21. The simulated ignition timing is about 4 degree earlier than the measured one for engine operation at 5 Nm. For higher engine loads, the difference of ignition timing is about 2 degree, and the difference of peak of pressure rises is wider.

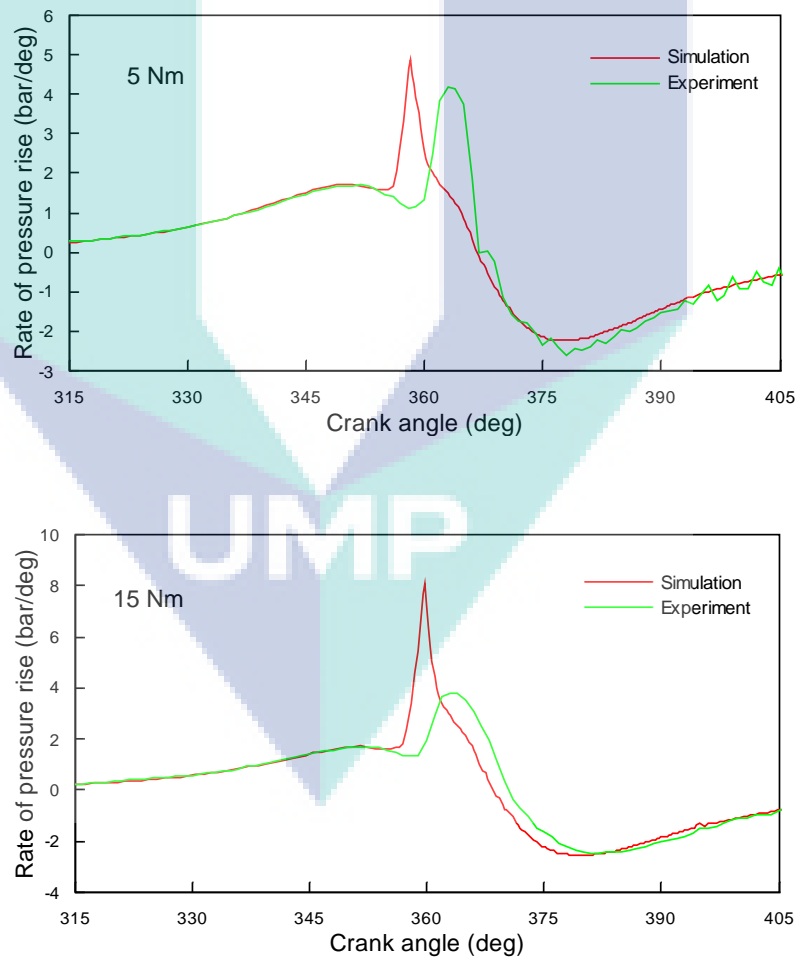


Figure 4.21. Rate of pressure rise for diesel combustion at 2000 rpm.

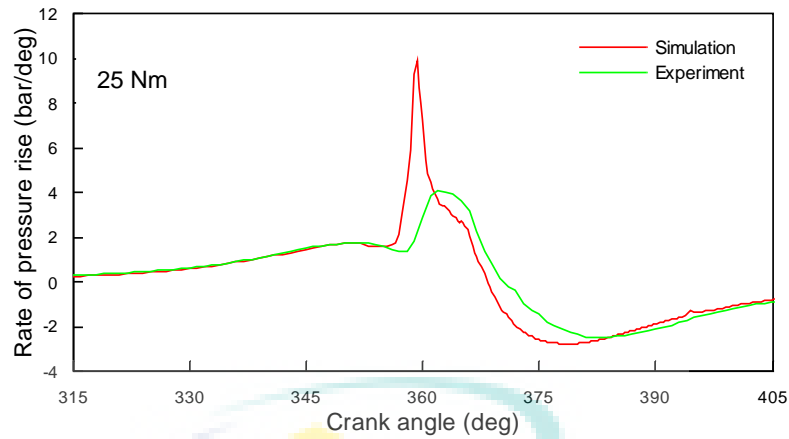
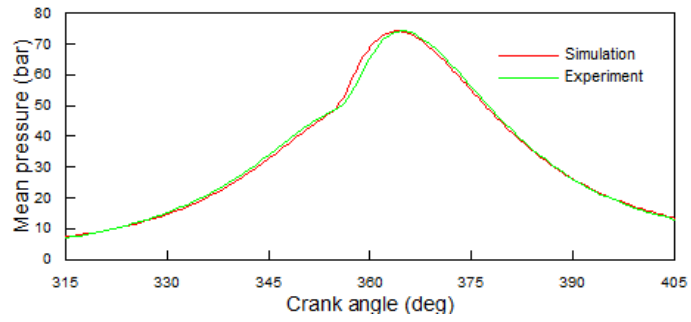


Figure 4.21. Continued.

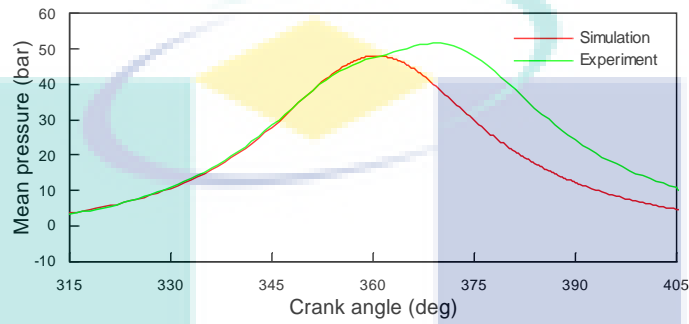
4.5.3 Validation of Dual Fuel Simulation

The CFD simulation of dual fuel combustion was focused at two loads operating condition, 10 and 20 Nm which represents the low and high load. For the same hydrogen flow rates, these two loads resulted in different combustion characteristics. Hydrogen addition tends to decrease the peak cylinder pressures at the engine operation of 10 Nm. On the other hand, higher cylinder peak pressures were achieved when hydrogen was introduced at the higher load.

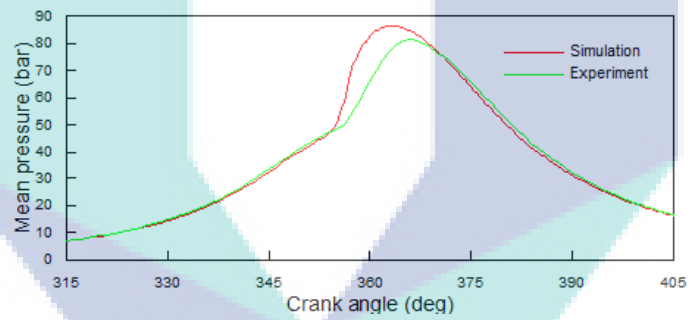
Figure 4.22 illustrated the comparison of simulation and experimental data of the dual fuel engine combustion characteristic. The compression and expansion strokes were good predicted by the simulation when the smallest amount of hydrogen was introduced in this case (see Figure 4.22(a) and (c)). The start of combustion and cylinder peak pressure at 10 Nm load and hydrogen flow rate 21.4 l/min were quite accurately met the experimental results. The simulation cannot predict the combustion when hydrogen was added at the highest amount at low load as depicted in Figure 4.22(b). Experiment result shows that the combustion started later in the expansion stroke and resulted a small increase in cylinder pressure.



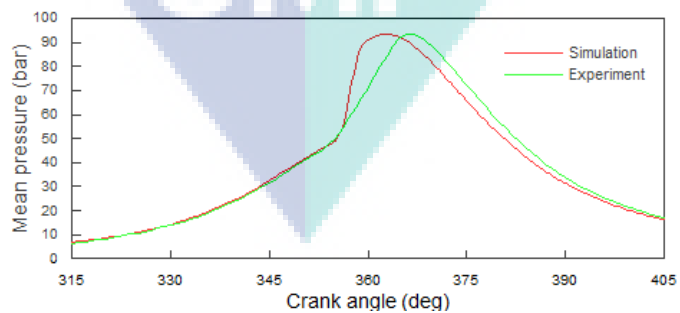
(a) 10 Nm, $H_2 = 21.4$ l/min



(b) 10 Nm, $H_2 = 49.6$ l/min



(c) 20 Nm, $H_2 = 21.4$ l/min



(d) 20 Nm, $H_2 = 49.6$ l/min

Figure 4.22. Comparison of cylinder pressure for dual fuel operation.

The comparison of simulation and experimental results of dual fuel operation at higher load is shown in Figure 4.22(c) and (d). The compression and expansion stroke

can be predicted quite accurately. The simulated ignition timing is about 2 degree earlier than the measured one in case of hydrogen addition at low flow rate. The pressure rise was faster, and the peak pressure was about 4 bar higher at advanced phasing. At higher hydrogen flow rate, faster combustion was predicted but the start of combustion and the peak pressure was almost the same but with the advanced phasing as can be seen in Figure 4.22(d).

4.5.4 Characteristics of Mixture Formation

In the dual fuel operation, the pilot diesel fuel was injected into the compressed hydrogen-air mixture during the compression stroke. The liquid fuel exits the injection nozzle at high speed and interacts with a highly compressed hydrogen-air mixture. As a result, the fuel jet disintegrates into small droplets. The drops are heated up as a result of convective heat transfer and temperature radiation of the hot chamber walls and the fuel finally begins to evaporate. Figure 4.23 depicts the injection rate profile and the corresponding fuel evaporation progress. The period between the start of injection and the start of combustion is the ignition delay. There are two process during the ignition delay: physical delay and chemical delay (Ganesan, 2012). During the physical delay period, the fuel is atomized, vaporized, mixed with air and raised to its self-ignition temperature. As can be observed from Figure 4.23, the evaporation started about 4 °CA after the injection started. It means that it takes about 0.33 ms for the injected fuel to disintegrate and be heated up before evaporated. It is seen that the injected fuel was completely evaporated at about 2 °CA after the end of injection.

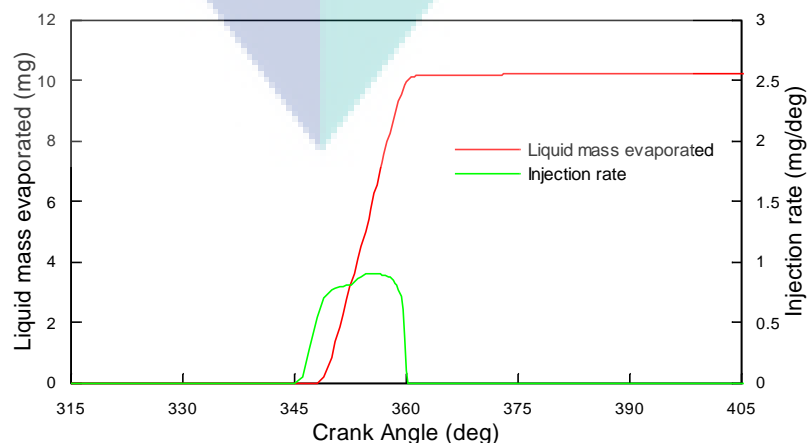


Figure 4.23. The injection rate and the evaporated fuel mass: case 2000 rpm, 20 Nm, H₂ flow = 42.8 l/min.

Figure 4.24 shows the spray evolution and the mass fraction distribution of diesel fuel (n-heptane) from 2 °CA after the start of injection until the TDC (360 °CA). From the top view of the cut plane at $Z = -3$ mm can be seen the influence of the swirl motion on the spray. The effect of swirl on the droplet path is highlighted, particularly for the droplets near the wall of the cylinder, where the tangential velocity is higher and the droplets have a small size with respect to the injected size (injection droplet radius = 105 μm , equal to the nozzle radius).

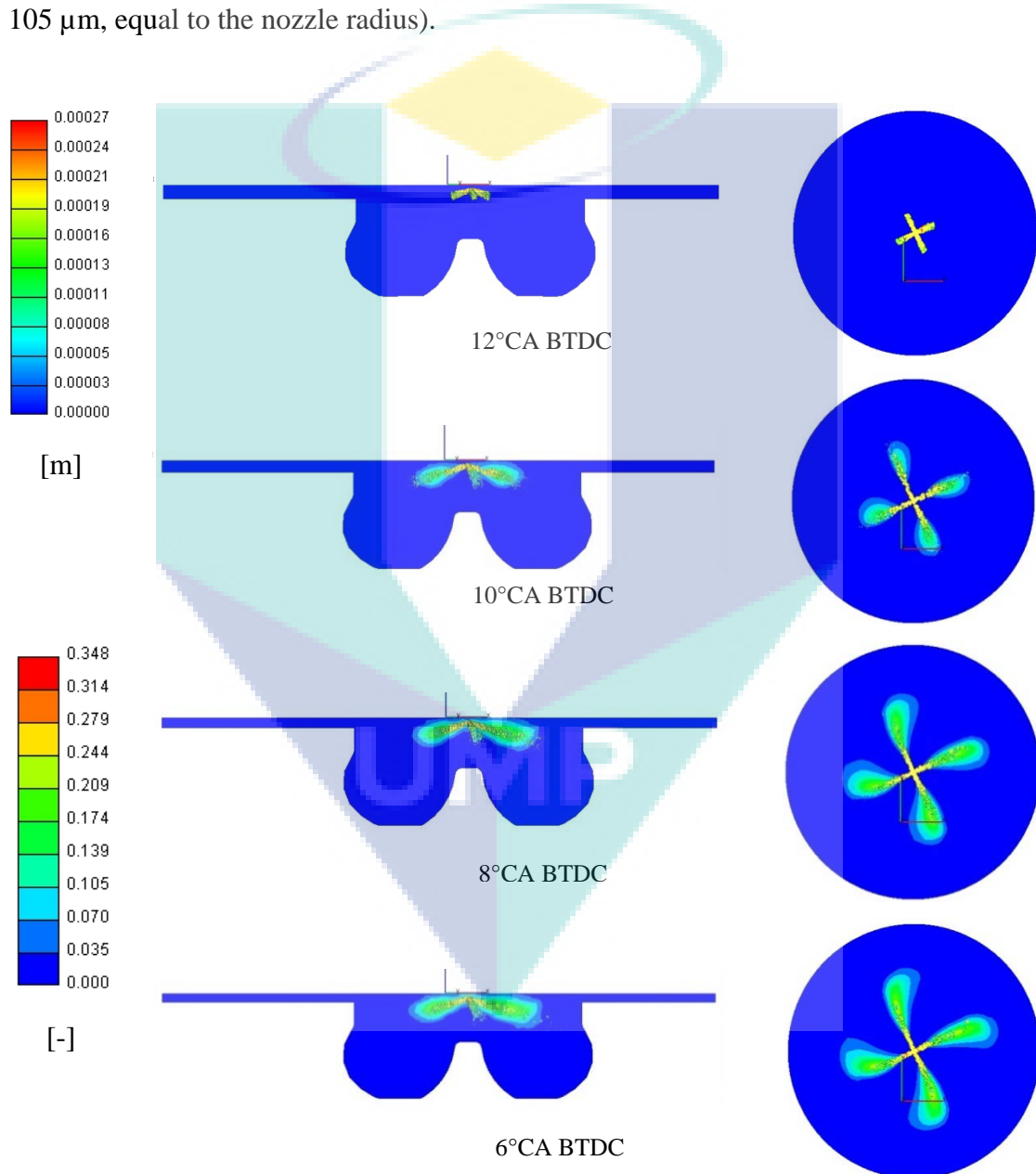


Figure 4.24. Spray evolution and the mass fraction distribution of diesel fuel: 2000 rpm, 20 Nm, H_2 flow = 42.8 l/min.

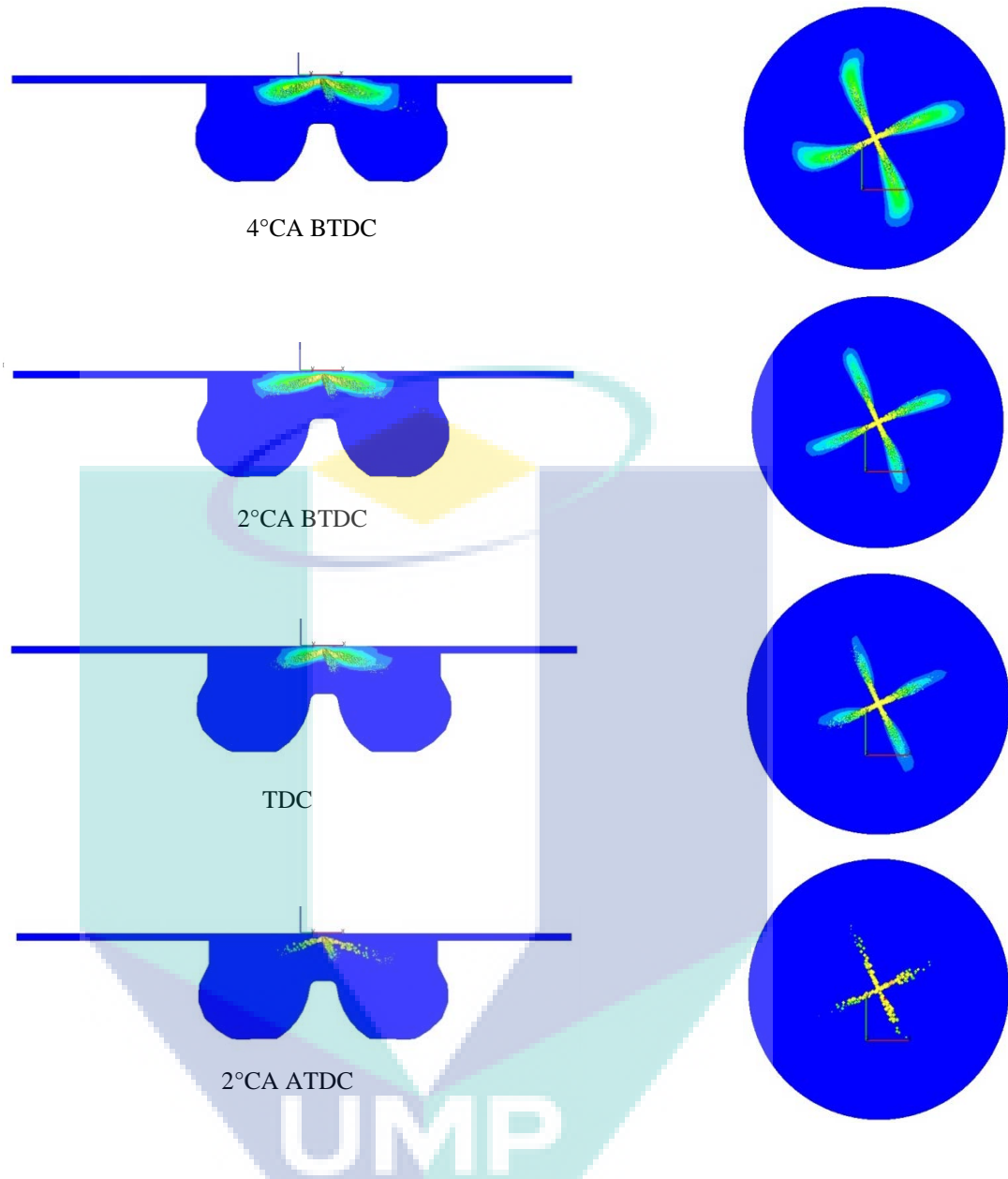


Figure 4.24. Continued.

Most of diesel fuel vaporizes near the spray tips; zones of main evaporation are located far from the nozzle direction. The smaller droplets that located on the outer part of the spray are first vaporized. It is noted from the both cut planes, the area of fuel vapour expanded until the start of ignition was commenced at 6 °CA before TDC. The diesel fuel vapour was then consumed rapidly until the piston reached TDC position. There are no more diesel vapour at these cut plane, however small amount of diesel vapour still existed in the cylinder.

4.5.5 Effects of Hydrogen Addition on Engine Combustion

Simulation results on the effect of hydrogen addition on cylinder pressures for engine operation at 10 and 20 Nm are illustrated in Figure 4.25. Hydrogen addition on the engine operation at 10 Nm resulted in the lower pressure. On the other hand, higher peak cylinder pressures were achieved when hydrogen was added at higher load.

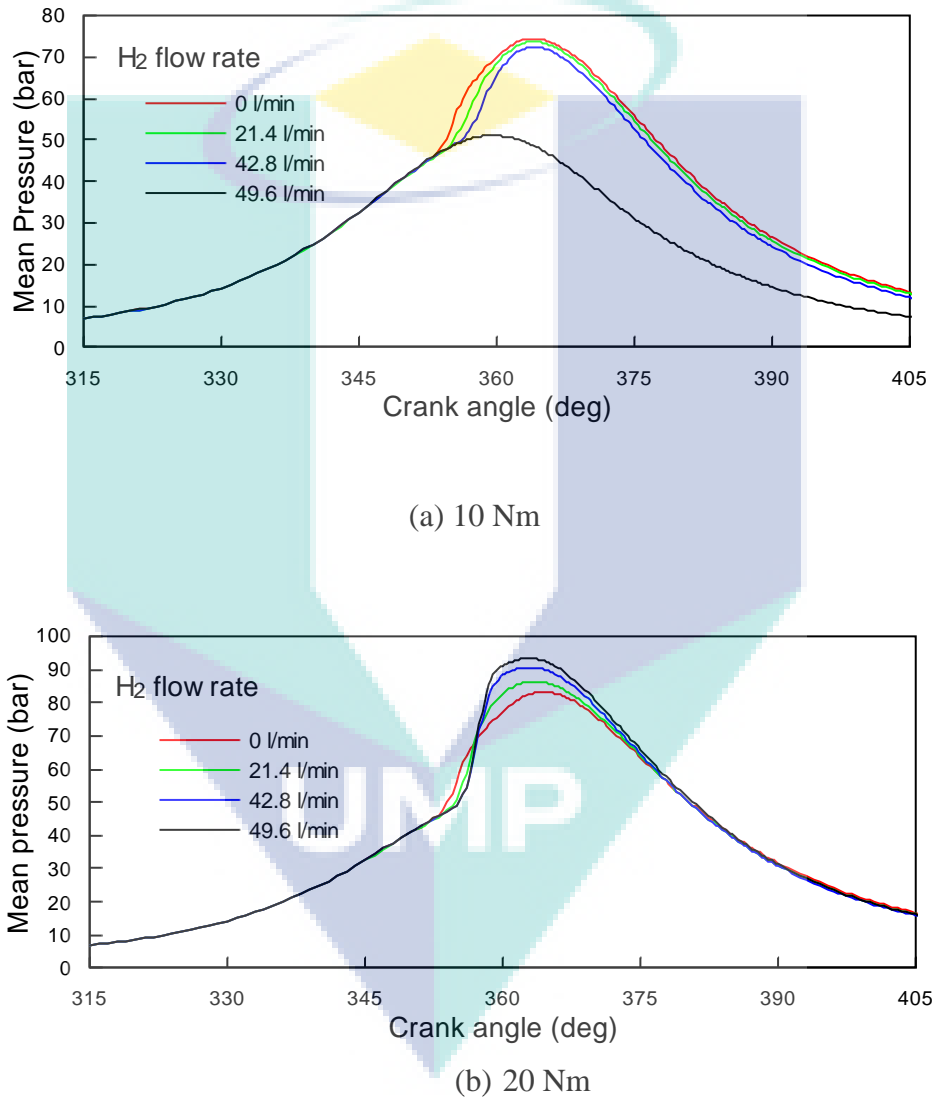


Figure 4.25. Simulation result of the effect of H₂ addition on cylinder pressures.

On the engine operation at 10 Nm load, higher hydrogen flow rates retards the start of combustion as can be observed in the rate of heat release graph as depicted in Figure 4.26(a). Hydrogen addition at 21.4 l/min retarded the start of ignition by 2 °CA and reduced of rate of heat release by 10 J/deg. The cylinder peak pressure was slightly

reduced at retarded phasing. Further hydrogen addition at 42.8 l/min retarded the start of by about 7 °CA. The peak value was almost the same with that of pure diesel operation. Thus, the peak cylinder pressure was lower due to late combustion. A very low heat release was noticed at hydrogen flow rate of 49.6 l/min, and no combustion was detected.

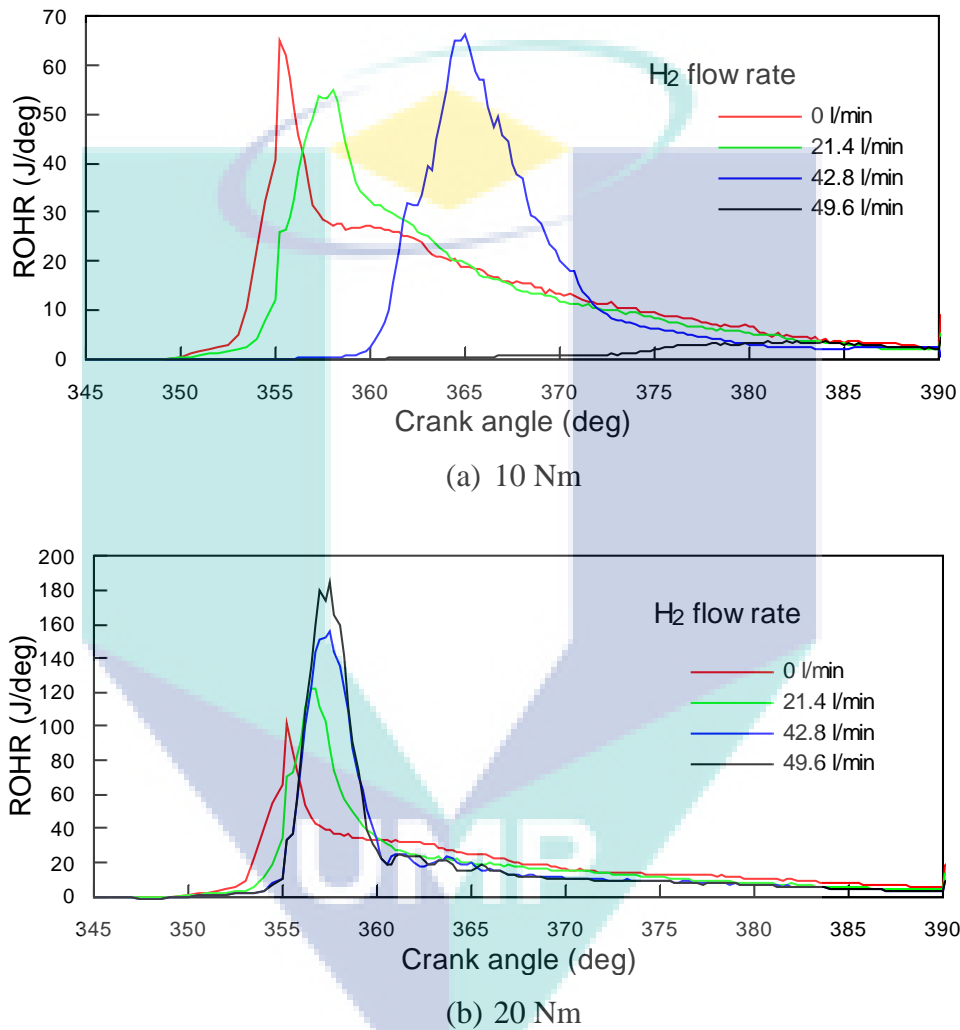


Figure 4.26. Simulation result of the effect of H₂ addition on rate of heat releases.

Figure 4.25(b) shows the simulation result of the effect of hydrogen addition on the cylinder pressures at 20 Nm load. In contrast to the case of lower engine load, hydrogen introduction at higher load resulted in higher cylinder pressures. Hydrogen addition slightly retarded the start of combustion but increased the peak value as shown in rate of heat release graph in Figure 4.26(b). Most of combustion occurred before

reaching the TDC. More heat was released with the increase of hydrogen flow rate resulted in higher cylinder peak pressures.

The start of ignition has an important role on the combustion process of dual fuel engine. The auto-ignition of diesel pilot fuel is a chain-branching process including the four reaction classes of chain initiation, chain propagation, chain branching, and chain termination. After the start of injection, ignition occurs after a certain period, the ignition delay. During this time delay, fuel droplet breakup and evaporates until a first region of ignitable mixture with an air-fuel ratio of $0.5 < \lambda < 0.7$ is formed (Baumgarten, 2006). The chemical reactions in this region have to produce enough fuel radicals in order to start the combustion process. The auto-ignition occurs when hydrogen peroxide (H_2O_2) that has been accumulating in the reactive mixture, begins to decompose producing two hydroxyl (OH) radicals (Warnatz, Maas, & Dibble, 2006). The importance of this reaction is clearly depicted in Figure 4.27. During the compression stroke, H_2O_2 was formed in the reactive mixture. The concentration of H_2O_2 decreases rapidly as OH radicals is being formed, increasing the temperature of the reacting mixture.

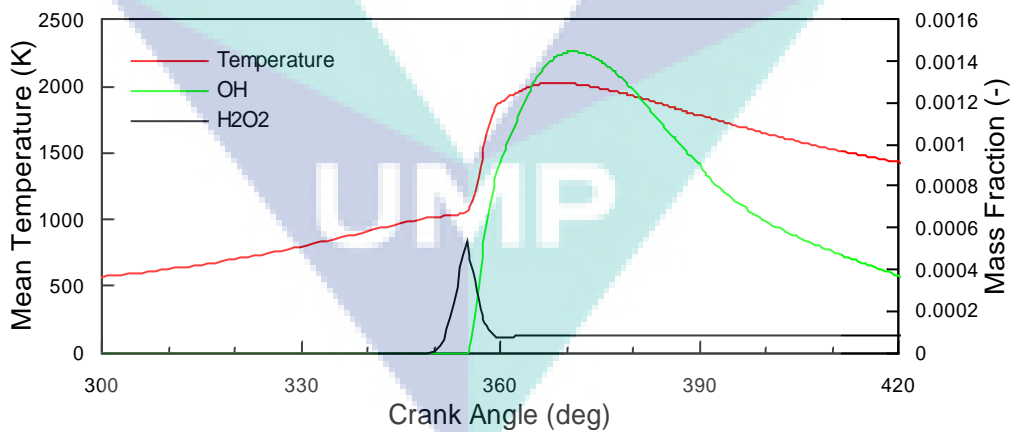
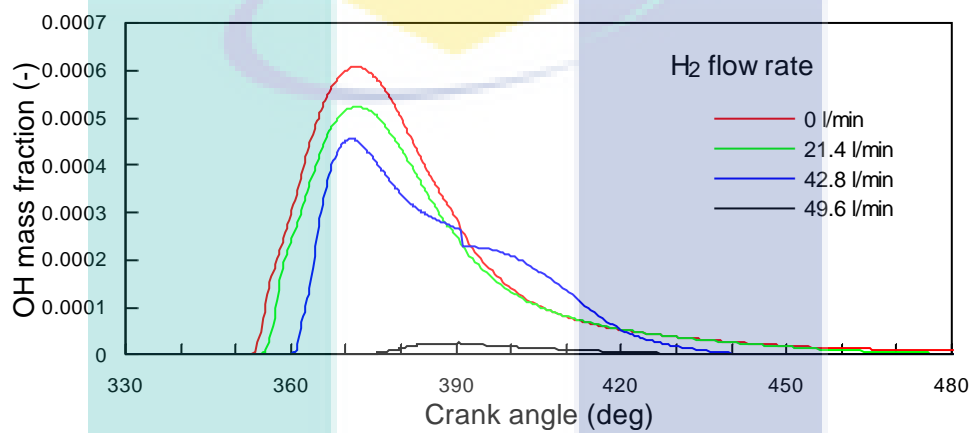


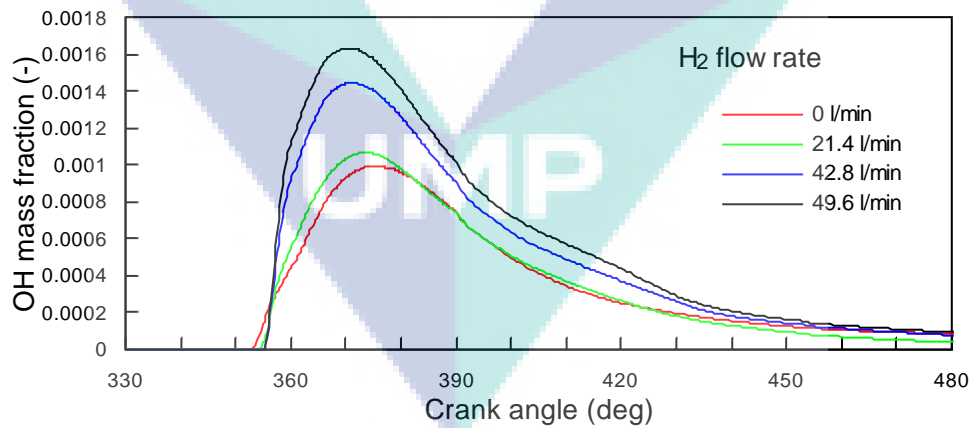
Figure 4.27. Radicals (H_2O_2 and OH) mass fraction decomposition and formation.

Figure 4.28 shows the effect of hydrogen addition on the formation of OH radical. In the engine operation of 10 Nm, hydrogen addition retarded the start of OH radicals' formation. The maximum OH mass fractions were also reduced with hydrogen

addition. OH formation will increase the in-cylinder temperature. When the start of OH formation was retarded, temperature increase was retarded as well. The start of formation and the amount of OH radical will influence the in-cylinder temperature as shown in Figure 4.29(a). In case of hydrogen addition at higher load, the start of OH formations were slightly retarded but the maximum value of OH radicals' mass fraction were higher. The start of temperature rise was slightly retarded. Faster combustion was noted at higher hydrogen flow rate, resulted in higher temperature as illustrated in Figure 4.29(b).

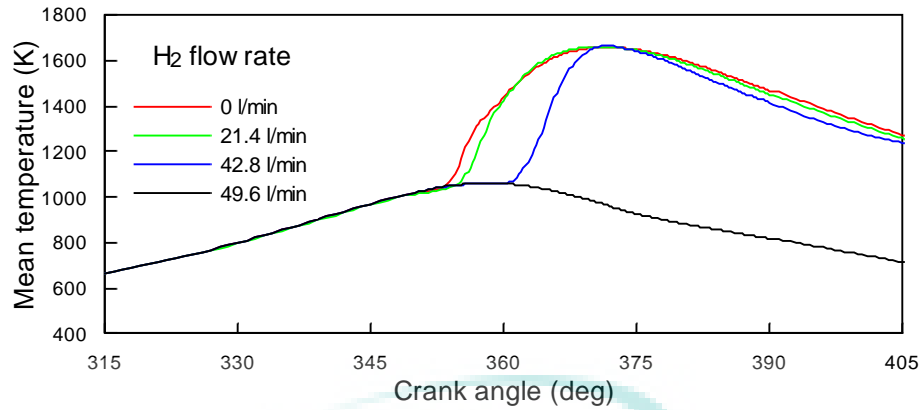


(a) 10 Nm

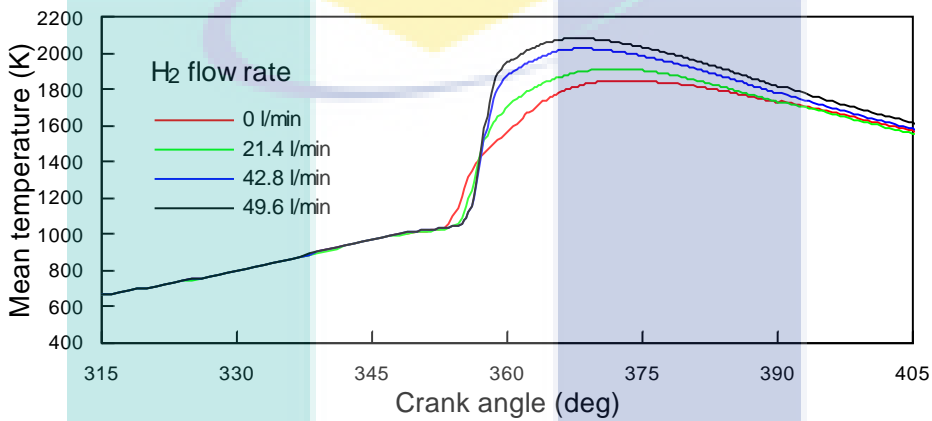


(b) 20 Nm

Figure 4.28. Time-histories of average OH mass fraction.



(a) 10 Nm



(b) 20 Nm

Figure 4.29. Effect of hydrogen addition on cylinder temperature.

During the combustion process, hydrogen was consumed when the combustion initiated by the diesel pilot was commenced. The progress of hydrogen consumptions are illustrated in Figure 4.30. For hydrogen flow rate of 21.4 l/min, the initial mass fractions at low and high load operations were 0.0028 and 0.0033 respectively. At the end of calculation at 130 °CA after TDC the mass fraction became 0.000529 and 0.000376 respectively. It means that around 81 % and 89 % of hydrogen were converted into the combustion products. In case of the highest hydrogen flow rate of 49.6 l/min applied, the initial and final hydrogen mass fractions for low load operation were 0.0091 and 0.0080 respectively. Less than 12 % of hydrogen was converted into the combustion products. For higher load operation, around 89 % of hydrogen can be converted. The hydrogen conversion rate for both cases is shown in Figure 4.31. Hydrogen conversion rate for engine operation at 20 Nm are around 90 % for all hydrogen flow rate. For a lower load, a high conversion rate around 80 % was achieved for hydrogen flow rate of 21.4 and 42.8 l/min, but it dropped to 12 % for higher

hydrogen flow rate. It means that only small amount of hydrogen was combusted. The amount of diesel pilot fuel in this likely cannot sustain the combustion (Ganesan, 2012). A very small amount of OH radical was produced and it was occurred in the expansion stroke (about 20 °CA ATDC) as illustrated in Figure 4.28(a). The combustion almost undetected as shown by the in-cylinder temperature. Only small amount of hydrogen was converted into the combustion product.

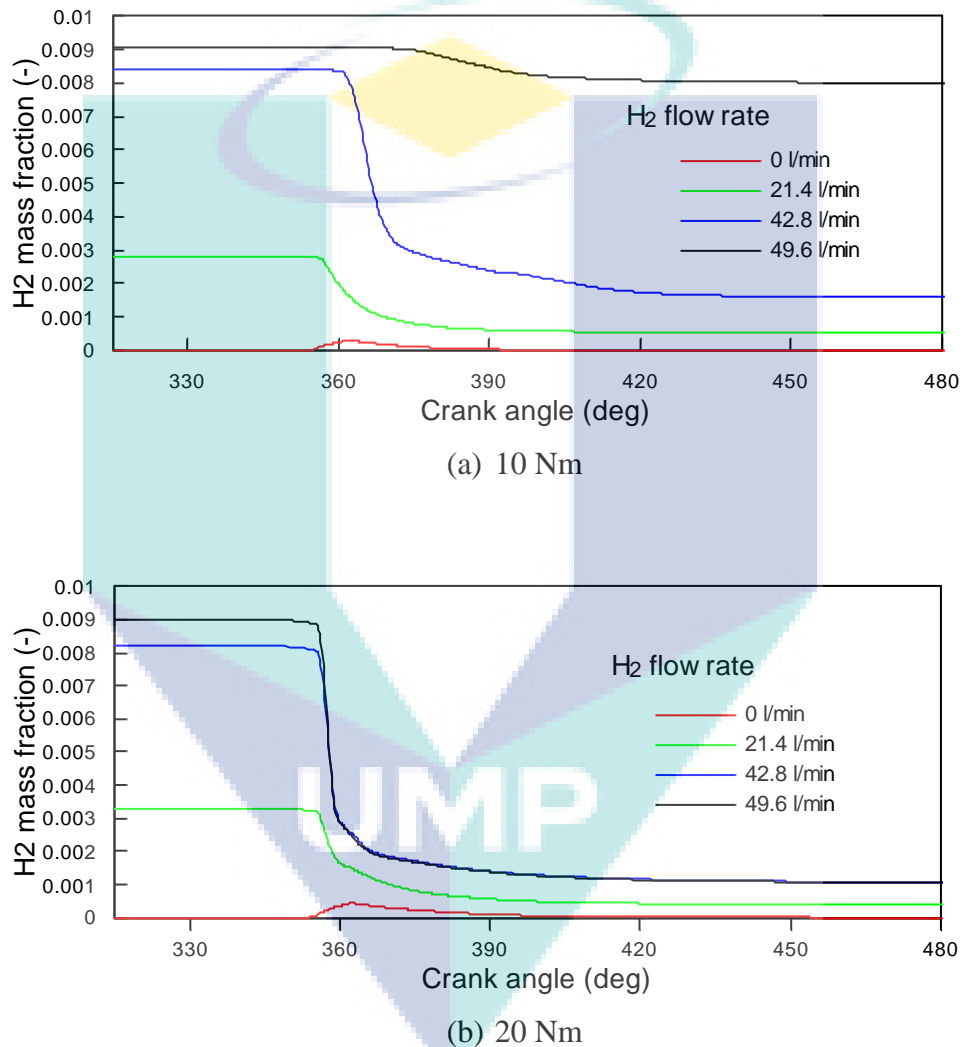


Figure 4.30. Time-histories of average hydrogen mass fraction.

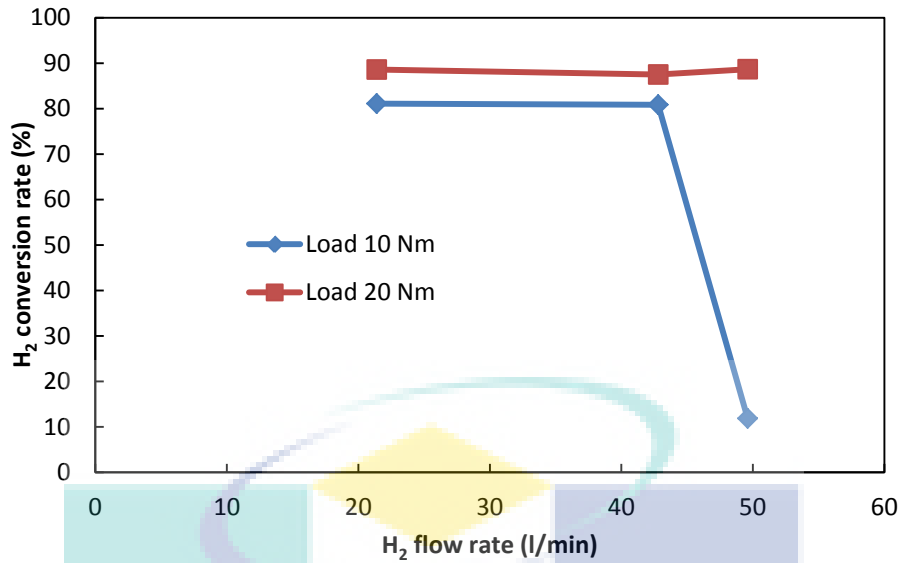


Figure 4.31. Effect of hydrogen addition on hydrogen conversion rate.

4.5.6 Characteristics of Diesel Dual Fuel during Compression and Combustion

The spatial distributions of the instantaneous values of the various variables such as velocity, temperature and the species mass fraction change continuously with time as the piston move from BDC to TDC and as combustion takes place. Investigation of the changes of these distributions can provide further understanding of how the mixture formation and the combustion take place. The different key physical and chemical factors that affect the combustion of hydrogen-air mixture and the pilot diesel fuel are of interest in this investigation.

A specific representative operating condition at the speed of 2000 rpm and the load of 20 Nm was chosen for this purpose. Dual fuel operation with hydrogen addition at the flow rates of 42.8 l/min was the focus of investigation. The distribution of the variables under investigation was visualized at the cut plane located along the spray axis and at the position of 1 mm under the bottom plane of the cylinder head.

Figure 4.32 shows the typical distributions of velocity and the surrogate diesel fuel (n-heptane) mass fraction 2 °CA after the start of pilot injection, at 14 °CA before TDC. It can be observed that there are strong swirls at the top of piston bowl caused by the intake generated swirl as shown in Figure 4.32(a). High velocity was noted near the

edge of piston bowl. In this location, the intensive squish turbulent was also detected as illustrated in Figure 4.32(b). These swirl and squish flow affect the liquid fuel distribution due to the tangential velocity as shown in Figure 4.32(c) and (d), and accordingly the distribution of other species within the combustion chamber.

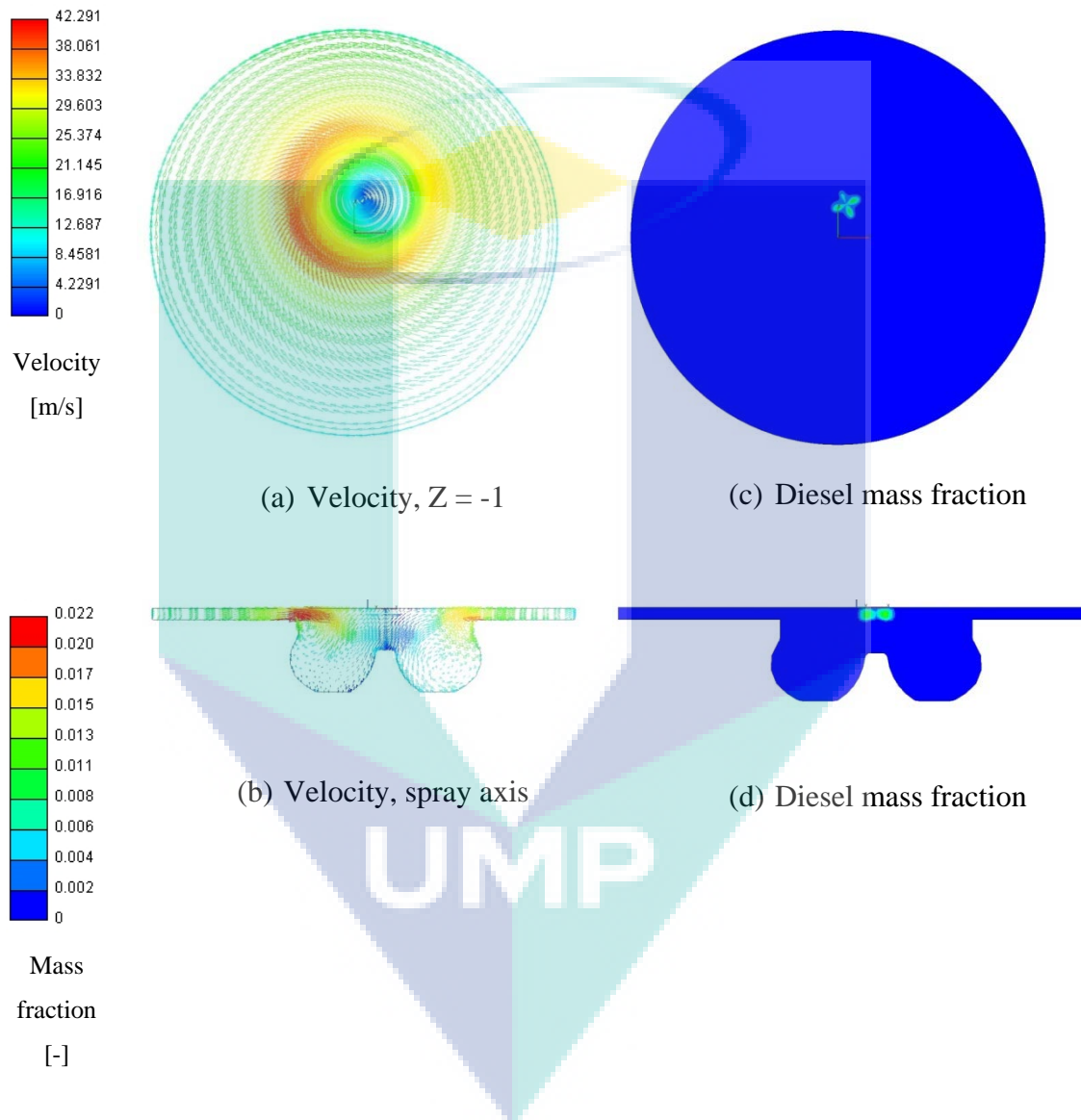


Figure 4.32. Velocity and diesel (nC_7H_{16}) mass fraction distribution at 12 °CA before TDC.

It was assumed that the diesel pilot fuel temperature during injection was 350 K. The initial cylinder temperature at the start of calculation was 488 K. The mean cylinder temperature increased during compression and reach about 1000 K at 12 °CA BTDC. The temperature distribution was homogeneous because the combustion has not initiated yet. The temperature was slightly lower at the spray position due to the lower fuel temperature as depicted in Figure 4.33(a). The corresponding mass fraction distribution of oxygen and hydrogen are shown in Figure 4.33(b) and (c) respectively. Mass fraction distribution was homogeneous due to assumption that hydrogen-air mixture was homogeneous at the start of calculation. The oxygen and hydrogen mass fraction at this position were 20.79 and 0.82 % respectively. The mass fractions of these species were slightly lower due to spray occupation at the nozzle position.

Figures 4.34-4.37 illustrated the commencement of the combustion process. The combustion started around 5 °CA before TDC when the formation of OH radical began as shown in Figure 4.28 and Figure 4.36. Some figures below give an illustration of the commencement of the combustion in more detail. Figure 4.34 shows the temperature distribution across the cut planes at 4 °CA before TDC. There are four regions with the highest temperature in the vicinity of the fuel spray, which are also the regions where the ignition first started. The corresponding mass fraction distributions of carbon monoxide in Figure 4.35 also indicate these regions of ignition. It can be noticed that more carbon dioxide was formed at that moment as shown in Figure 4.37. Small amount of carbon dioxide was defined as the initial value at the start of calculation. The formation of CO₂ due to combustion appears to lag by nearly 5 °CA behind that of CO as shown in Figure 4.38.

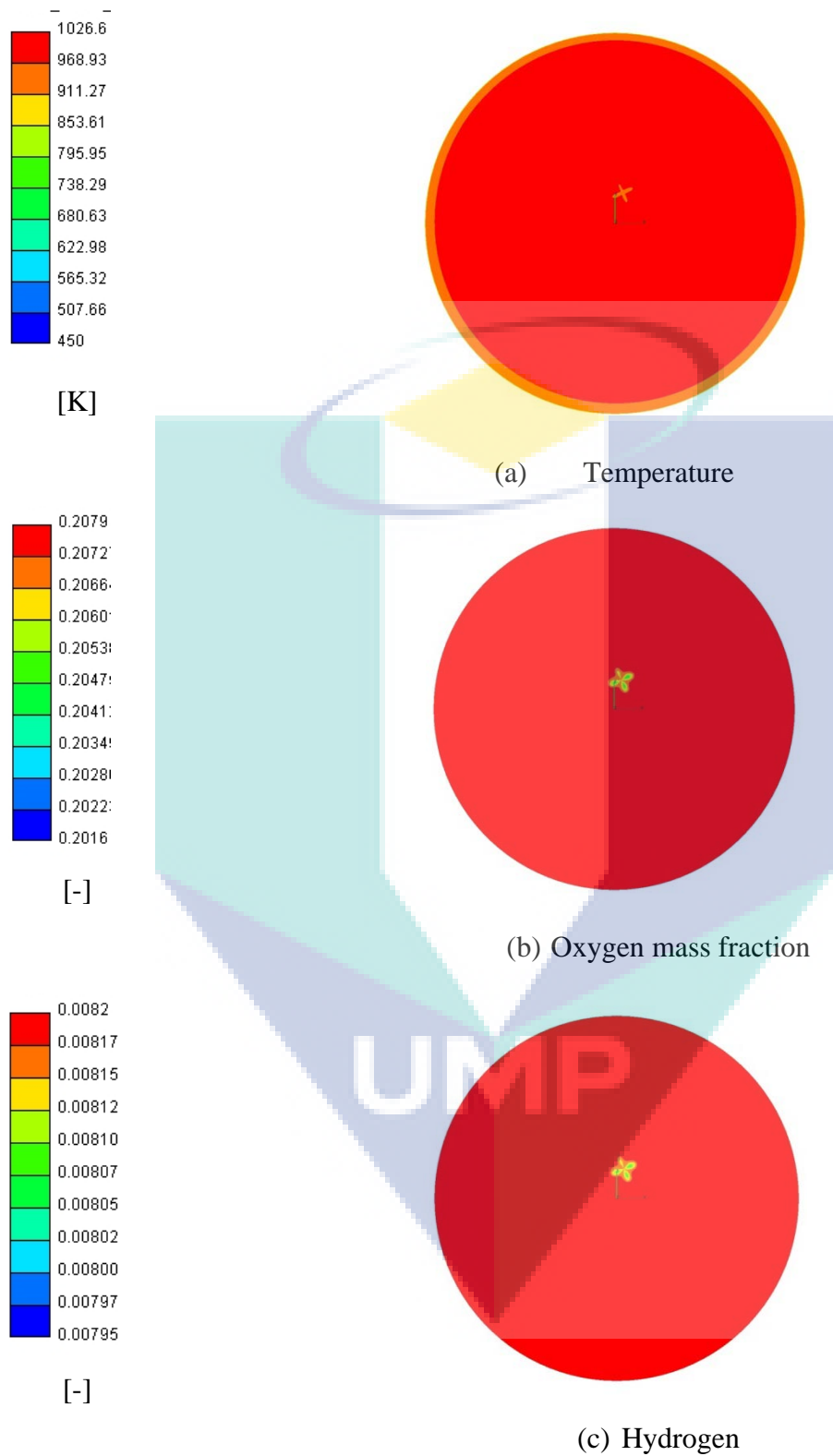


Figure 4.33. Temperature and species mass fraction distribution at 12 °CA before TDC.

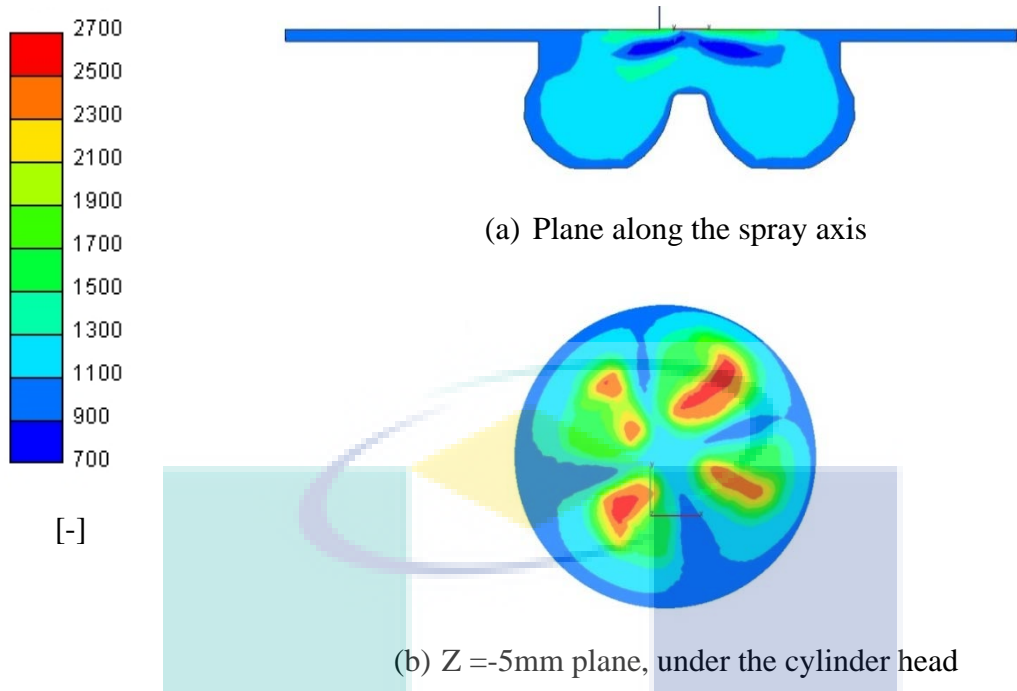


Figure 4.34. Temperature distribution at 4 °CA before TDC.

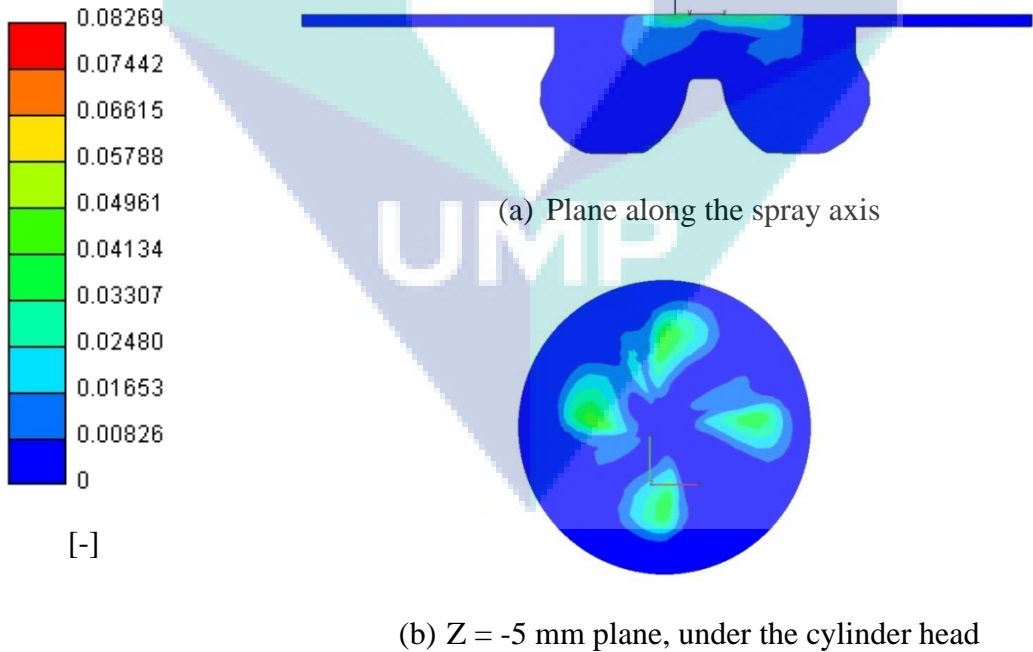


Figure 4.35. Carbon monoxide mass fraction distribution at 4 °CA before TDC.

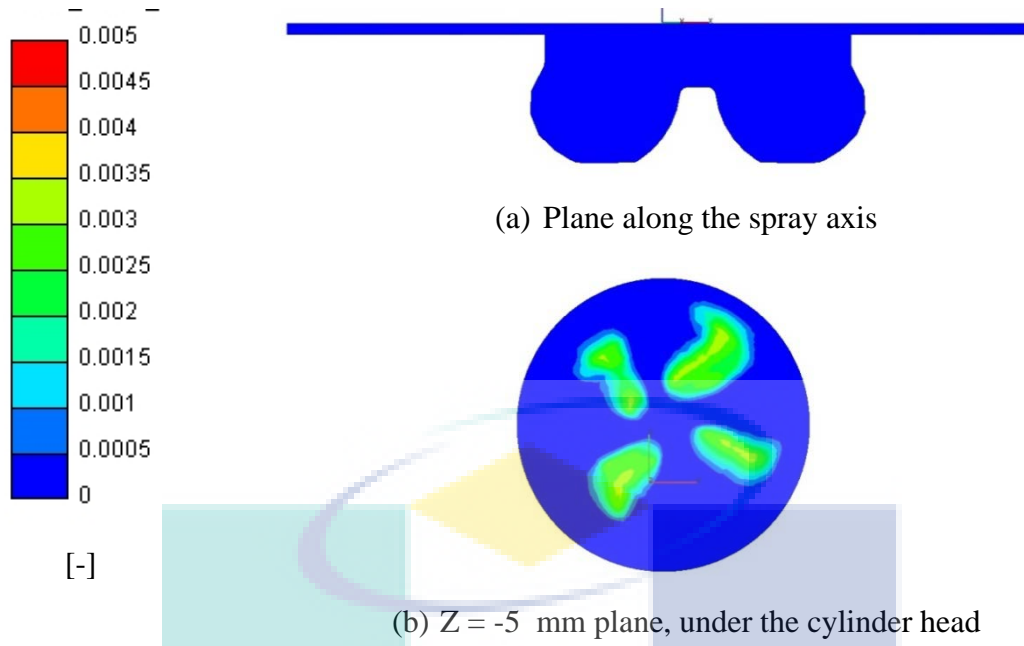


Figure 4.36. OH mass fraction distribution at 4 °CA before TDC.

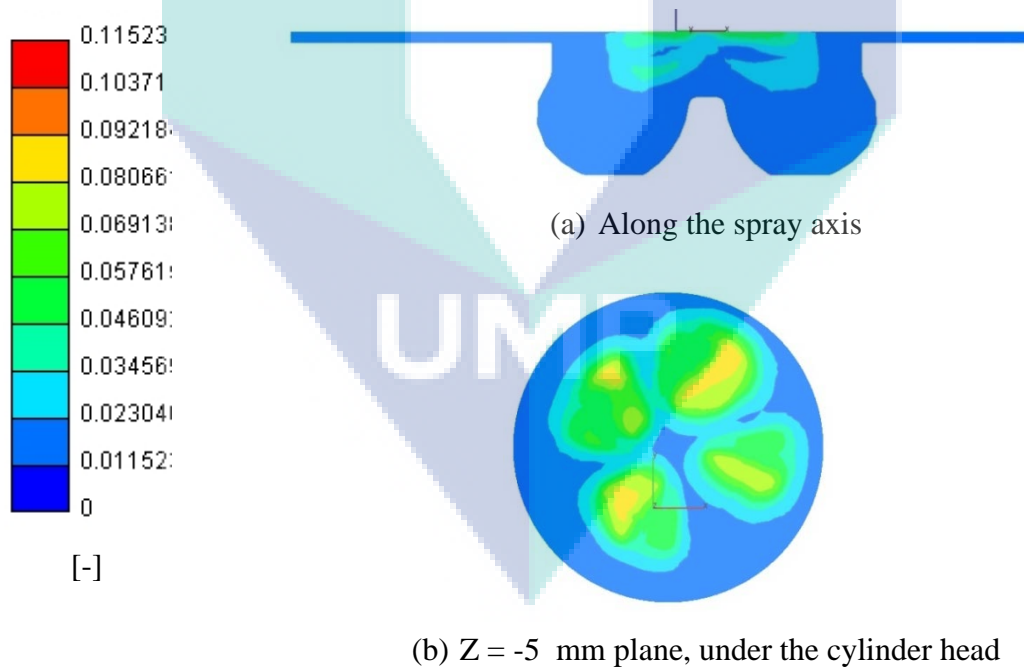


Figure 4.37. Carbon dioxide mass fraction distribution at 4 °CA before TDC.

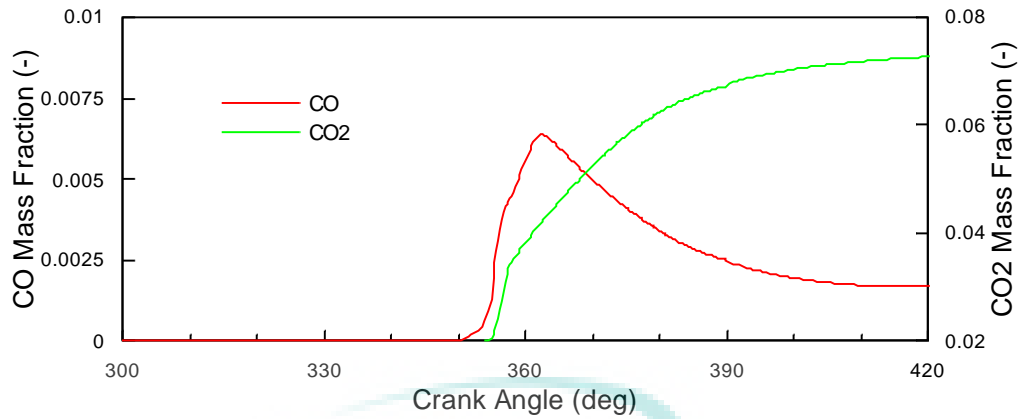


Figure 4.38. Time-histories of average carbon monoxide and carbon dioxide concentration.

The combustion process after the start of combustion is depicted in Figures 4.39-4.44. The ignition was initiated by the diesel pilot fuel and the flame then propagated to combust the hydrogen-air mixture. Hydrogen was rapidly consumed during the time of start of combustion until top dead centre as discussed earlier and has been shown globally in Figure 4.30. The hydrogen mass fraction distribution during this fast combustion is shown in Figures 4.39-4.40. Hydrogen occupied almost all the cylinder volume at 5-4 °CA BTDC. The areas where the hydrogen mass fractions were reduced seem to be occupied by the diesel vapour as described in the mixture formation discussion. On the next step, 3 °CA BTDC, the majority of hydrogen was located near the wall of piston bowl and the squish area. Small amount of hydrogen was also noticed under the cylinder head which was not affected by the combustion as can be seen in Figure 4.40. The hydrogen was then consumed by the flame propagation that started in the vicinity of the spray towards the piston bowl as shown by the temperature distribution in Figure 4.41-Figure 4.42. As can be seen at the spray cut plane, the area in the vicinity of the spray shows the temperature increase. The area then spread towards the piston bowl as the flame propagated. The flame propagation in the radial direction can be illustrated by the temperature distribution in the cut plane under the cylinder head as illustrated in Figure 4.42. The mean cylinder temperature increased from 1060 K until 1880 K during this compression stroke.

The combustion process can also be characterised by the consumption of oxygen. The fuel alongside the oxygen was taken part in the combustion process. Diminishing of oxygen during combustion process in the compression stroke is depicted

in Figure 4.43. The similar shape of oxygen distribution with that of hydrogen and temperature represented the combustion process of this dual fuel engine. During this compression stroke, the hydrogen near the cylinder liner wall has not been combusted yet as noticed in Figure 4.39. It is confirmed by Figure 4.43 that oxygen near the cylinder wall has not combusted until the TDC, and the flame propagation has not reached the wall as shown by temperature distribution in Figure 4.41.

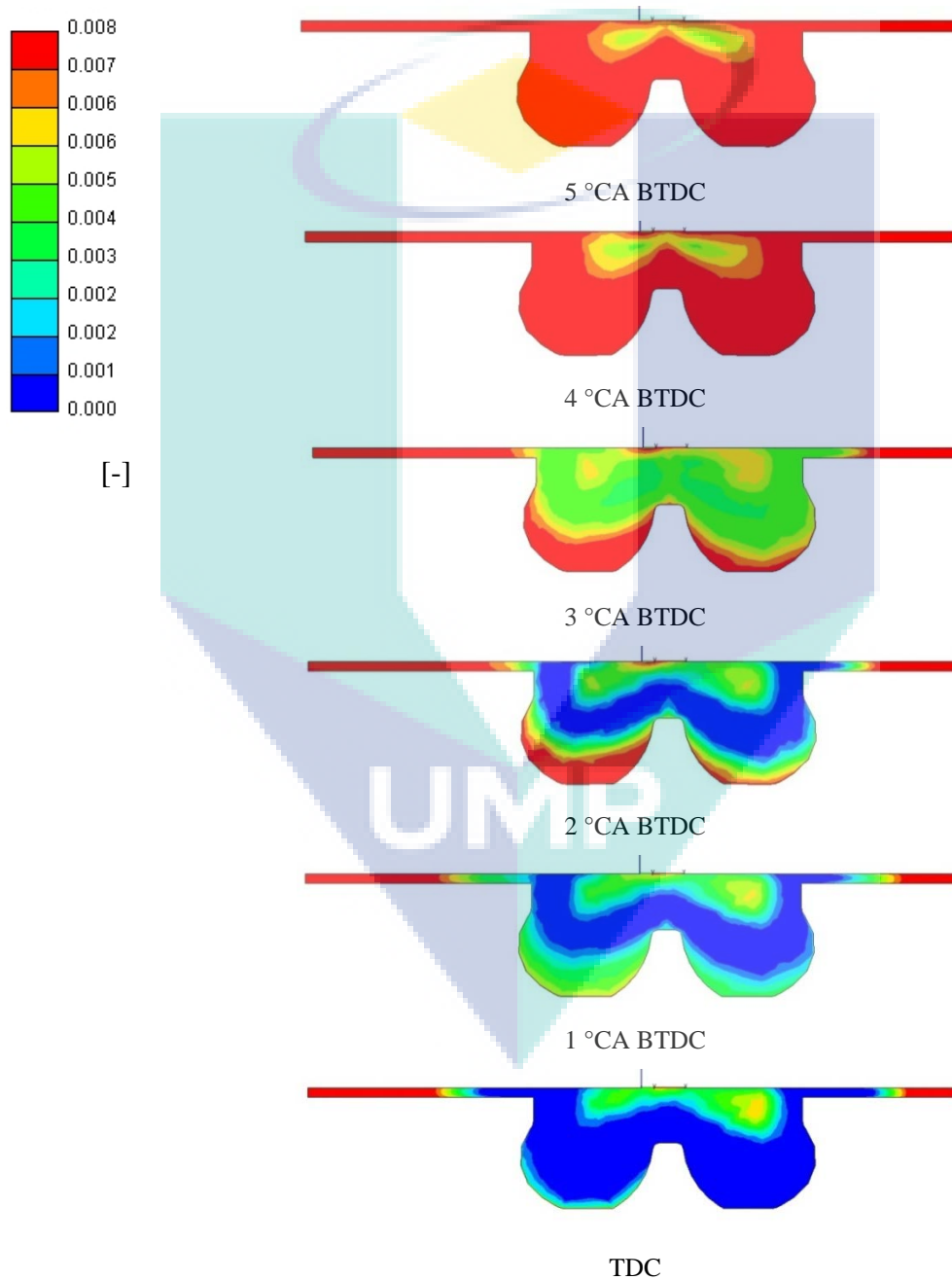


Figure 4.39. Hydrogen mass fraction distribution from 5°CA BTDC until TDC, cut plane along the spray axis.

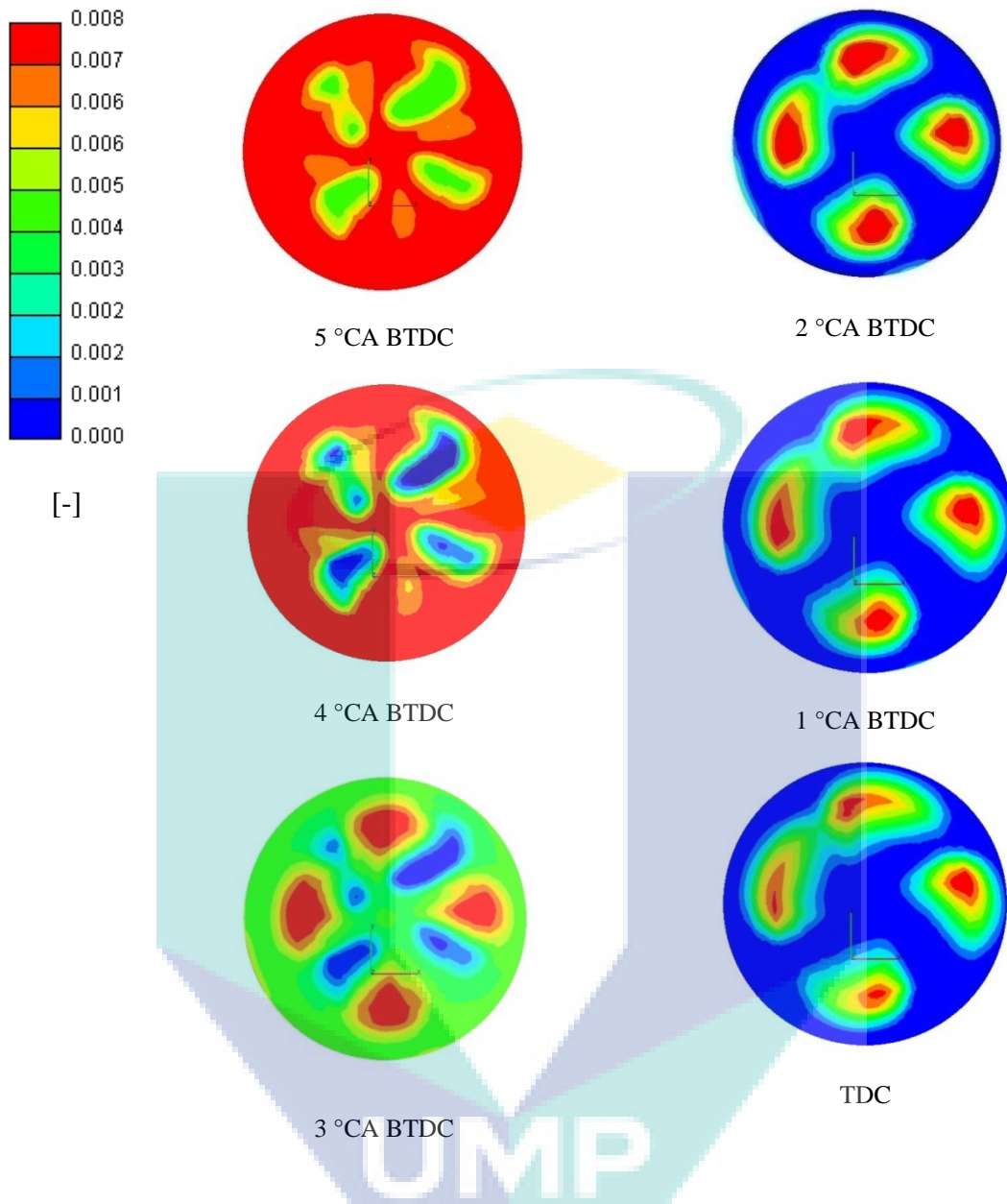


Figure 4.40. Hydrogen mass fraction distribution from 5°CA BTDC until TDC, cut plane at Z=-5 mm.

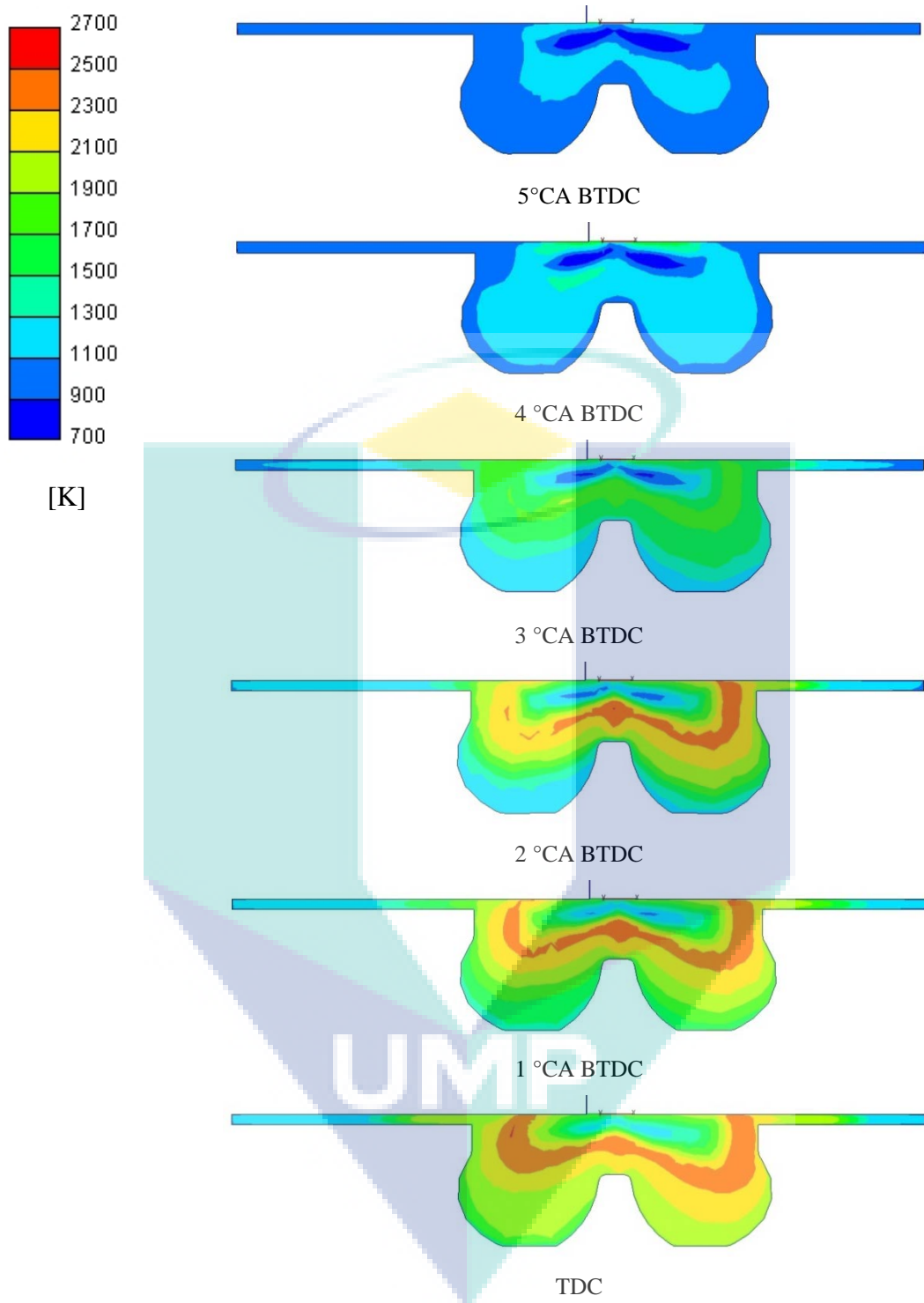


Figure 4.41. Temperature distribution across the spray axis from 5°CA BTDC until TDC.

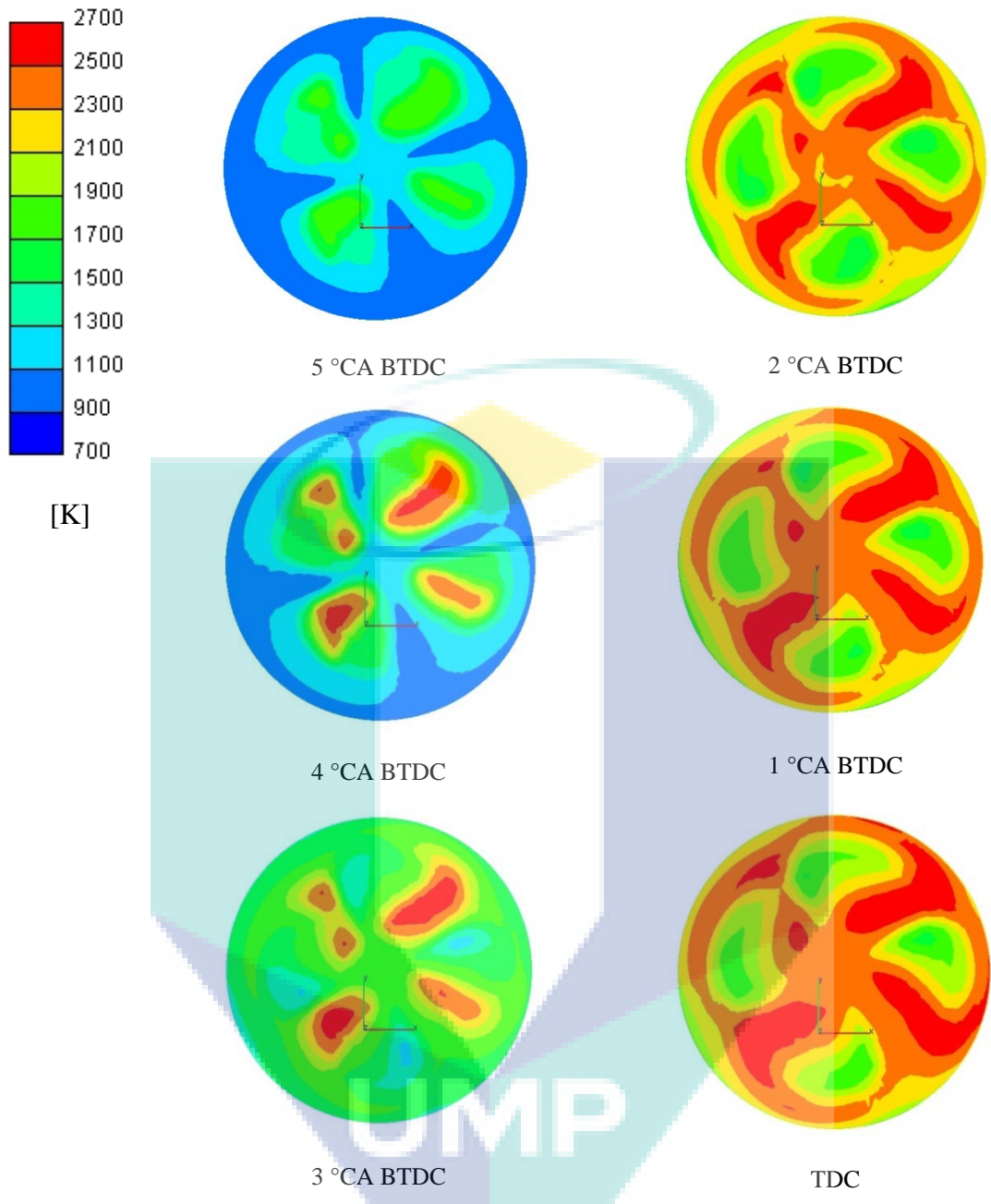


Figure 4.42. Temperature distribution from 5°CA BTDC until TDC, cut plane Z = -5 mm.

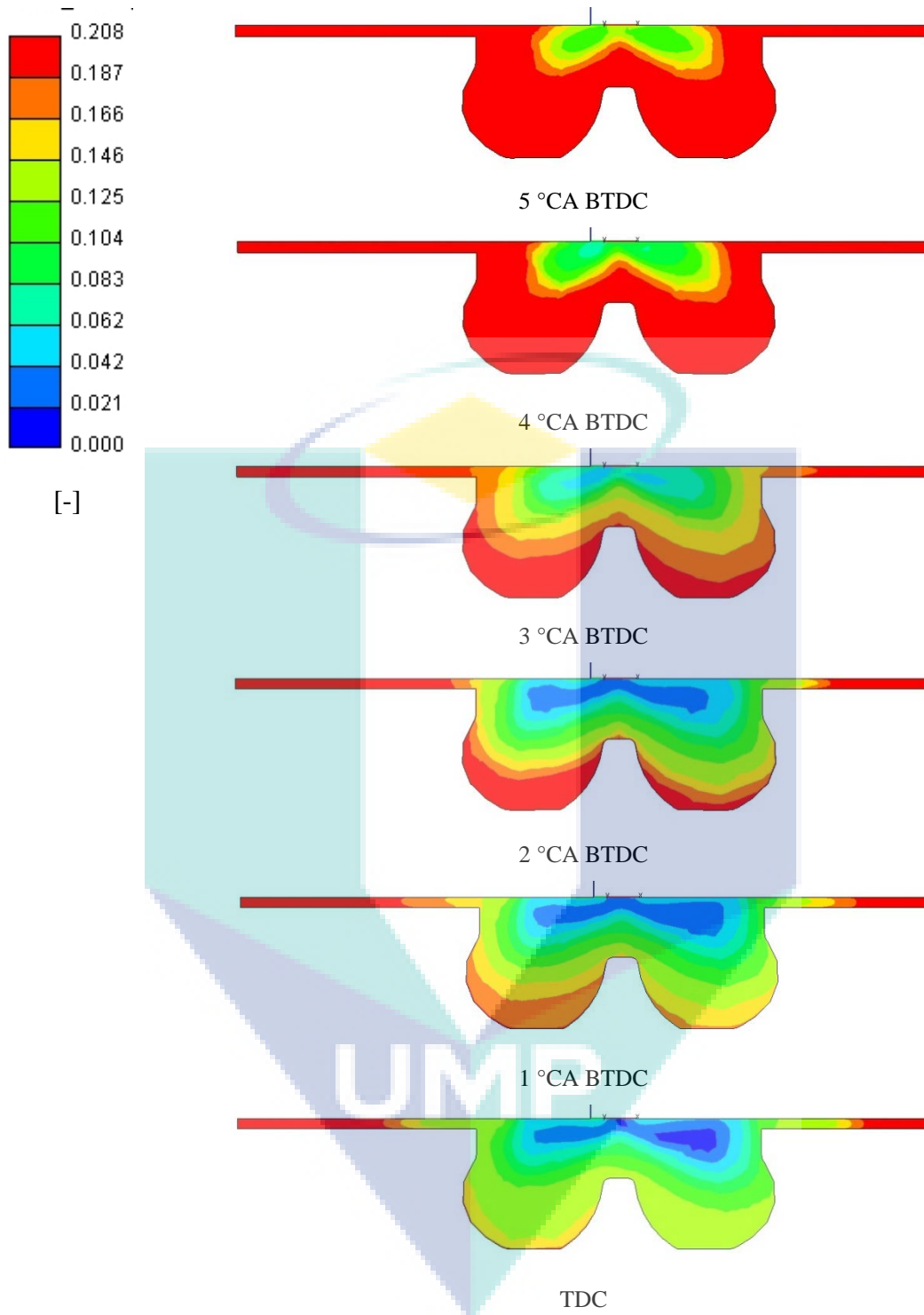


Figure 4.43. Oxygen mass fraction distribution across the spray axis from 5°CA BTDC until TDC.

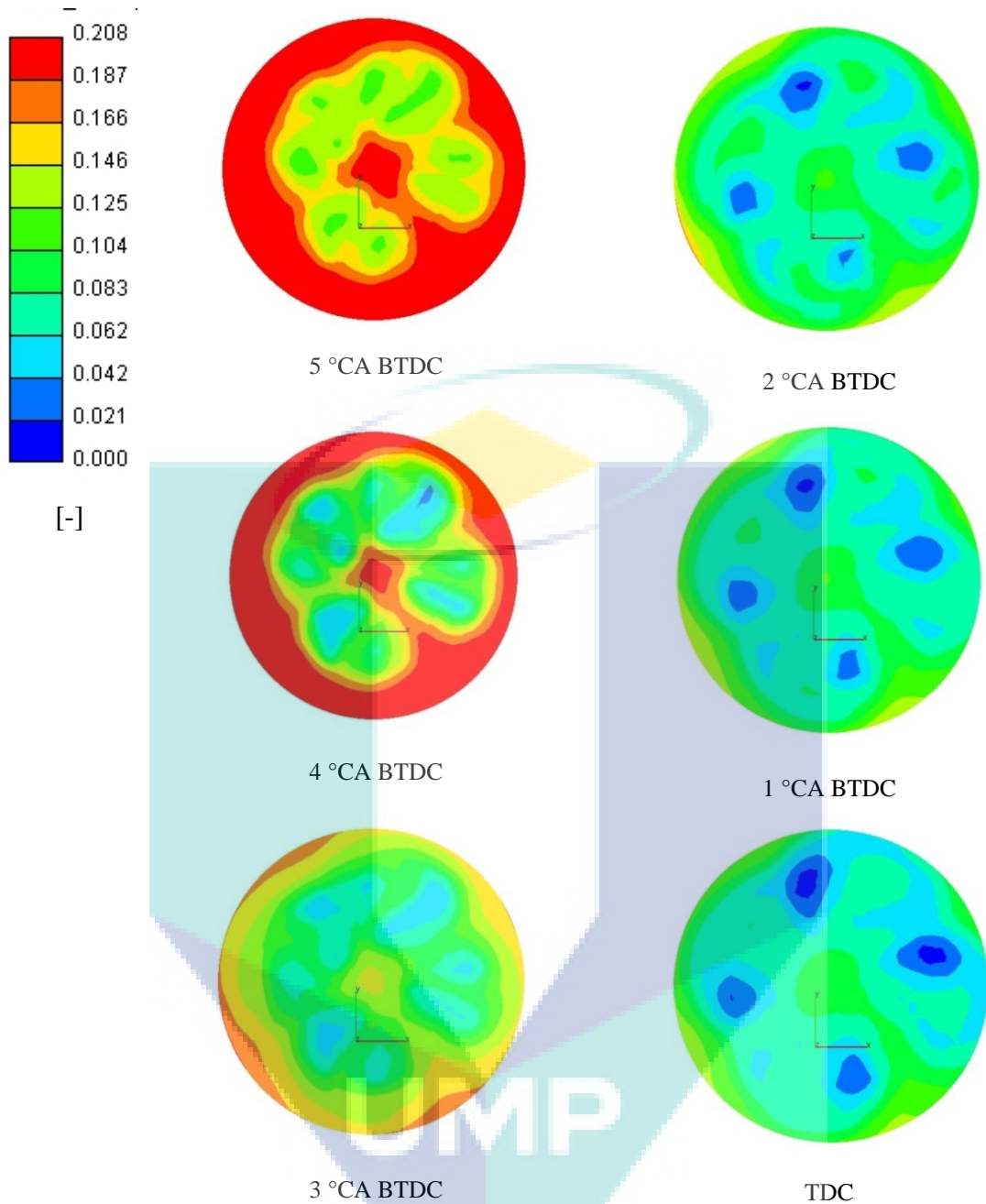


Figure 4.44. Oxygen mass fraction distribution from 5°CA BTDC until TDC, cut plane $Z = -5$ mm.

Combustion process from the start of ignition until the TDC was characterized by the fast heat release rate. The mean mass fraction of the pilot fuel (n-heptane) and the main fuel (hydrogen) is shown in Figure 4.45. It is noticed that hydrogen was oxidized rapidly some degrees crank angle after the ignition of diesel fuel started. It can be seen by the rapid degradation of hydrogen mass fraction when reaching the TDC. The similar

fast consumption of pilot fuel was also noticed. The slower combustion was observed during the expansion stroke when most of the fuels have been oxidized.

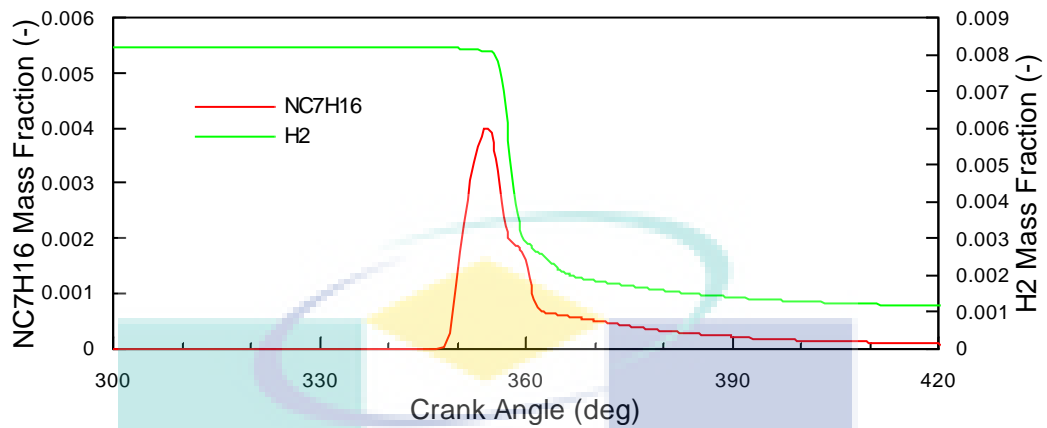


Figure 4.45. Time-histories of mean n-heptane and hydrogen concentration.

Figures 4.46-4.48 depict the progress of temperature distribution, hydrogen mass fraction, and oxygen mass fraction respectively at different crank angles according to time sequence starting from 4 °CA until 20 °CA after TDC. During this expansion stroke, the flame propagated toward the cylinder liner wall as shown by temperature progress in Figure 4.46. The hottest temperature area moved via the squish area to reach the liner wall. The mean temperature increased until 9°CA ATDC and then gradually decreased. This can be seen on the temperature distribution at frontal cut plane ($Z = -5$ mm). Distribution of hydrogen and oxygen shown in Figures 4.47-4.48 confirmed the flame propagation and the combustion process. The hydrogen mass fraction distribution in Figure 4.47 gives the illustration of the progress of hydrogen oxidation in the radial direction to the cylinder wall.

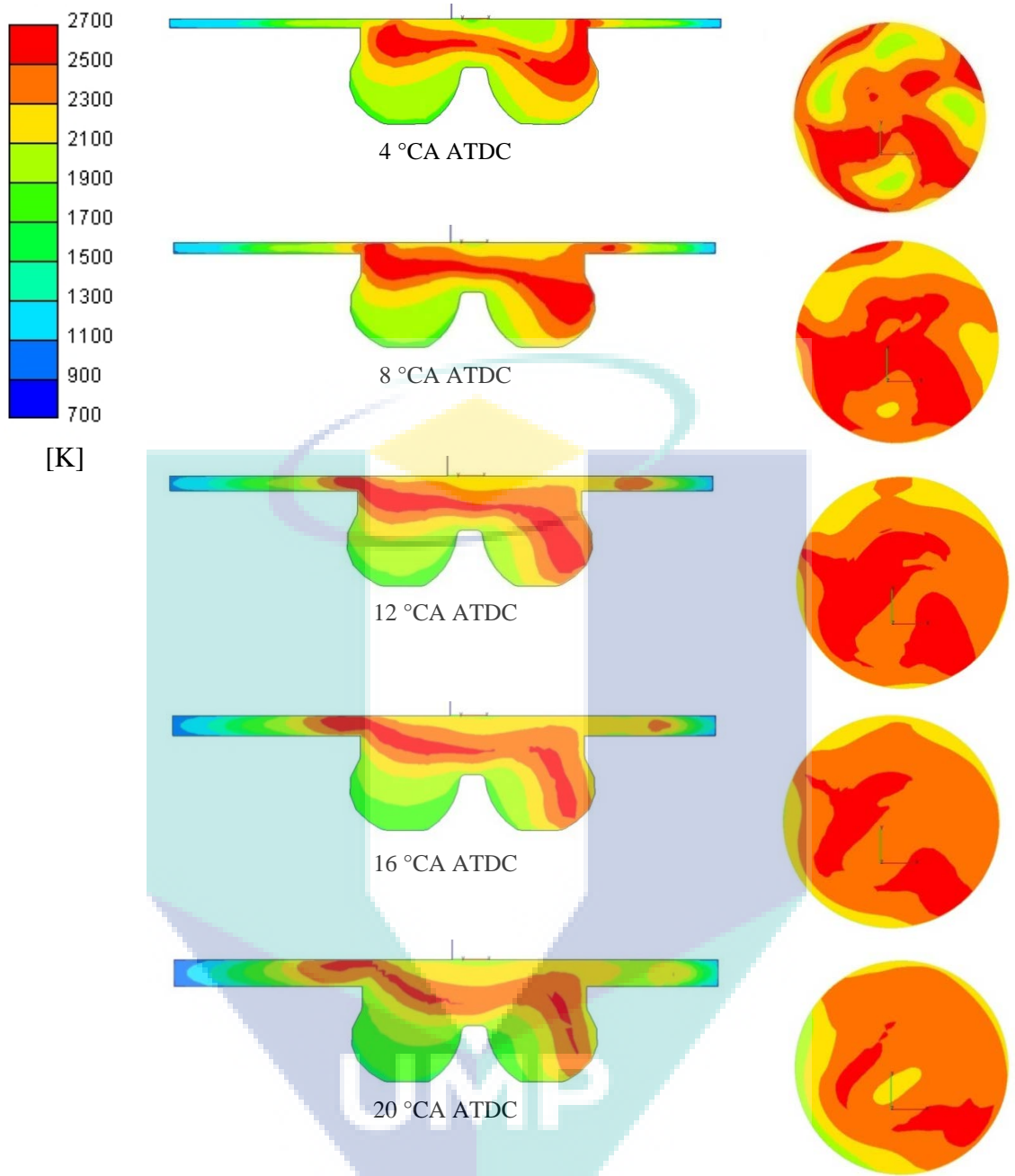


Figure 4.46. Progress of temperature distribution from 4°CA-20°CA ATDC.

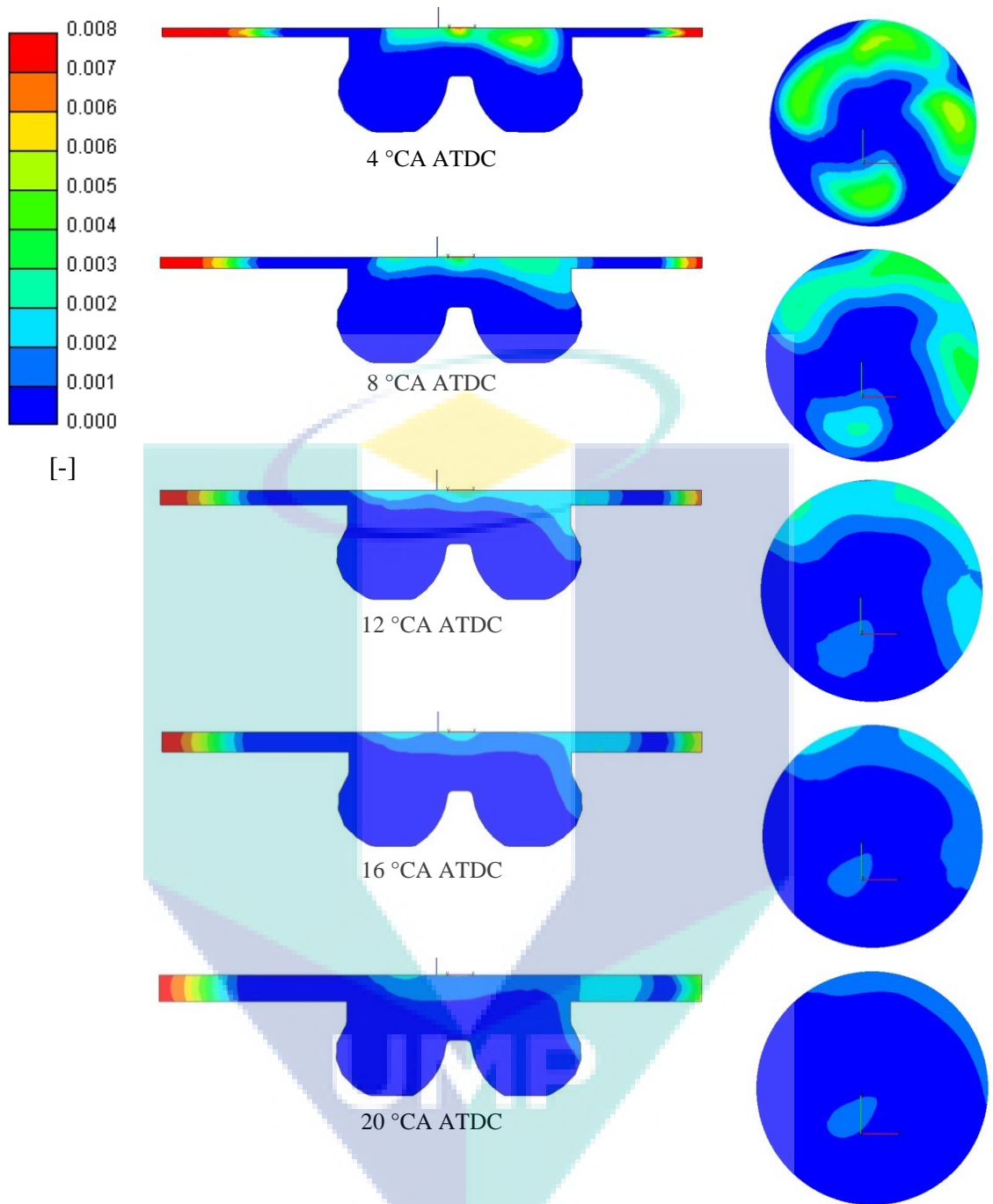


Figure 4.47. Progress of hydrogen mass fraction distribution from 4°CA-20°CA ATDC.

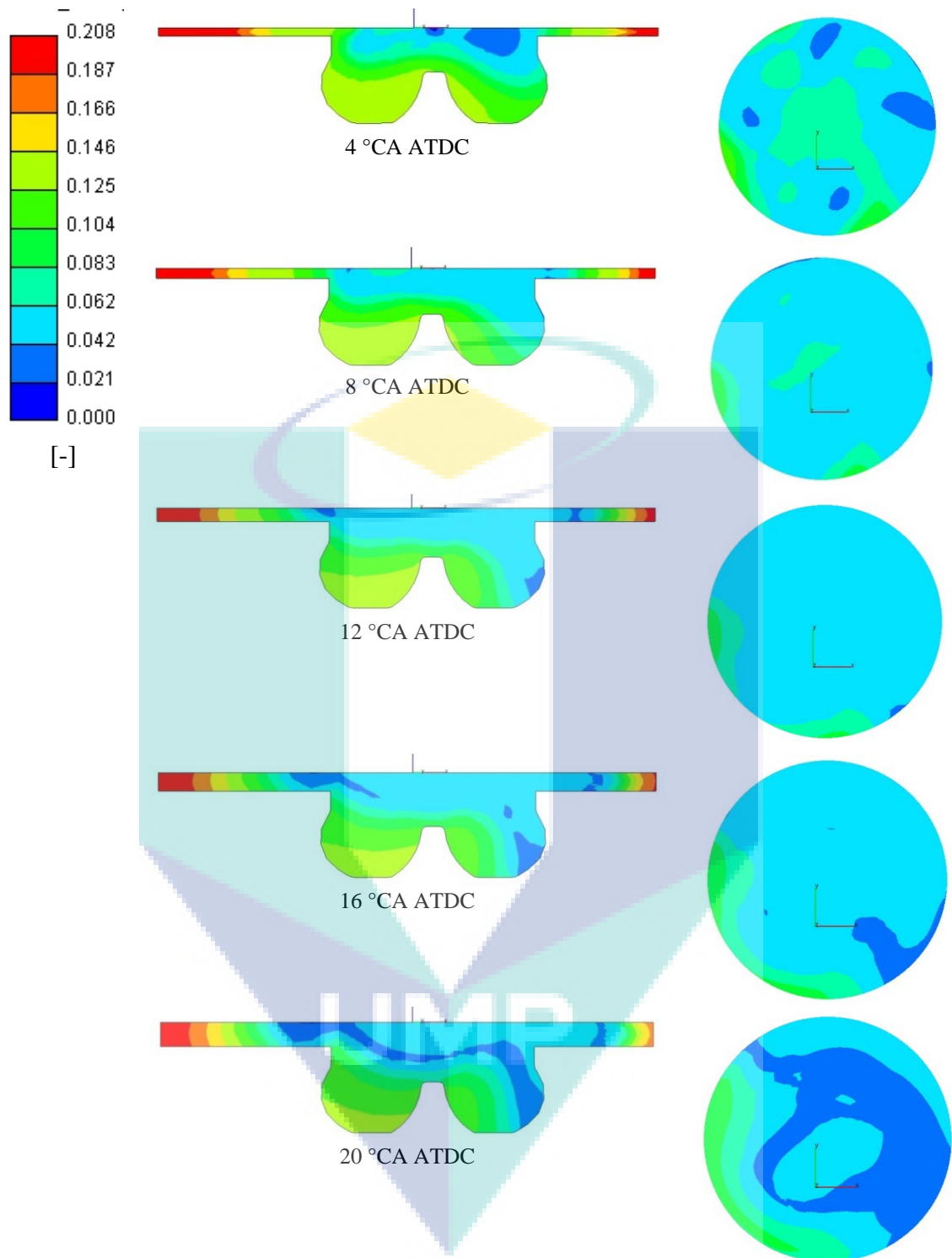
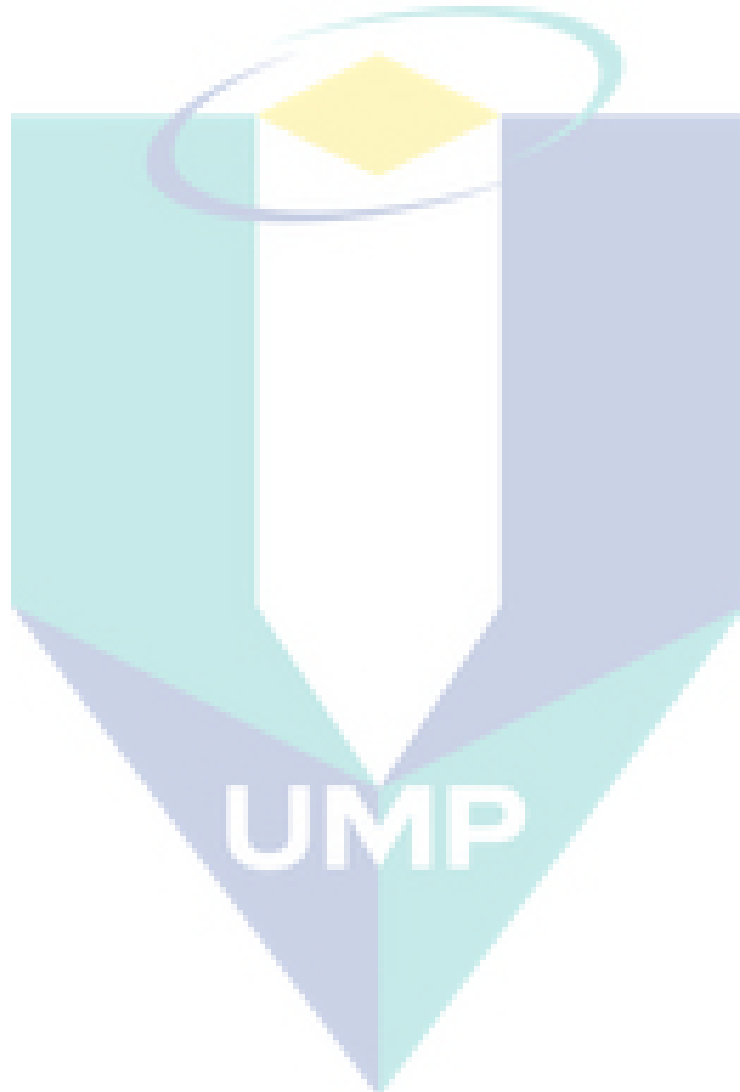


Figure 4.48. Oxygen mass fraction distribution from 5 °CA-20 °CA ATDC.

The end phase of the combustion during the expansion stroke is illustrated in Figures 4.49-4.51. In this phase, the combustion becomes slower with the lower temperature. Figure 4.49 shows the hydrogen mass fraction distributions at 55-65 °CA after TDC, a position where most of the hydrogen has been oxidized. Most of the

unburned hydrogen can be found in the low temperature regions near the wall. As can be seen in Figure 4.50, the movement of in-cylinder gases was insufficient to help the unburned hydrogen to mix effectively with the high temperature gases. The flow movement tends to push the gas to the cylinder wall and to the bottom of piston bowl, while the high temperature region was located in the region near the piston top. As can be seen in Figure 4.51, the temperature is lowered in the burned zone next to the area containing unburned hydrogen near the cylinder wall (liner).



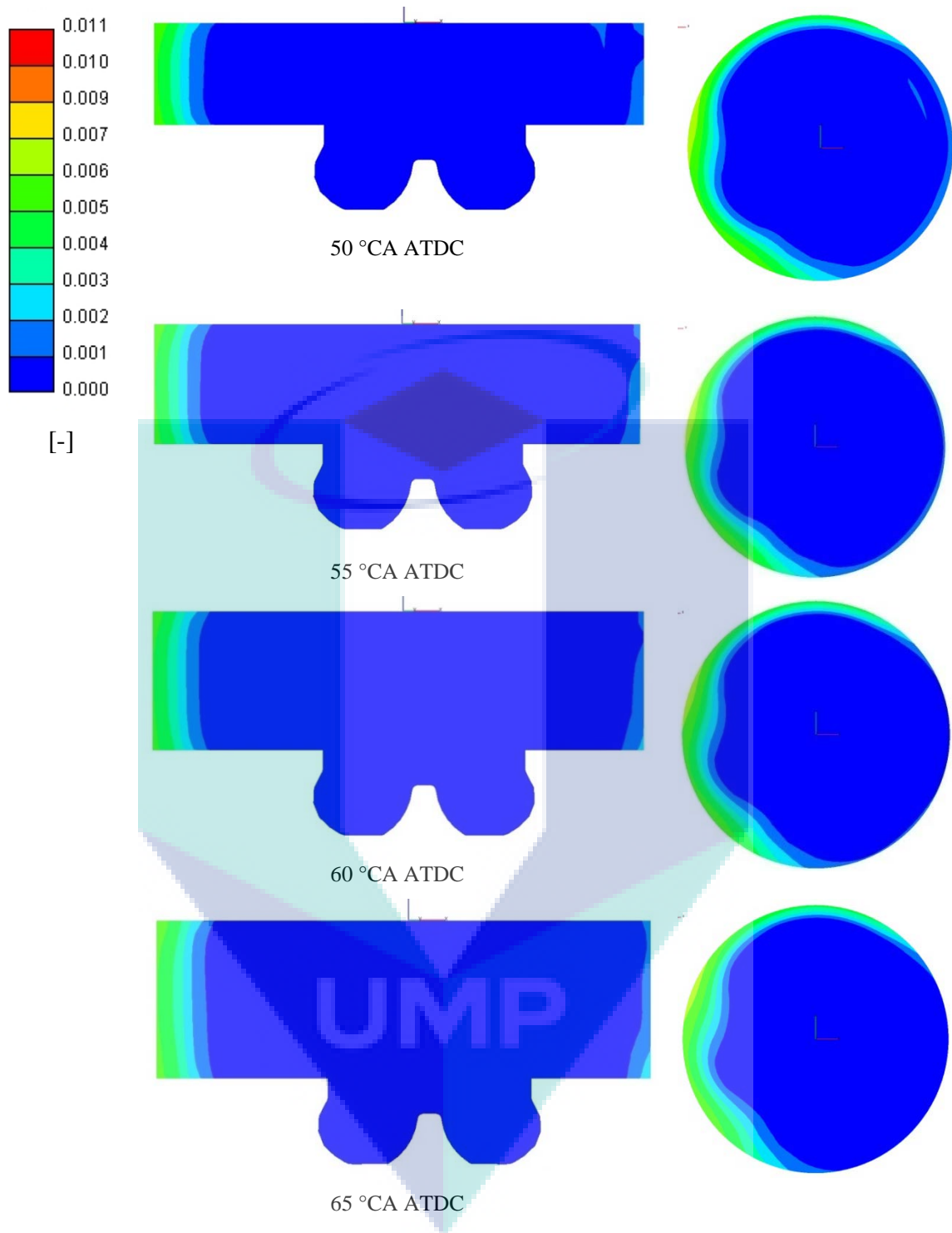


Figure 4.49. Hydrogen mass fraction distribution during the end of combustion phase (50-65 °CA after TDC).

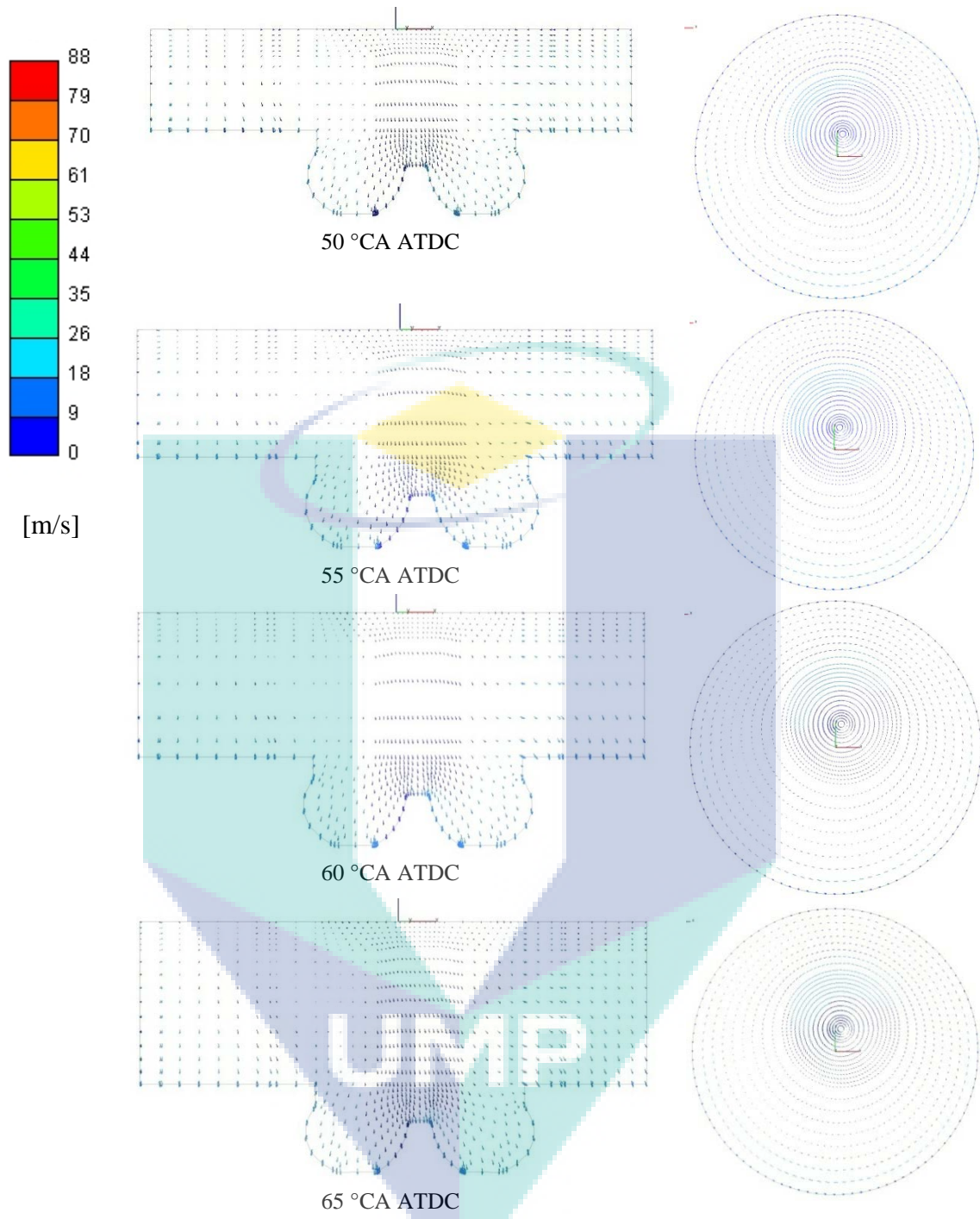


Figure 4.50. Velocity distribution during the end of combustion phase (50-65 °CA after TDC).

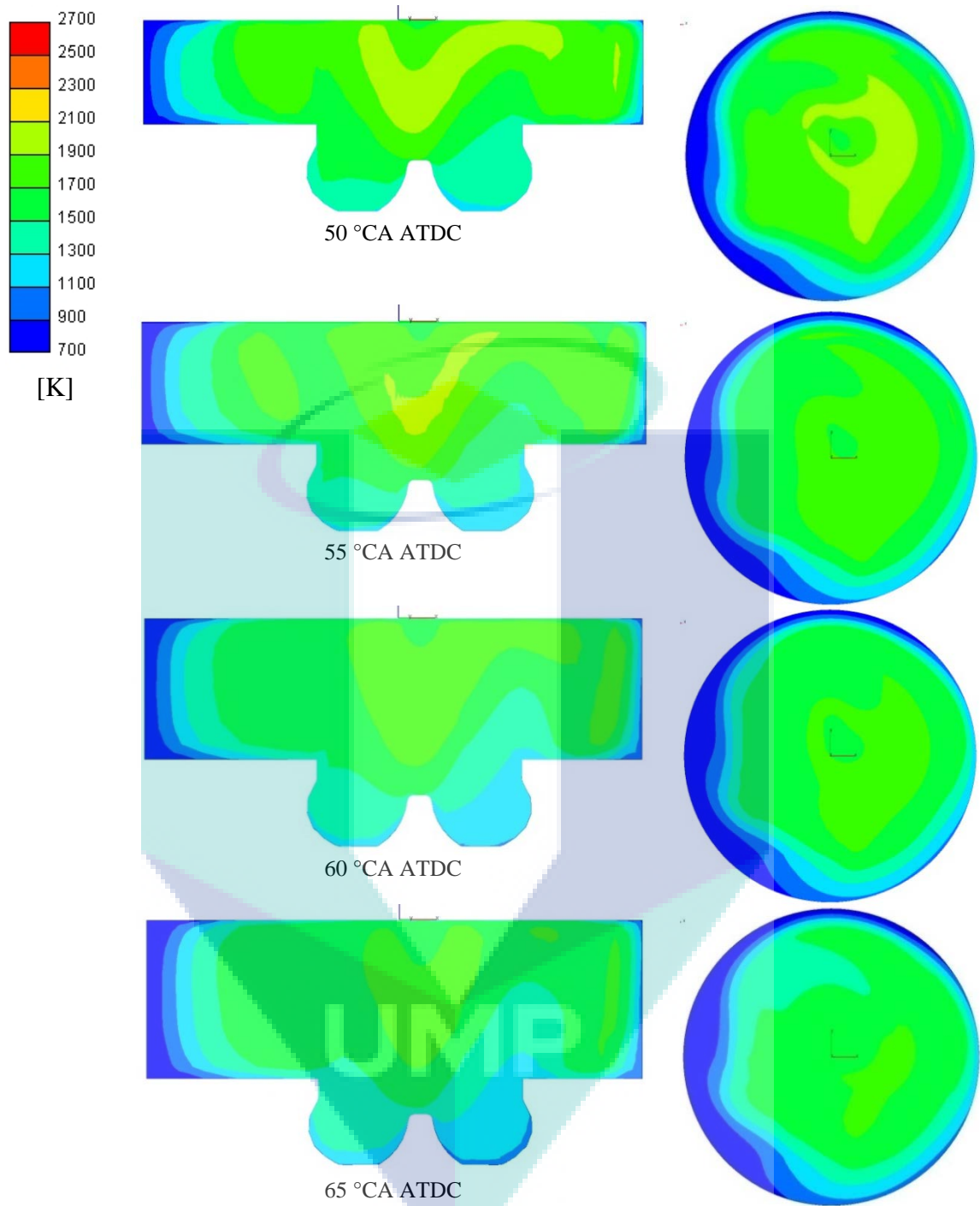


Figure 4.51. Temperature distribution during the end of combustion phase (50-65 °CA after TDC).

4.6 SUMMARY

Engine performance, combustion, and emission have been revealed and discussed in this chapter. Hydrogen can be utilized as fuel for diesel engine, either as supplement or main fuel when the portion of hydrogen sharing was more than 50 % on energy basis. In general, hydrogen additions slightly reduce the engine efficiency. The combustion instability was noticed at low load operations and high hydrogen flow rates. Knock occurrence was detected at high load operation. This abnormal combustion limited the use hydrogen enrichment.

Superior exhaust gas emissions were achieved over the conventional diesel combustion. The use of no carbon fuel reduced the emission except the NO_x at high load operation. CO was reduced due to lean combustion. The absence of carbon in hydrogen reduced CO_2 emission. Smokeless operation was achieved at almost all operating condition.

Predicted results of the 3-D CFD model with a reduced kinetics of 130 elementary reaction steps with 41 chemical species for the diesel combustion process in homogeneously premixed hydrogen-air mixture validated well with some corresponding experimental results. Mixture formation and combustion processes of diesel dual fuel has been investigated and analysed using a CFD tool. The injection process, fuel evaporation, fuel oxidation, species formation and consumption are amongst the physical and chemical interaction in the combustion chamber that can be deeply understood through the simulation.

The engine load represented by the amount of diesel pilot fuel has an important role on the combustion process in case the hydrogen was introduced at the same flow rate. The amount of diesel pilot fuel resulted in the different combustion characteristics for the low and higher loads. Hydrogen introduction at low load engine operation will deteriorate the engine performance. On contrary, better engine performance was achieved at higher loads operation with the same hydrogen introduction. The role of OH radical that triggered the ignition can be revealed by the simulation.

CHAPTER 5

CONCLUSIONS AND RECOMMENDATION FOR FUTURE WORK

5.1 SUMMARY OF FINDINGS

Experimental and simulation works have been carried out to investigate, observe, and analyse the mixture formation and combustion process of diesel-hydrogen dual fuel engine. The main findings are summarized in the following sections:

5.1.1 Dual Fuel Experiment

A single cylinder DI diesel engine was converted to utilize hydrogen as fuel under dual fuel operation. The engine was connected to a dynamometer to control the speed or the load. During the hydrogen addition, the load and speed were kept constant. Experimental results showed that in all engine speed, hydrogen admission tends to achieve similar results. In the loads of 5 and 10 Nm, hydrogen additions reduced the peak cylinder pressures. The rate of pressure rises were also reduced, the peak value of the rise shifted a few degree crank angle. This indicates slower combustion rates. The combustion efficiency was also lower and indicated by the lower indicated efficiency and higher specific energy consumption (SEC). At the higher loads of 15, 20, and 25 Nm, hydrogen introduction increased the peak cylinder pressures. The diesel energy sharing based on energy was more than 35 % that seems to be sufficient to achieve the efficient combustion. However, knock occurrence was detected when hydrogen was introduced at the highest flow rate.

NO_x tends to decrease with hydrogen addition at low loads (5 and 10Nm). This is due to lower cylinder pressures and temperatures. At higher loads, NO_x slightly increased when hydrogen was introduced. NO_x formation related to cylinder temperature. Hydrogen resulted in a clean combustion. No smoke (particulate) was detected except for the highest load where the percentage of diesel based on fuel energy was the highest among the experimental cases in this research. Since the overall air-fuel mixture was lean, no CO emissions were detected for all cases. The formation of carbon dioxide was reduced with the increase of hydrogen flow rates. The reduction of CO_2 emission was due to reduced intake air, means that the mixture become richer.

5.1.2 Cyclic Variability

Cyclic variability tends to increase with the increase of hydrogen enrichment. It is obvious especially at low load and hydrogen enrichment more than 30 l/min. It is found that cyclic variability is reduced at higher engine load operation. At higher load and the same hydrogen flow rate, diesel percentage on energy basis increased. The amount of diesel fuel to ignite the premixing of hydrogen with air was increased and resulted in better combustion stability.

5.1.3 CFD Simulation

The CFD simulation in this study incorporated a direct integration of the chemical kinetic model into the CFD code. The integration of the chemical kinetics resolves the species conversion rates by considering detailed chemistry for modelling engine combustion processes. The PRF kinetic model with modified species reaction rate was used throughout the simulation, both for pure diesel and dual fuel simulation. Fairly good agreement was achieved, especially for engine load operation and lower hydrogen flow rates. Simulation results of the engine modelling showed that:the burning of hydrogen-air mixtures essentially occurs around the regions in the vicinity of the spray with high temperature.

The simulation showed a good prediction of the effect of hydrogen addition on the cylinder pressure both for the low and high loads. The results showed the similar trend compared to those of the experimental results. At the low load, hydrogen addition

retarded the start of combustion. Some cases showed the same peak value of the heat release rate, however, the start of ignition was retarded some degree crank angle. A very low heat release was noticed at hydrogen flow rate of 49.6 l/min, and no combustion was detected. In contrast to the case of lower engine load, hydrogen introduction at higher load resulted in higher cylinder pressures. Hydrogen addition slightly retarded the start of combustion but more heat was released resulted in higher cylinder peak pressures. Hydrogen-air mixture was rapidly oxidized, initiated by pilot diesel fuel ignition. The combustion rate was slower when most of the pilot fuel was consumed. About 90 % of hydrogen was converted into the combustion product for engine operating at high load (20 Nm). At lower load (10 Nm), 80 % of hydrogen was converted, and dropped until 13% for the highest hydrogen flow rate.

5.2 CONTRIBUTIONS OF THE PRESENT WORK

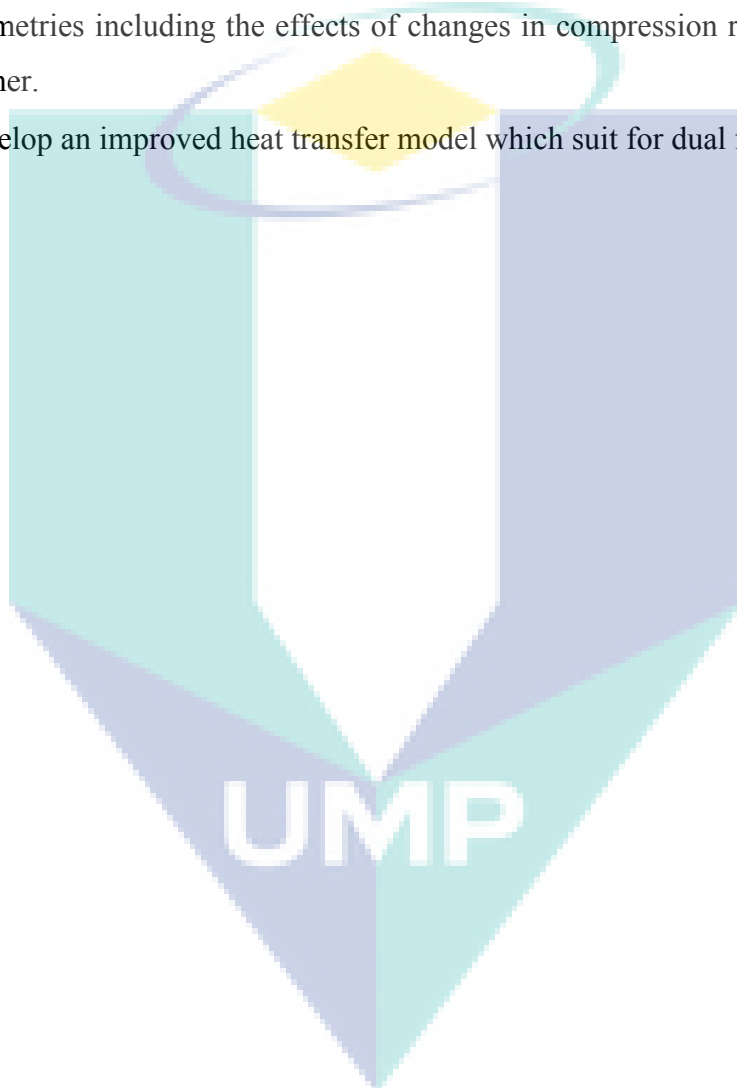
The present work involves the following contribution:

- Investigating the performance, combustion process, and emission of dual fuel engine utilising hydrogen at wide range of hydrogen enrichment.
- Investigating the cyclic variability of hydrogen-diesel dual fuel engine.
- Developing a multidimensional model for dual fuel simulation. The model is developed for investigating the interaction of liquid fuel spray with hydrogen air mixture.
- Modifying and integrating a kinetic model into a CFD simulation tool. Both chemical and turbulence effects on combustion were considered.

5.3 RECOMMENDATION FOR FUTURE WORK

Through the extensive experimental and numerical investigation into the diesel-hydrogen dual fuel engine, some valuable insight and new ideas were identified. These inevitably could not have been pursued more fully further within the present research. The following may be considered as some possible future research:

- Incorporate a detailed pilot fuel injection model which can provide more accurate results for pilot injection. Measured rate of injection would be a valuable parameter for simulation input
- Modify or develop an improved kinetic model for dual fuel combustion processes with gaseous fuel as the main fuel.
- Develop a full engine model including intake and exhaust port to take into consideration the air flow into the cylinder. Different combustion chamber geometries including the effects of changes in compression ratio can be studied further.
- Develop an improved heat transfer model which suit for dual fuel combustion



REFERENCES

- Abdelaal, M.M. and Hegab, A.H. (2012). Combustion and emission characteristics of a natural gas-fueled diesel engine with EGR. *Energy Conversion and Management*, 64(0), 301-312.
- Abramzon, B. and Sirignano, W.A. (1989). Droplet vaporation model for spray combustion calculations. *International Journal of Heat Mass Transfer*, 32(9), 1605-1618.
- An, H., Yang, W.M., Maghbouli, A., Li, J., Chou, S.K. and Chua, K.J. (2013). A numerical study on a hydrogen assisted diesel engine. *International Journal of Hydrogen Energy*, 38(6), 2919-2928.
- An, H., Yang, W.M., Maghbouli, A., Li, J., Chou, S.K., Chua, K.J., Wang, J.X. and Li, L. (2014). Numerical investigation on the combustion and emission characteristics of a hydrogen assisted biodiesel combustion in a diesel engine. *Fuel*, 120(0), 186-194.
- AVL. (2011). *AVL FIRE v2011 manual*. Graz: AVL List GmbH.
- Barboza, A.B.V., Yagnesh Sharma, N. and Sudhir, C.V. (2010). Cyclic combustion studies of a CI engine operating on jatropa B20 fuel. *Proceeding of the Int. Conf. on Mechanical and Electrical Technology*, pp. 43-46.
- Bari, S. and Mohammad Esmaeil, M. (2010). Effect of H₂/O₂ addition in increasing the thermal efficiency of a diesel engine. *Fuel*, 89(2), 378-383.
- Basara, B. (2006). Eddy viscosity transport model based on elliptic relaxation approach. *AIAA Journal*, 44(7), 1686-1690.
- Baumgarten, C. (2006). *Mixture formation in internal combustion engines*. Heidelberg: Springer.
- Bean, M.A. (2001). *Probability: The science of uncertainty*. Boston: Brooks/Cole.
- Bizon, K., Continillo, G., Leistner, K.C., Mancaruso, E. and Vaglieco, B.M. (2009). POD-based analysis of cycle-to-cycle variations in an optically accessible diesel engine. *Proceedings of the Combustion Institute*, 32(2), 2809-2816.
- Bose, P.K. and Maji, D. (2009). An experimental investigation on engine performance and emissions of a single cylinder diesel engine using hydrogen as inducted fuel and diesel as injected fuel with exhaust gas recirculation. *International Journal of Hydrogen Energy*, 34(11), 4847-4854.
- Brenn, G., Deviprasath, L.J., Durst, F. and Fink, C. (2007). Evaporation of acoustically levitated multi-component liquid droplets. *International Journal of Heat and Mass Transfer*, 50(25-26), 5073-5086.
- Brookshear, D.W., Nam, J.-g., Nguyen, K., Toops, T.J. and Binder, A. (2015). Impact of sulfation and desulfation on NO_x reduction using Cu-chabazite SCR catalysts. *Catalysis Today*, 258, Part 2, 359-366.
- Choi, I.S. and Milton, B.E. (1997). Dual-fuel combustion model for premixed natural gas with distillate ignition in a quiescent bomb. *Numerical Heat Transfer, Part A: Applications*, 31(7), 725-743.

- Das, L.M. (1996). Hydrogen-oxygen reaction mechanism and its implication to hydrogen engine combustion. *International Journal of Hydrogen Energy*, 21(8), 703-715.
- de Morais, A.M., Mendes Justino, M.A., Valente, O.S., Hanriot, S.d.M. and Sodré, J.R. (2013). Hydrogen impacts on performance and CO₂ emissions from a diesel power generator. *International Journal of Hydrogen Energy*, 38(16), 6857-6864.
- de Palacio, L. and Busquin, P. (2003). Hydrogen energy and fuel cells (Technical Report). Brussel:European Commission
- Deb, M., Sastry, G.R.K., Bose, P.K. and Banerjee, R. (2015). An experimental study on combustion, performance and emission analysis of a single cylinder, 4-stroke DI-diesel engine using hydrogen in dual fuel mode of operation. *International Journal of Hydrogen Energy*, 40(27), 8586-8598.
- Dhole, A.E., Yarasu, R.B., Lata, D.B. and Priyam, A. (2014). Effect on performance and emissions of a dual fuel diesel engine using hydrogen and producer gas as secondary fuels. *International Journal of Hydrogen Energy*, 39(15), 8087-8097.
- Ekins, P. (Ed.). (2010). *Hydrogen energy : Economic and social challenges*. London: Earthscan.
- Friedrich, K.A., Büchi, F.N., Li, Z.P., Kiesgen, G., Leinhos, D.C., Rottengruber, H.S., Bowman, R.C. and Ratnakumar, B.V. (2008). *Hydrogen as a future energy carrier*. Weinheim: Wiley-VCH Verlag GmbH & Co. KGaA.
- Fulton, J., Lynch, F. and Marmora, R. (1993). Hydrogen for reducing emissions from alternative fuel vehicle. *SAE Technical Paper*, 931813, 1-7.
- Ganesan, V. (2012). *IC engine*. New Delhi: Tata McGraw-Hill.
- Ghazal, O.H. (2013). Performance and combustion characteristic of CI engine fueled with hydrogen enriched diesel. *International Journal of Hydrogen Energy*, 38(35), 15469-15476.
- Gu, H., Chun, K.M. and Song, S. (2015). The effects of hydrogen on the efficiency of NO_x reduction via hydrocarbon-selective catalytic reduction (HC-SCR) at low temperature using various reductants. *International Journal of Hydrogen Energy*, 40(30), 9602-9610.
- Gupta, R.B. (2009). *Hydrogen Fuel: Production, Transport, and Storage*. Boca Raton: CRC Press.
- Hanjalić, K., Popovac, M. and Hadžiabdić, M. (2004). A robust near-wall elliptic-relaxation eddy-viscosity turbulence model for CFD. *International Journal of Heat and Fluid Flow*, 25(6), 1047-1051.
- Heywood, J.B. (1988). *Internal combustion engine fundamentals* (2nd ed.). Singapore: McGraw-Hill International Editions.
- Hočevar, S. and Summers, W. (2008). *Hydrogen production*. A. Léon (Ed.). Berlin: Springer.
- Hollinger, T. and Bose, T. (2008). *Status on existing technologies*. A. Léon (Ed.). Berlin: Springer.
- Huang, B., Hu, E., Huang, Z., Zheng, J., Liu, B. and Jiang, D. (2009). Cycle-by-cycle variations in a spark ignition engine fueled with natural gas-hydrogen blends

- combined with EGR. *International Journal of Hydrogen Energy*, 34(19), 8405-8414.
- ISO. (1993). *International vocabulary of basic and general terms in metrology*. Geneva: International Organization for Standardization
- ISO. (2005). *ISO/IEC 17025:2005 General requirements for the competence of testing and calibration laboratories*. Geneva: International Organization for Standardization
- JCGM. (2008). *Evaluation of measurement data — Guide to the expression of uncertainty in measurement*. Sèvres: Joint Committee for Guides in Metrology
- Kang, W. and Choi, B. (2016). Effect of copper precursor on simultaneous removal of PM and NO_x of a 2-way SCR/CDPF. *Chemical Engineering Science*, 141, 175-183.
- Karim, G.A. (2015). *Dual-fuel diesel engines*. Boca Raton: CRC Press
- Kong, S.C., Han, Z. and Reitz, R.D. (1995). The development and application of a diesel ignition and combustion model for multidimensional engine simulation. *SAE Technical Paper*, 950278, 1-11.
- Kong, S.C., Marriot, C.D., Reitz, R.D. and Christensen, M. (2001). Modeling and experiments of HCCI engine combustion using detailed chemical kinetics with multidimensional CFD. *SAE Technical Paper*, 2001-01-1026, 1-12.
- Köse, H. and Ciniviz, M. (2013). An experimental investigation of effect on diesel engine performance and exhaust emissions of addition at dual fuel mode of hydrogen. *Fuel Processing Technology*, 114(0), 26-34.
- Kumar, M.S., Ramesh, A. and Nagalingam, B. (2003). Use of hydrogen to enhance the performance of a vegetable oil fuelled compression ignition engine. *International Journal of Hydrogen Energy*, 28(10), 1143-1154.
- Lakshminarayanan, P.A. and Aghav, Y.V. (2010). *Modelling diesel combustion*: Springer Netherlands.
- Lanz, A. (2001). Hydrogen Fuel Cell Engine, Module 3: Hydrogen Use in Internal Combustion Engines. *College of The Dessert, Revision 0*.
- Lata, D.B. and Misra, A. (2010). Theoretical and experimental investigations on the performance of dual fuel diesel engine with hydrogen and LPG as secondary fuels. *International Journal of Hydrogen Energy*, 35(21), 11918-11931.
- Lata, D.B., Misra, A. and Medhekar, S. (2012). Effect of hydrogen and LPG addition on the efficiency and emissions of a dual fuel diesel engine. *International Journal of Hydrogen Energy*, 37(7), 6084-6096.
- Leon, A. (Ed.). (2008). *Hydrogen Technology: Mobile and Portable Applications*. Berlin: Springer-Verlag.
- Liew, C., Li, H., Nuskowski, J., Liu, S., Gatts, T., Atkinson, R. and Clark, N. (2010). An experimental investigation of the combustion process of a heavy-duty diesel engine enriched with H₂. *International Journal of Hydrogen Energy*, 35(20), 11357-11365.

- Lilik, G.K., Zhang, H., Herreros, J.M., Haworth, D.C. and Boehman, A.L. (2010). Hydrogen assisted diesel combustion. *International Journal of Hydrogen Energy*, 35(9), 4382-4398.
- Liu, C. and Karim, G.A. (2009). Three-dimensional computational fluid simulation of diesel and dual fuel engine combustion. *Journal of Engineering for Gas Turbines and Power*, 131(1), 012804-012809.
- Liu, S., Li, H., Liew, C., Gatts, T., Wayne, S., Shade, B. and Clark, N. (2011). An experimental investigation of NO₂ emission characteristics of a heavy-duty H₂-diesel dual fuel engine. *International Journal of Hydrogen Energy*, 36(18), 12015-12024.
- Liu, Z. and Karim, G.A. (1995). Knock characteristics of dual-fuel engines fuelled with hydrogen fuel. *International Journal of Hydrogen Energy*, 20(11), 919-924.
- Liu, Z. and Karim, G.A. (1997). Simulation of combustion processes in gas-fuelled diesel engines. *Proceedings of the Institution of Mechanical Engineers -- Part A -- Power & Energy*, 211(2), 159-169.
- Lloyd, A.C. and Cackette, T.A. (2001). Diesel Engines: Environmental Impact and Control. *Journal of the Air & Waste Management Association*, 51(6), 809-847.
- Ma, F., Ding, S., Wang, Y., Wang, Y., Wang, J. and Zhao, S. (2008). Study on combustion behaviors and cycle-by-cycle variations in a turbocharged lean burn natural gas S.I. engine with hydrogen enrichment. *International Journal of Hydrogen Energy*, 33(23), 7245-7255.
- Maghbouli, A., Yang, W., An, H., Shafee, S., Li, J. and Mohammadi, S. (2014). Modeling knocking combustion in hydrogen assisted compression ignition diesel engines. *Energy*, 76(0), 768-779.
- Mansour, C., Bounif, A., Aris, A. and Gaillard, F. (2001). Gas-Diesel (dual-fuel) modeling in diesel engine environment. *International Journal of Thermal Sciences*, 40(4), 409-424.
- Marbán, G. and Valdés-Solís, T. (2007). Towards the hydrogen economy? *International Journal of Hydrogen Energy*, 32(12), 1625-1637.
- Martyr, A.J. and Plint, M.A. (2007). *Test cell cooling water and exhaust gas systems*. A. J. Martyr & M. A. Plint (Ed.). Oxford: Butterworth-Heinemann.
- Masood, M. and Ishrat, M.M. (2008). Computer simulation of hydrogen-diesel dual fuel exhaust gas emissions with experimental verification. *Fuel*, 87(7), 1372-1378.
- Masood, M., Ishrat, M.M. and Reddy, A.S. (2007). Computational combustion and emission analysis of hydrogen-diesel blends with experimental verification. *International Journal of Hydrogen Energy*, 32(13), 2539-2547.
- McAllister, S., Chen, H. and Fernandez-Pello, A.C. (2011). *Fundamental of combustion processes*. New York: Springer.
- McWilliam, L., Megaritis, T. and Zhao, H. (2008). Experimental investigation of the effects of combined hydrogen and diesel combustion on the emissions of a HSDI diesel engine. *SAE Technical Paper*, 2008-01-1787, 1-9.
- Merker, G.P., Schwarz, C., Stiesch, G. and Otto, F. (2006). *Simulating combustion*. Berlin: Springer.

- Merker, G.P., Schwarz, C. and Teichmann, R. (Eds.). (2012). *Combustion engine development*. Berlin: Springer-Verlag.
- Miao, H. and Milton, B. (2002). Modeling of the gas/diesel dual-fuel combustion process for conditions applicable to engines. *Numerical Heat Transfer; Part A: Applications*, 41(6), 725-739.
- Miao, H. and Milton, B. (2005). Numerical simulation of the gas/diesel dual-fuel engine in-cylinder combustion process. *Numerical Heat Transfer; Part A: Applications*, 47(6), 523-547.
- Midilli, A. and Dincer, I. (2008). Hydrogen as a renewable and sustainable solution in reducing global fossil fuel consumption. *International Journal of Hydrogen Energy*, 33(16), 4209-4222.
- Miyamoto, T., Hasegawa, H., Mikami, M., Kojima, N., Kabashima, H. and Urata, Y. (2011). Effect of hydrogen addition to intake gas on combustion and exhaust emission characteristics of a diesel engine. *International Journal of Hydrogen Energy*, 36(20), 13138-13149.
- Miyamoto, T., Kobayashi, B., Mikami, M. and Kojima, N. (2008). Exhaust emission characteristics of a diesel engine with small amounts of hydrogen added to the intake air. *Proceeding of The Seventh International Conference on Modeling and Diagnostics for Advanced Engine Systems (COMODIA 2008)*, pp. 759-764.
- Mohamed Ibrahim, M., Varuna Narasimhan, J. and Ramesh, A. (2015). Comparison of the predominantly premixed charge compression ignition and the dual fuel modes of operation with biogas and diesel as fuels. *Energy*, 89, 990-1000.
- Papagiannakis, R.G., Hountalas, D.T. and Rakopoulos, C.D. (2007). Theoretical study of the effects of pilot fuel quantity and its injection timing on the performance and emissions of a dual fuel diesel engine. *Energy Conversion and Management*, 48(11), 2951-2961.
- Perry, R.H. and Green, D.W. (1984). *Perry's chemical engineers' handbook*. New York: McGraw-Hill.
- Pirouzpanah, V. and Saray, R.K. (2006). A predictive model for the combustion process in dual fuel engines at part loads using quasi dimensional multi zone model and detailed chemical kinetics mechanism. *IJE Transactions B: Applications*, 19, 83-98.
- Pischinger, R., Klell, M., Sam, T. (2002). *Thermodynamik der Verbrennungskraftmaschine*. Graz: Springer.
- Popovac, M. and Hanjalic, K. (2007). Compound wall treatment for RANS computation of complex turbulent flows and heat transfer. *Flow, Turbulence and Combustion*, 78(2), 177-202.
- Pundir, B.P. and Kumar, R. (2007). Combustion and smoke emission studies on a hydrogen fuel supplemented DI diesel engine. *SAE Technical Paper, 2007-01-0055*, 1-9.
- Ra, Y. and Reitz, R.D. (2008). A reduced chemical kinetic model for IC engine combustion simulations with primary reference fuels. *Combustion and Flame*, 155(4), 713-738.

- Rao, H.B., Shrivastava, K.N. and Bhakta, H.N. (1983). Hydrogen for dual fuel engine operation. *International Journal of Hydrogen Energy*, 8(5), 381-384.
- Reitz, R.D. (2013). Directions in internal combustion engine research. *Combustion and Flame*, 160(1), 1-8.
- Reitz, R.D. and Diwakar, R. (1987). Structure of high pressure fuel sprays. *SAE Transaction*, 96, 492-509.
- Sahoo, B.B., Sahoo, N. and Saha, U.K. (2009). Effect of engine parameters and type of gaseous fuel on the performance of dual-fuel gas diesel engines--A critical review. *Renewable and Sustainable Energy Reviews*, 13(6-7), 1151-1184.
- Saravanan, N. and Nagarajan, G. (2008a). An experimental investigation of hydrogen-enriched air induction in a diesel engine system. *International Journal of Hydrogen Energy*, 33(6), 1769-1775.
- Saravanan, N. and Nagarajan, G. (2008b). An experimental investigation on a diesel engine with hydrogen fuel injection in intake manifold. *SAE Technical Paper*, 2008-01-1784, 1-15.
- Saravanan, N. and Nagarajan, G. (2009). An insight on hydrogen fuel injection techniques with SCR system for NOX reduction in a hydrogen-diesel dual fuel engine. *International Journal of Hydrogen Energy*, 34(21), 9019-9032.
- Saravanan, N. and Nagarajan, G. (2010). Performance and emission studies on port injection of hydrogen with varied flow rates with Diesel as an ignition source. *Applied Energy*, 87(7), 2218-2229.
- Saravanan, N., Nagarajan, G., Dhanasekaran, C. and Kalaiselvan, K.M. (2007a). Experimental investigation of hydrogen fuel injection in DI dual fuel diesel engine. *SAE Technical Paper*, 2007-01-1465, 1-10.
- Saravanan, N., Nagarajan, G., Dhanasekaran, C. and Kalaiselvan, K.M. (2007b). Experimental investigation of hydrogen port fuel injection in DI diesel engine. *International Journal of Hydrogen Energy*, 32(16), 4071-4080.
- Saravanan, N., Nagarajan, G., Kalaiselvan, K.M. and Dhanasekaran, C. (2008). An experimental investigation on hydrogen as a dual fuel for diesel engine system with exhaust gas recirculation technique. *Renewable Energy*, 33(3), 422-427.
- Saravanan, N., Nagarajan, G. and Narayanasamy, S. (2007). Experimental investigation on performance and emission characteristics of di diesel engine with hydrogen fuel. *SAE Technical Paper*, 2007-26-030, 1-6.
- Saravanan, N., Nagarajan, G. and Narayanasamy, S. (2008). An experimental investigation on DI diesel engine with hydrogen fuel. *Renewable Energy*, 33(3), 415-421.
- Schmidt, D.P. and Rutland, C.J. (2000). A new droplet collision algorithm. *J. Comp. Phys*(164), 62-80.
- Sebastian, V., Thomas, W. and Roger, S. (2014). *Hydrogen-fueled internal combustion engines*. New York: CRC Press.
- Selim, M.Y.E. (2004). Sensitivity of dual fuel engine combustion and knocking limits to gaseous fuel composition. *Energy Conversion and Management*, 45(3), 411-425.

- Selim, M.Y.E. (2005). Effect of engine parameters and gaseous fuel type on the cyclic variability of dual fuel engines. *Fuel*, 84(7–8), 961-971.
- Sen, A.K., Longwic, R., Litak, G. and Górski, K. (2008). Analysis of cycle-to-cycle pressure oscillations in a diesel engine. *Mechanical Systems and Signal Processing*, 22(2), 362-373.
- Sharma, S. and Ghoshal, S.K. (2015). Hydrogen the future transportation fuel: From production to applications. *Renewable and Sustainable Energy Reviews*, 43(0), 1151-1158.
- Sherif, S.A., Barbir, F. and Veziroglu, T.N. (2014). *Hydrogen economy*. New York: CRC Press.
- Shi, Y., Ge, H.-W. and Reitz, R.D. (2011). *Computational optimization of internal combustion engine*. London: Springer-Verlag.
- Shi, Y. and Reitz, R.D. (2010). *Multi-dimensional modelling of diesel combustion: Review*. F. F. Ling (Ed.). Heidelberg: Springer.
- Shin, B., Cho, Y., Han, D., Song, S. and Chun, K.M. (2011). Hydrogen effects on NO_x emissions and brake thermal efficiency in a diesel engine under low-temperature and heavy-EGR conditions. *International Journal of Hydrogen Energy*, 36(10), 6281-6291.
- Shioji, M., Ishiyama, T. and Ikegami, M. (2000). Approach to high thermal-efficiency in high compression ratio natural gas engine. *Proceeding of 7th International Conference and Exhibition on Natural Gas Vehicle*, pp. 13-21.
- Shudo, T., Nabetani, S. and Nakajima, Y. (2001). Influence of specific heats on indicator diagram analysis in a hydrogen-fuelled SI engine. *JSAE Review*, 22(2), 224-226.
- Steinfeld, A. (2014). *Overview of hydrogen production*. S. A. Sherif, D. Y. Goswami, E. K. Stefanakos & A. Steinfeld (Ed.). New York: CRC Press.
- Stetson, N.T., Bowman, R.C. and Olson, G.L. (2014). *Overview of hydrogen storage, transportation, handling, and distribution*. S. A. Sherif, D. Y. Goswami, E. K. Stefanakos & A. Steinfeld (Ed.). New York: CRC Press.
- Stiesch, G. (2010). *Modeling engine spray and combustion processes*: Springer.
- Szwaja, S. and Grab-Rogalinski, K. (2009). Hydrogen combustion in a compression ignition diesel engine. *International Journal of Hydrogen Energy*, 34(10), 4413-4421.
- Tang, D., Ge, J., Duan, R. and Zhang, Y. (2011, 15-17 April 2011). Investigation on the combustion cyclic variability in a non-road diesel engine fuelled with diesel/bio-diesel blends. pp. 2286-2289.
- Tomita, E., Kawahara, N., Piao, Z. and Fujita, S. (2001). Hydrogen combustion and exhaust emissions ignited with diesel oil in a dual fuel engine. *SAE Technical Paper*, No. 2001-01-3503, 1-10.
- Tsolakis, A., Hernandez, J.J., Megaritis, A. and Crampton, M. (2005). Dual fuel diesel engine operation using H₂ : Effect on particulate emissions. *Energy & Fuels*, 19(2), 418-425.

- Tsolakis, A. and Megaritis, A. (2005). Partially premixed charge compression ignition engine with on-board production by exhaust gas fuel reforming of diesel and biodiesel. *International Journal of Hydrogen Energy*, 30(7), 731-745.
- Tsolakis, A., Megaritis, A. and Wyszynski, M.L. (2003). Application of exhaust gas fuel reforming in compression ignition engines fueled by diesel and biodiesel fuel mixtures. *Energy and Fuels*, 17(6), 1464-1473.
- Valencia, M., López, E., Andrade, S., Iris, M.L., Pérez, V.R., Salinas Martínez de Lecea, C. and Bueno López, A. (2014). Proof of concept of the SCR of NO_x in a real diesel engine exhaust using commercial diesel fuel and a full size Pt/beta zeolite/honeycomb monolith. *Catalysis Communications*, 46, 86-89.
- Verhelst, S. and Wallner, T. (2009). Hydrogen-fueled internal combustion engines. *Progress in Energy and Combustion Science*, 35(6), 490-527.
- Wang, J., Chen, H., Liu, B. and Huang, Z. (2008). Study of cycle-by-cycle variations of a spark ignition engine fueled with natural gas-hydrogen blends. *International Journal of Hydrogen Energy*, 33(18), 4876-4883.
- Warnatz, J., Maas, U. and Dibble, R.W. (2006). *Combustion*. Heidelberg: Springer-Verlag.
- White, C.M., Steeper, R.R. and Lutz, A.E. (2006). The hydrogen-fueled internal combustion engine: a technical review. *International Journal of Hydrogen Energy*, 31(10), 1292-1305.
- Xiao, F. and Karim, G. (2011). An Investigation of the combustion in an IDI diesel engine with low concentrations of added hydrogen. *SAE Technical Paper*, 2011-01-0676, 1-10.
- Zhang, H., Lilik, G.K., Boehman, A.L. and Haworth, D.C. (2009). Effect of hydrogen addition on NO_x emissions in hydrogen-assisted diesel combustion. *Proceedings of International Multidimensional Engine Modeling User Group*, pp. 1-6.
- Zuettel, A., Borgschulte, A. and Schlapbach, L. (Eds.). (2008). *Hydrogen as a Future Energy Carrier*. Weinheim: Wiley-VCH.

APPENDICES

A. LIST OF PUBLICATION

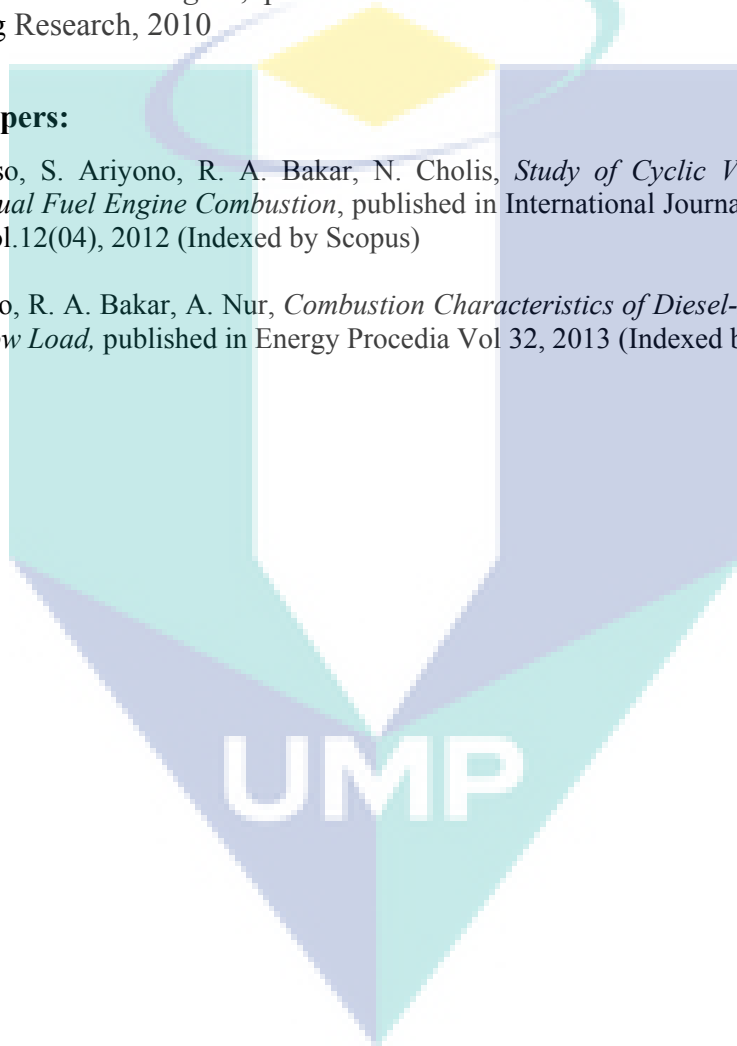
Conference Papers:

W.B. Santoso, A. Nur, S. Ariyono, R.A. Bakar, *Combustion Characteristics of a Diesel-Hydrogen Dual Fuel Engine*, presented at 2nd National Conference on Mechanical Engineering Research, 2010

Journal Papers:

W.B. Santoso, S. Ariyono, R. A. Bakar, N. Cholis, *Study of Cyclic Variability in Diesel-Hydrogen Dual Fuel Engine Combustion*, published in International Journal of Engineering and Sciences, Vol.12(04), 2012 (Indexed by Scopus)

W.B. Santoso, R. A. Bakar, A. Nur, *Combustion Characteristics of Diesel-Hydrogen Dual Fuel Engine at Low Load*, published in Energy Procedia Vol 32, 2013 (Indexed by Scopus)



B. PRF CHEMICAL KINETICS

1	IC8H18+H=C8H17+H2		4.3800E+07	2.000	3.9054E+03
2	IC8H18+OH=C8H17+H2O		3.4700E+07	1.800	1.4001E+02
3	IC8H18+HO2=C8H17+H2O2		2.2300E+14	0.000	9.5370E+03
4	IC8H18+O2=C8H17+HO2		2.2200E+15	0.000	2.1592E+04
5	C8H17+O2=C8H17OO		1.0500E+11	0.000	0.0000E+00
6	C8H17OO+O2=IC8KET21+OH		8.7000E+15	0.000	1.0686E+04
7	IC8KET21=CH2O+C6H13CO+OH		1.7800E+14	0.000	1.9678E+04
8	C6H13CO=C4H9+C2H4+CO		4.9200E+16	0.000	2.0232E+04
9	C4H9=C3H6+CH3		4.5600E+13	0.000	1.8571E+04
10	C8H17=C3H7+C2H4+C3H6		2.1600E+16	0.000	1.8420E+04
11	IC8H18+C7H15-2<=>NC7H16+C8H17		5.0100E+10	0.000	5.6366E+03
12	NC7H16+H=C7H15-2+H2		4.3800E+07	2.000	2.3956E+03
13	NC7H16+OH=C7H15-2+H2O		1.3600E+10	1.300	3.4726E+02
14	NC7H16+HO2=C7H15-2+H2O2		3.3000E+14	0.000	8.5304E+03
15	NC7H16+O2=C7H15-2+HO2		1.2500E+14	0.000	1.9076E+04
16	C7H15-2+O2=C7H15O2		2.3400E+12	0.000	0.0000E+00
17	C7H15O2+O2=C7KET12+OH		3.2900E+14	0.000	9.1760E+03
18	C7KET12=C5H11CO+CH2O+OH		6.0100E+14	0.000	2.0684E+04
19	C5H11CO=C2H4+C3H7+CO		9.8400E+15	0.000	2.0232E+04
20	C7H15-2=C2H5+C2H4+C3H6		4.0400E+14	0.000	1.7413E+04
21	C3H7=C2H4+CH3		9.6000E+13	0.000	1.5576E+04
22	C3H7=C3H6+H		1.2500E+14	0.000	1.8571E+04
23	C3H6+CH3=C3H5+CH4		9.0000E+12	0.000	4.2677E+03
24	C3H5+O2=C3H4+HO2		6.0000E+11	0.000	5.0327E+03
25	C3H4+OH=C2H3+CH2O		1.0000E+12	0.000	0.0000E+00
26	C3H4+OH=C2H4+HCO		1.0000E+12	0.000	0.0000E+00
27	CH3+HO2=CH3O+OH		5.0000E+13	0.000	0.0000E+00
28	CH3+OH=CH2+H2O		7.5000E+06	2.000	2.5164E+03
29	CH2+OH=CH2O+H		2.5000E+13	0.000	0.0000E+00
30	CH2+O2=HCO+OH		4.3000E+10	0.000	-2.5164E+02
31	CH2+O2=CO2+H2		6.9000E+11	0.000	2.5164E+02
32	CH2+O2=CO+H2O		2.0000E+10	0.000	-5.0327E+02
33	CH2+O2=CH2O+O		5.0000E+13	0.000	4.5294E+03
34	CH2+O2=CO2+H+H		1.6000E+12	0.000	5.0327E+02
35	CH2+O2=CO+OH+H		8.6000E+10	0.000	-2.5164E+02
36	CH3O+CO=CH3+CO2		3.9200E+13	0.000	5.9386E+03
37	CO+OH=CO2+H		1.2600E+07	1.300	-3.8148E+02
38	O+CO (+M) <=> CO2 (+M)		1.8000E+10	0.000	1.2003E+03
	Fall-Off LOW Parameters	6.0200E+14	0.0000E+00	1.5098E+03	
	H2	3rd body:	2.0000E+00		
	O2	3rd body:	6.0000E+00		
	H2O	3rd body:	6.0000E+00		
	CO	3rd body:	1.5000E+00		
	CO2	3rd body:	3.5000E+00		
39	O2+CO<=>O+CO2		2.5000E+12	0.000	2.4056E+04
40	HO2+CO<=>OH+CO2		4.7600E+13	0.000	1.1877E+04
41	O+OH=O2+H		4.0000E+13	-0.500	0.0000E+00
42	H+HO2=OH+OH		1.7000E+14	0.000	4.4036E+02
43	OH+OH=O+H2O		6.0000E+08	1.300	0.0000E+00
44	H+O2 (+M) =HO2 (+M)		1.4800E+12	0.600	0.0000E+00
	Fall-Off LOW Parameters	3.5000E+16	-4.1000E-01	-	
	TROE Parameters	5.0000E-01	1.0000E-30	1.0000E+30	1.0000+100
	H2	3rd body:	2.0000E+00		
	H2O	3rd body:	1.2000E+01		
	CO	3rd body:	1.9000E+00		
	CO2	3rd body:	3.8000E+00		
45	OH+OH (+M) =H2O2 (+M)		1.2400E+14	-0.400	0.0000E+00
	Fall-Off LOW Parameters	3.0410E+30	-4.6300E+00	1.0312E+03	
	TROE Parameters	4.7000E-01	1.0000E+02	2.0000E+03	1.0000E+15
	H2	3rd body:	2.0000E+00		
	H2O	3rd body:	1.2000E+01		
	CO	3rd body:	1.9000E+00		
	CO2	3rd body:	3.8000E+00		
46	H2O2+H=HO2+H2		1.9800E+06	2.000	1.2255E+03

47	H2O2+H=OH+H2O		3.0700E+13	0.000	2.1223E+03
48	H2O2+O=OH+HO2		9.5500E+06	2.000	1.9980E+03
49	H2O2+OH=H2O+HO2		2.4000E+00	4.000	-1.0881E+03
50	H2+OH=H2O+H		1.1700E+09	1.300	1.8249E+03
51	HO2+HO2=H2O2+O2		3.0000E+12	0.000	0.0000E+00
52	CH2O+OH=HCO+H2O		5.5600E+10	1.100	-3.8500E+01
53	CH2O+HO2=HCO+H2O2		3.0000E+12	0.000	4.0262E+03
54	HCO+O2=HO2+CO		3.3000E+13	-0.400	0.0000E+00
55	HCO+M=H+CO+M		1.5900E+18	0.900	2.8542E+04
56	CH3+CH3O=CH4+CH2O		4.3000E+13	0.000	0.0000E+00
57	C2H4+OH=CH2O+CH3		1.2000E+14	0.000	4.8314E+02
58	C2H4+OH=C2H3+H2O		8.0200E+13	0.000	2.9970E+03
59	C2H3+O2=CH2O+HCO		4.0000E+12	0.000	-1.2582E+02
60	C2H3+HCO=C2H4+CO		6.0300E+13	0.000	0.0000E+00
61	C2H5+O2=C2H4+HO2		2.0000E+10	0.000	-1.1072E+03
62	CH4+O2=CH3+HO2		7.9000E+13	0.000	2.8183E+04
63	OH+HO2=H2O+O2		7.5000E+12	0.000	0.0000E+00
64	CH3+O2=CH2O+OH		3.8000E+11	0.000	4.5294E+03
65	CH4+H=CH3+H2		6.6000E+08	1.600	5.4555E+03
66	CH4+OH=CH3+H2O		1.6000E+06	2.100	1.2380E+03
67	CH4+O=CH3+OH		1.0200E+09	1.500	4.3301E+03
68	CH4+HO2=CH3+H2O2		9.0000E+11	0.000	9.4112E+03
69	CH4+CH2=CH3+CH3		4.0000E+12	0.000	-2.8686E+02
70	C3H6=C2H3+CH3		3.1500E+15	0.000	4.3030E+04
71	CH2+CH2=C2H2+H2		1.2000E+13	0.000	4.0262E+02
72	CH2+CH2=C2H2+H+H		1.2000E+14	0.000	4.0262E+02
73	C2H4+M=C2H2+H2+M		1.5000E+15	0.000	2.8083E+04
74	C2H2+O2=HCO+HCO		4.0000E+12	0.000	1.4092E+04
75	C2H2+O=CH2+CO		1.0200E+07	2.000	9.5622E+02
76	C2H2+H+M=C2H3+M		5.5400E+12	0.000	1.2129E+03
77	C2H3+H=C2H2+H2		4.0000E+13	0.000	0.0000E+00
78	C2H3+OH=C2H2+H2O		3.0000E+13	0.000	0.0000E+00
79	C2H3+CH2=C2H2+CH3		3.0000E+13	0.000	0.0000E+00
80	C2H3+C2H3=C2H2+C2H4		1.4500E+13	0.000	0.0000E+00
81	C2H3+O=C2H2+OH		1.0000E+13	0.000	0.0000E+00
82	C2H2+OH=CH3+CO		4.8300E-04	4.000	-1.0065E+03
83	C2H3=C2H2+H		4.6000E+40	-8.800	2.3251E+04
84	C3H6+H=C3H5+H2		5.0000E+12	0.000	7.5491E+02
85	C3H6+O2=C3H5+HO2		4.0000E+12	0.000	2.0081E+04
86	CH2CHO+H=CH3+HCO		2.2000E+13	0.000	0.0000E+00
87	CH2O+O2=HCO+HO2		6.2000E+13	0.000	1.9628E+04
88	CH2O+O=HCO+OH		4.1000E+11	0.600	1.3890E+03
89	CH2O+H=HCO+H2		2.1900E+08	1.800	1.5098E+03
90	CH2O+M=CO+H2+M		6.2500E+15	0.000	3.4997E+04
91	CH2O+M=HCO+H+M		3.3000E+16	0.000	4.0765E+04
92	HCO+OH=H2O+CO		1.0000E+14	0.000	0.0000E+00
93	HCO+O=OH+CO		3.0000E+13	0.000	0.0000E+00
94	HCO+O=H+CO2		3.0000E+13	0.000	0.0000E+00
95	HCO+HO2=CO2+OH+H		3.0000E+13	0.000	0.0000E+00
96	C2H6+CH3=C2H5+CH4		1.5100E-07	6.000	3.0433E+03
	REV Parameters	9.6500E-10	6.6000E+00	5.1434E+03	
97	C2H6+H=C2H5+H2		5.3700E+02	3.500	2.6170E+03
	REV Parameters	9.7200E+02	3.5000E+00	1.3749E+04	
98	C2H6+OH=C2H5+H2O		5.1200E+06	2.100	4.3030E+02
	REV Parameters	1.0100E+07	2.1000E+00	1.1565E+04	
99	C2H6+O=C2H5+OH		1.1300E+14	0.000	3.9507E+03
	REV Parameters	2.0800E+13	0.0000E+00	6.4016E+03	
100	CH3+CH3 (+M)=C2H6 (+M)		7.3700E+16	-1.200	3.1998E+02
	Fall-off LOW Parameters	9.0880E+35	-5.2460E+00	8.5808E+02	
	TROE Parameters	4.0500E-01	1.1200E+03	6.9600E+01	1.0000E+15
101	C2H6+O2=C2H5+HO2		4.0000E+13	0.000	2.5617E+04
	REV Parameters	3.0000E+11	0.0000E+00	0.0000E+00	
102	C2H6+HO2=C2H5+H2O2		1.7000E+13	0.000	1.0297E+04
	REV Parameters	1.0700E+11	2.0000E-01	3.9467E+03	
103	C2H6+C2H4=C2H5+C2H5		5.0000E+11	0.000	3.0196E+04
	REV Parameters	5.0000E+11	0.0000E+00	0.0000E+00	
104	C2H6+M=C2H5+H+M		8.8500E+20	-1.200	5.1434E+04

105	REV Parameters	1.1500E+13	3.0000E-01	-	
	C2H6+CH2=C2H5+CH3		2.2000E+13	0.000	4.3634E+03
	REV Parameters	2.6600E+10	6.0000E-01	8.5858E+03	
106	C2H6+CH3O2=C2H5+CH3O2H		1.7000E+13	0.000	1.0297E+04
	REV Parameters	7.5000E+11	0.0000E+00	6.4419E+02	
107	C3H6+C2H5=C3H5+C2H6		1.0000E+11	0.000	4.9321E+03
	REV Parameters	5.3700E+05	1.3000E+00	8.2738E+03	
108	C3H5+C2H5=C2H6+C3H4		4.0000E+11	0.000	0.0000E+00
	REV Parameters	1.8000E+12	1.0000E-01	2.0297E+04	
109	C2H4+O=CH2CHO+H		3.3900E+06	1.900	9.0086E+01
110	C2H3+O2=CH2CHO+O		3.5000E+14	-0.600	2.6472E+03
111	CH2CHO+O2=CH2O+CO+OH		2.0000E+13	0.000	2.1137E+04
112	C2H2+OH=CH2CO+H		2.1900E-04	4.500	-5.0327E+02
113	CH2CO+H=CH3+CO		1.1000E+13	0.000	1.7111E+03
114	CH2CO+O=CH2+CO2		1.7500E+12	0.000	6.7942E+02
115	CH2CO(+M)=CH2+CO(+M)		3.0000E+14	0.000	3.5722E+04
	Fall-Off LOW Parameters	3.6000E+15	0.0000E+00	2.9829E+04	
116	C3H6+O=CH2CO+CH3+H		2.5000E+07	1.800	3.8249E+01
117	CH2CHO=CH2CO+H		3.0900E+15	-0.300	2.5576E+04
118	CH3+O2+M=CH3O2+M		5.4400E+25	-3.300	0.0000E+00
119	CH3O2+CH3=CH3O+CH3O		2.4100E+12	0.000	0.0000E+00
120	CH3O2+O=CH3O+O2		3.6100E+13	0.000	0.0000E+00
121	CH3O2+H=CH3O+OH		9.6400E+13	0.000	0.0000E+00
122	CH3O+H=CH3+OH		1.0000E+14	0.000	0.0000E+00
123	CH3+O=CH2O+H		8.0000E+13	0.000	0.0000E+00
124	CH3+O2=CH3O+O		2.0000E+18	-1.600	1.4701E+04
	REV Parameters	3.5800E+18	-1.6000E+00	-	
125	CH3+H(+M)=CH4(+M)		2.1400E+15	0.2004E+02	0.0000E+00
	Fall-Off LOW Parameters	3.3100E+30	-4.0000E+00	1.0609E+03	
	TROE Parameters	0.0000E+00	1.0000E-15	1.0000E-15	4.0000E+01
	H2 3rd body:	2.0000E+00			
	H2O 3rd body:	5.0000E+00			
	CO 3rd body:	2.0000E+00			
	CO2 3rd body:	3.0000E+00			
126	CH3O2H=CH3O+OH		6.3100E+14	0.000	2.1288E+04
127	CH3O2+CH2O=CH3O2H+HCO		1.9900E+12	0.000	5.8732E+03
128	C2H4+CH3O2=C2H3+CH3O2H		1.1300E+13	0.000	1.5315E+04
129	CH4+CH3O2=CH3+CH3O2H		1.8100E+11	0.000	9.3005E+03
130	CH3O2+HO2=CH3O2H+O2		1.7500E+10	0.000	-1.6482E+03
	>>> No. of reac. with 3rd body :		13		
	>>> No. of reac. with fall off :		6		
	>>> No. of "REV" reactions :		13		
	>>> No. of real RO reactions :		0		